SYMMETRY AND CONSTRAINTS IN HYDRODYNAMICS AND MECHANICAL LOCOMOTION

by

Michael Joel Fairchild

A dissertation submitted to the faculty of
The University of North Carolina at Charlotte
in partial fulfillment of the requirements
for the degree of Doctor of Philosophy in
Applied Mathematics

Charlotte

2015

Approved by:

_____
Dr. Douglas S. Shafer

_____
Dr. Scott D. Kelly

_____
Dr. Evan G. Houston

_____
Dr. Gregory J. Gbur

ABSTRACT

MICHAEL JOEL FAIRCHILD. Symmetry and constraints in hydrodynamics and mechanical locomotion. (Under the direction of DR. DOUGLAS S. SHAFER)

This dissertation introduces new models for the locomotion and control of mechanical and hydrodynamic systems that exhibit symmetry, constraints, and control. I introduce the class of unbalanced Chaplygin control systems and analyze the dynamics and control of two new examples in this class — the Chaplygin beanie and the Chaplygin pendulum. I then prove for the former, and numerically verify for the latter, that a single-input control strategy is able to generate locomotion and asymptotically control both heading and speed. The resulting underactuated control strategy provides a basis for single-input navigation of planar robots subject to a nonholonomic no-slip constraint. Next, I introduce a new model for the locomotion of articulated rigid bodies in ideal fluids and demonstrate that even in the absence of added-mass effects arising from an asymmetric shape, these swimmers may nevertheless locomote provided symmetry of the fluid boundary is broken. I also show that an underlying geometric phase may govern their motion. I then introduce a new technique for devising reduced-order models of the interaction of infinitesimal, stationary rigid bodies immersed in inviscid incompressible fluids with point vorticity. The rigid bodies considered in this dissertation impose four types of constraints on the fluid flow — velocity, direction (or tangency), distance, and position constraints. It is found that energy is generally conserved but that linear and angular impulse of the fluid are not, and that the constraints may dramatically alter the system dynamics.

I also show that this technique may be used to generate approximate models for the interaction of moving rigid bodies and vortical fluids. Finally, motivated by both the relevance of principal bundles to locomotion and by the mismatch between the data needed to prove important theorems vs. the data available in a typical application, I elucidate the relationship between three definitions of a principal bundle appearing in the literature, introduce a new definition, and demonstrate mutual equivalence of all four.

TABLE OF CONTENTS

CHAPTER 1: OUTLINE OF CONTRIBUTIONS 1

CHAPTER 2: PRELIMINARIES 6

2.1. Submersions, Fiber Bundles, and Ehresmann Connections 6

2.2. Geometric Mechanics 14

2.3. Geometry of Locomotion 19

CHAPTER 3: ON THE DEFINITION OF A PRINCIPAL BUNDLE 22

3.1. Introduction 22

3.2. On the Definition of a Principal Bundle 23

3.3. Vertical Spaces in a Principal Bundle 32

3.4. Summary 33

CHAPTER 4: CHAPLYGIN CONTROL SYSTEMS 35

4.1. Introduction 36

4.2. Chaplygin Control Systems 36

4.3. The Chaplygin Sleigh 47

4.4. The Chaplygin Beanie 54

4.5. The Chaplygin Pendulum 68

4.6. Summary 76

CHAPTER 5: LOCOMOTION IN FLUIDS VIA BROKEN SYMMETRY 78

5.1. Introduction 78

5.2. Three-Link Swimmer 81

5.3. A Symmetric Scallop Near a Wall 85

5.4. An Articulated Swimmer Near a Wall 97

5.5. Summary 105

CHAPTER 6: CONSTRAINED VORTEX MOTION 107

6.1. Introduction 108

6.2. The Classical N-Vortex Problem 109

6.3. The Constrained N-Vortex Problem 113

6.4. Velocity Constraint 116

6.5. Direction Constraint 122

6.6. Distance Constraint 127

6.7. Point Vortex and a Rigid Body 131

6.8. Summary 137

CHAPTER 7: FUTURE WORK 138

REFERENCES 140

APPENDIX A: MORE ABOUT CONNECTIONS 144

A.1. Factoring an Ehresmann Connection 144

A.2. Principal Connections 147

A.3. Parallel Transport in Principal Bundles 151

A.4. The Mechanical Connection and the Master Formula 153

A.5. Elroy's Beanie 156

APPENDIX B: AN EXAMPLE OF DIRAC'S METHOD 161

CHAPTER 1: OUTLINE OF CONTRIBUTIONS

The theme of this dissertation is geometry, locomotion, and reduced-order models for mechanical and hydrodynamic systems exhibiting symmetry, nonholonomic constraints, and control. The interaction between these three features leads to rich nonlinear dynamics and enables such phenomena as locomotion generation and underactuated control.

I introduce the class of *Chaplygin control systems*, obtained by adjoining internal degrees of freedom to the Chaplygin sleigh. This work extends the previous literature in that I consider control of the unbalanced sleigh, whereas previous work considers control of the balanced sleigh. The equations of motion are significantly more complicated in the unbalanced case. After studying the general features of these systems and recovering the known dynamics of the sleigh as a special case, I introduce two new examples in this class, the Chaplygin beanie and the Chaplygin pendulum. For these two systems I analyze a single-input control strategy and find that it is possible to control the asymptotic evolution of two outputs — heading and speed — with only a single input, thus demonstrating a form of underactuated control. I give a rigorous proof for the former system and a numerical verification for the latter. I also demonstrate that both systems exhibit the phenomenon of locomotion generation, whereby starting from rest a net locomotion through the environment is induced by the actuation of internal shape variables.

Turning to hydrodynamics, I introduce a new class of articulated rigid bodies swimming in an inviscid incompressible fluid. Unlike previous work in this area, the swimmers considered here have completely symmetric inertia tensors and therefore do not benefit from added-mass effects arising from their shape. I compensate for this by breaking a symmetry in the boundary of the fluid region and show that this broken symmetry enables their locomotion. Although the broken symmetry rules out the relevance of the mechanical connection, I do find numerical evidence for an underlying geometric phase and suggest that a hidden connection may be relevant to the locomotion of these systems.

I then introduce a reduced-order model for the dynamics of fixed, infinitesimal rigid bodies immersed in an inviscid incompressible fluid with point vorticity. The bodies impose hydrodynamic constraints on the evolution of the fluid. I first consider three constraints of this kind — velocity constraints, direction (or tangency) constraints, and distance constraints. The first arises from a small cylinder in the flow, the second from a small fin, and the third from a vortex dipole. The idea of the model is to capture the essential physics using a system of finitely many ordinary differential equations without requiring the full power of the Euler or Navier-Stokes equations. I do this by expressing the fluid constraints in terms of the evolution of the vortices and then applying Dirac's method of constraints to the Hamiltonian formulation of the classical N-vortex problem. I find that for the constraints considered here, energy is conserved but linear and angular impulse of the fluid are not, and that the constraints may alter the system dynamics dramatically — in one case changing a symmetric periodic vortex orbit to an asymmetric scattering orbit. I then consider a

fourth kind of constraint, the position constraint, and show that it may be used to derive an approximate reduced-order model for the dynamic interaction of a moving cylinder with an external point vortex. The resulting model produces dynamics with qualitative similarities to the known solution. Although not exact in its details, the benefit is that it does not require a detailed control-volume analysis but rather only a judicious choice of image vortices that satisfy certain boundary conditions.

Returning to geometry and locomotion, I elucidate the relationship between three different definitions of principal bundle appearing in the literature, introduce a new definition, and demonstrate that all four are mutually equivalent. This is motivated not only by the importance of principal bundles and connections to the geometry and dynamics of locomotion, as explained in the preliminary material, but also by the mismatch between the data one needs to prove important results and the data available at hand in a typical application. Specifically, it is demonstrated through proofs appearing in the appendices that important results in locomotion rely on the presence of an atlas of equivariant charts for a principal bundle, whereas the data at hand in a typical mechanics application is the smooth, free, and proper action of a Lie group on the system's configuration space. Hence it is of significant benefit to know that the latter set of data implies the former. Although this result is known, I have not yet found a proof in the literature, nor of the other equivalences established in this work. I present this material at the beginning of the dissertation because the resulting geometry of locomotion is invoked in the interpretation of later examples.

This concludes the discussion of the original research material, and I now discuss the appendices, which serve two purposes — to give additional details and explicit

examples that aid in the understanding of the new research material but whose inclusion in the body of the dissertation would be disruptive, and to rigorously establish known "folklore" results whose proofs I did not find in the literature. The first appendix discusses Ehresmann and principal connections in detail, giving an explicit example in coordinates of an Ehresmann connection and the local factorization of its connection form. In the mechanics literature on principal bundles, much attention is understandably given to left principal bundles, because it is left multiplication that leads to symmetry in particle and rigid body mechanics. However, right multiplication is what gives symmetry in ideal hydrodynamics, and by working through explicit proofs I show how to handle this case as well. Since I define connections geometrically in terms of a direct-sum splitting of tangent spaces, whereas in applications it is connection forms that are used, I explain in detail the relation between the two, again with an emphasis on the distinction between left and right multiplication. Of course these considerations are not of concern for abelian bundles, but most of the Lie groups relevant to mechanics are nonabelian, such as the rotation groups $SO(n)$ and the rigid motion groups $SE(n)$. I give an alternate proof of the classical reconstruction formula for parallel transport in abelian principal bundles by using a formula for the derivative of the exponential map, rather than using the usual structure theorem for abelian Lie groups. Next, because the mechanical connection is discussed at least three times in the dissertation, and because I find somewhat unsatisfactory the usual definition of it in terms of its connection form, I give its geometric definition as the metric connection induced by the kinetic-energy metric. I then prove that this geometric definition induces the usual "master formula" for the connection form, and

I then treat Elroy's beanie as a concrete example of the mechanical connection and geometric phase. Finally, the last appendix gives an example of Dirac's method of constraints.

The literature relevant to the material in this dissertation is reviewed in context in the individual chapters.

CHAPTER 2: PRELIMINARIES

I assume the reader is familiar with the theory of differentiable manifolds and Lie groups. This purpose of this chapter is to concisely gather together only those key concepts from the theory of bundles and connections and from geometric mechanics needed to understand the new material in the sequel. Principal references for the differential geometry material are [35], [32], [43], [9], [62], and [16], and references for geometric mechanics include [1], [36], [38], [37], [25], [7], and [8].

2.1 Submersions, Fiber Bundles, and Ehresmann Connections

Recall that a smooth map $\pi : M \to N$ between manifolds is a *submersion* if its differential is everywhere surjective. A *local section* for π is an open set $U \subset N$ together with a smooth map $\sigma : U \to M$ such that $\pi \circ \sigma = \mathrm{id}_U$; the section is *global* if $U = N$. The following theorem is proved in [35].

THEOREM 1. *A map $\pi : M \to N$ is a submersion if and only if M is covered by the images of local sections. Every submersion is an open map, and a surjective submersion is a quotient map.*

THEOREM 2. *Let a surjective submersion $\pi : M \to N$ and a map $f : N \to P$ be given. Then f is smooth if and only if its lift $f \circ \pi : M \to P$ is smooth. If f is a smooth bijection and its lift $f \circ \pi$ is a submersion, then f is a diffeomorphism.*

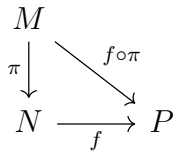

Proof. This first part of this theorem is proved in [35]. To prove the last part, assume f is a smooth bijection. Then f^{-1} is smooth by a similar diagram but with P and N swapped, f^{-1} on the bottom, $f \circ \pi$ on the left, and $f^{-1} \circ (f \circ \pi) = \pi$ on the diagonal. □

Finally, recall the level set theorem, whose proof may be found in [35].

THEOREM 3 (Level Set). *Each level set of a smooth map of constant rank r is a properly embedded submanifold of codimension r. In particular, a regular level set of a submersion $M \to N$ is a properly embedded submanifold of codimension* $\dim N$.

A *fiber bundle* is a quadruple (Q, π, M, F) comprising smooth manifolds Q, M, F and a smooth surjection $\pi : Q \to M$ such that to each $p \in M$ there corresponds an open set $U \subset M$ about p and a *fiber-preserving* diffeomorphism $\phi : \pi^{-1}(U) \to U \times F$, which means the diagram

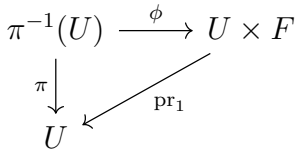

commutes, where $\mathrm{pr}_1 : U \times F \to U : (r, s) \mapsto r$ is the projection onto the first factor. It follows that ϕ may be factored as $\phi(q) = (\pi(q), \tilde{\phi}(q))$, which defines the *principal part* $\tilde{\phi} : \pi^{-1}(U) \to F$ of ϕ. We call Q the *total space*, M the *base space*, F the *model fiber* (or *typical fiber*), π the *projection*, and say that Q is an F *bundle over* M. A pair (U, ϕ) as in the definition is called a *local trivialization*, as illustrated in Figure 1. Given $p \in M$ the set $Q_p \coloneqq \pi^{-1}(p)$ is the *fiber over* p, and elements in Q_p are said

to be *over* p. Depending on the data to be emphasized, the bundle may be denoted (Q, π, M, F), or $F \hookrightarrow Q \xrightarrow{\pi} M$, or $\pi : Q \to M$, or just Q.

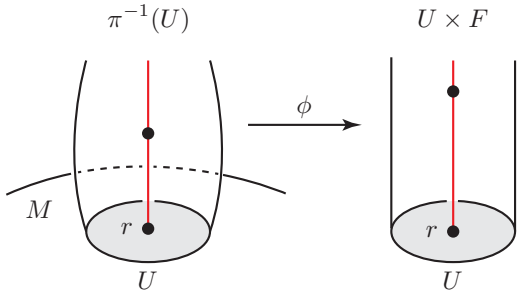

Figure 1: A local trivialization $\phi : \pi^{-1}(U) \to U \times F$ maps the cylinder $\pi^{-1}(U)$ diffeomorphically onto the product cylinder $U \times F$ while preserving fibers.

THEOREM 4. *In every fiber bundle the projection is a submersion and a quotient map, each fiber is a properly embedded submanifold diffeomorphic to the fiber, and the dimension of the total space equals the sum of the dimensions of the base and fiber.*

Proof. Let $\pi : Q \to M$ be an F-bundle. Let $q \in Q$ and choose a local trivialization (U, ϕ) with $q \in \pi^{-1}(U)$. Differentiate $\pi = \mathrm{pr}_1 \circ \phi$ at q to obtain $T_q\pi = T_{\phi(q)}\,\mathrm{pr}_1 \cdot T_q\phi$. Since $T_{\phi(q)}\,\mathrm{pr}_1$ is surjective, so too is $T_q\pi$ surjective, and hence π is a submersion. Since π is also surjective, it is a quotient map by Theorem 1. Finally, consider any fiber $\pi^{-1}(r)$. Choose a local trivialization (U, ϕ) with $r \in \pi(U)$. The level set theorem implies $\pi^{-1}(r)$ is a properly embedded submanifold of codimension $\dim M$. Hence the restriction of ϕ to $\pi^{-1}(r)$ is smooth; this restriction gives a diffeomorphism $\pi^{-1}(r) \to \{r\} \times F \cong F$, which also implies $\dim \pi^{-1}(r) = \dim F$. The codimension statement now gives $\dim Q - \dim \pi^{-1}(r) = \dim M$, so $\dim Q = \dim M + \dim F$. □

An important consequence of the local trivialization property is that locally coordinates can always be chosen that factor in a nice way. Indeed, if $\phi : \pi^{-1}(U) \to U \times F$ is

any local trivialization, then product coordinates on $U \times F$ may be pulled back along ϕ to obtain give *bundle coordinates* (or *product coordinates*) $q = (r, s)$ on $\pi^{-1}(U)$, where r encodes position along the base and s encodes position along the fiber.

A *smooth structure* (or *bundle atlas*) for a bundle $F \hookrightarrow Q \xrightarrow{\pi} M$ is a collection $\mathcal{G} = \{(U_\alpha, \phi_\alpha)\}$ of local trivializations such that $\bigcup U_\alpha = M$. By definition, every bundle comes equipped with a smooth structure. Two local trivializations (U_α, ϕ_α) and (U_β, ϕ_β) in $\mathcal{G}$ *overlap* if $U_{\alpha\beta} \coloneqq U_\alpha \cap U_\beta$ is nonempty, in which case the diagram

$$\begin{array}{ccccc} U_{\alpha\beta} \times F & \xleftarrow{\phi_\alpha} & \pi^{-1}(U_{\alpha\beta}) & \xrightarrow{\phi_\beta} & U_{\alpha\beta} \times F \\ & \searrow^{\mathrm{pr}_1} & \downarrow{\scriptstyle \pi} & \swarrow_{\mathrm{pr}_1} & \\ & & U_{\alpha\beta} & & \end{array}$$

commutes. Since ϕ_α and ϕ_β are fiber-preserving diffeomorphisms, so is

$$\phi_{\alpha\beta} \coloneqq \phi_\alpha \circ \phi_\beta^{-1} : U_{\alpha\beta} \times F \to U_{\alpha\beta} \times F.$$

Hence for each $r \in U_{\alpha\beta}$ there is a diffeomorphism $g_{\alpha\beta}(r) : F \to F$ defined by

$$\phi_{\alpha\beta}(r, s) = (r, g_{\alpha\beta}(r)(s)).$$

Letting r vary over $U_{\alpha\beta}$ gives a family $\{g_{\alpha\beta}(r) : r \in U_{\alpha\beta}\}$ of diffeomorphisms $F \to F$, one for each point of $U_{\alpha\beta}$. Let $\mathcal{D}(F)$ denote the group of diffeomorphisms $F \to F$ and define the *transition function*

$$g_{\alpha\beta} : U_{\alpha\beta} \to \mathcal{D}(F) : r \mapsto g_{\alpha\beta}(r).$$

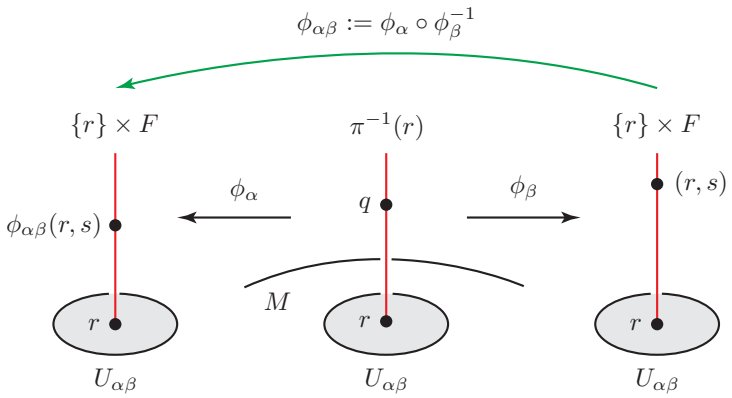

Figure 2: Two overlapping trivializations induce a diffeomorphism $F \to F$ (green) for each fiber (red) corresponding to a point r in the overlap $U_{\alpha\beta}$. Letting r vary over $U_{\alpha\beta}$ induces the transition function $g_{\alpha\beta} : U_{\alpha\beta} \to \mathcal{D}(F)$.

The transition function is illustrated in Figure 2. On a practical level, it relates two overlapping trivializations; indeed, if $\pi(q) \in U_\alpha \cap U_\beta$, then $\phi_\alpha(q)$ and $\phi_\beta(q)$ are related according to

$$\phi_\beta(q) = (r, s) \Rightarrow \phi_\alpha(q) = (r, g_{\alpha\beta}(r)(s)). \tag{1}$$

Every transition function $g_{\alpha\beta}$ is *differentiable* in the sense that $U_{\alpha\beta} \times F \to F : (r, s) \mapsto g_{\alpha\beta}(r)(s)$ is differentiable, which follows from differentiability of $\phi_{\alpha\beta}$. On triple overlaps $U_{\alpha\beta\gamma} := U_\alpha \cap U_\beta \cap U_\gamma \neq \varnothing$, the transition functions obey the *cocycle condition*

$$g_{\alpha\beta}(r) \circ g_{\beta\gamma}(r) = g_{\alpha\gamma}(r)$$

for every $r \in U_{\alpha\beta\gamma}$. The cocycle condition implies that for each $r \in M$ the collection $G_r := \{g_{\alpha\beta}(r)\}$ is a subgroup of $\mathcal{D}(F)$. In particular, $g_{\alpha\alpha}(r)$ is the identity diffeomorphism for every α, and $g_{\beta\alpha}(r)$ is the inverse of $g_{\alpha\beta}(r)$. If there is a fixed Lie group

$G \subset \mathcal{D}(F)$ in which all transition functions take their values, i.e. $G_r \subset G$ for every $r \in M$, then G is said to be a *structure group* of the bundle. Hence any larger Lie group $G \subset G' \subset \mathcal{D}(F)$ is also a structure group. To emphasize that G is a structure group, the bundle may be denoted (Q, π, M, F, G).

Associated to every fiber bundle $\pi : Q \to M$ is its *vertical distribution* $q \mapsto V_q$, defined by

$$V_q \coloneqq \ker(T_q\pi) = \{v_q \in T_qQ : T_q\pi \cdot v_q = 0\}.$$

We call V_q the *vertical space* at q.[1] An *Ehresmann connection* is a smooth distribution $q \mapsto H_q$ such that

$$T_qQ = H_q \oplus V_q. \tag{2}$$

We call H_q the *horizontal space* at q. There is no natural choice of a connection on a bundle unless that bundle has extra structure. Two examples for which there is such structure are product bundles $Q = M \times F$, in which case the direct sum $T_{(r,s)}Q = T_rM \oplus T_sF$ defines a connection $(r, s) \mapsto H_{(r,s)} \coloneqq T_rM$, and bundles Q endowed with a Riemannian metric g, in which case the *metric connection* $q \mapsto H_q$ is defined such that horizontal is metric orthogonal to vertical, i.e.

$$H_q \coloneqq V_q^{\perp} = \{v_q \in T_qQ : g(v_q, w_q) = 0 \text{ for all } w_q \in V_q\}. \tag{3}$$

The *horizontal bundle* H and the *vertical bundle* V are the subbundles of TQ whose fibers at q are H_q and V_q, respectively. A tangent vector $v_q \in TQ$ is *horizontal* or

[1] The word "vertical" is explained by that fact that fibers are typically drawn vertically over the base

vertical if $v \in H_q$ or $v \in V_q$, respectively; it need not be either. However, due to the direct sum (2), it is uniquely a sum of a horizontal and vertical vector, $v_q = \operatorname{hor} v_q + \operatorname{ver} v_q$. Likewise, a vector field X on Q is *horizontal* or *vertical* if for every $q \in Q$, $X_q \in H_q$ or $X_q \in V_q$, respectively, and every vector field on Q may be decomposed uniquely as the sum of a horizontal and a vertical vector field. Finally, a trajectory $\gamma : [a, b] \to Q$ is *horizontal* or *vertical* if $\dot\gamma(t) \in H_{\gamma(t)}$ or $\dot\gamma(t) \in V_{\gamma(t)}$, respectively, for every $t \in [a, b]$.

Given a bundle $\pi : Q \to M$, a base trajectory $r : [a, b] \to M$, and a point $q \in \pi^{-1}(r(a))$, the *parallel transport problem*, shown in Figure 3, is to find a trajectory $\gamma : [a, b] \to Q$ that is a *lift* through q of the base trajectory in the sense that $\gamma(a) = q$ and $\pi(\gamma(t)) = r(t)$ for all $t \in [a, b]$. In general there are many such lifts and no natural way of selecting among them. However, given a connection there is a unique such lift — at least on some subinterval $[a, a + \epsilon)$ — that is horizontal. Indeed, differentiation of $\pi(\gamma(t)) = r(t)$ shows that finding the horizontal lift γ of r amounts to solving the initial-value problem

$$T_{\gamma(t)}\pi \cdot \dot\gamma(t) = \dot r(t), \quad \dot\gamma(t) \in H_{\gamma(t)}, \quad \gamma(a) = q, \quad a \le t \le b,$$

but the local existence and uniqueness theory for ordinary differential equations only guarantees a solution on some small interval $[a, a+\epsilon)$. It is a theorem (see [32] or [43]) that a horizontal lift exists for all time $t \in [a, b]$ provided the model fiber is compact, or if the connection is a principal connection on a principal bundle. (Principal bundles are defined in §3.2, and principal connections are defined in §A.2).

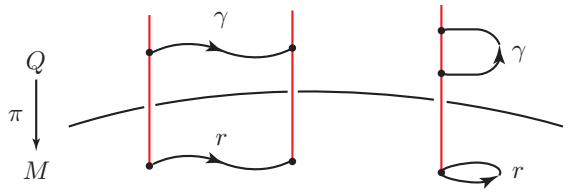

Figure 3: Parallel transport relative to an Ehresmann connection.

Note in Figure 3 that the lift of a closed loop in base space, although it must return to the same fiber, need not return to the same point along the fiber. This translation along the fiber associated with horizontal lifts of closed base loops is known as *geometric phase* when it is independent of the time parameterization along the trajectories.

Finally, because it is easier to work with maps than subspaces, it is helpful to have a characterization of an Ehresmann connection in terms of a map satisfying certain properties. Recall that a *projection* on a vector space W is a linear map $P : W \to W$ such that $P \circ P = P$. Such a projection induces the direct-sum decomposition $W = \ker P \oplus \operatorname{img} P$. Conversely, given any decomposition $W = U \oplus V$ where U, V of are subspaces of W, there is an associated projection operator $P : W \to W$ characterized by the property that $\ker P = U$. Applying this observation pointwise, it follows that to each connection $q \mapsto H_q$ there is a vertical-valued 1-form $A : TQ \to V$, called the *connection form*, with the property that for each q the restriction $A|_q : T_qQ \to V_q$ is a linear projection. So the connection form returns the vertical part of a vector, $A(v_q) = \operatorname{ver} v_q$. Then $\operatorname{hor} v_q = v_q - A(v_q)$, and $H_q = \ker(A_q)$. Conversely, a vertical-valued 1-form $A : TQ \to V$ satisfying the properties above induces the Ehresmann connection $q \mapsto H_q := \ker(A_q)$. More details are given in §A.1, where an explicit

example is worked out in coordinates.

2.2 Geometric Mechanics

The description of a mechanical system begins with its configuration manifold Q whose points encode the distinct configurations of the system. This is then enlarged to a phase space P that encodes additional dynamical variables, such as velocities or momenta, that are used to describe the governing equations of the system. These equations are obtained by the interaction between a given structure and a distinguished function on phase space. In Lagrangian mechanics the phase space is the tangent bundle TQ, the structure is Hamilton's principle, and the distinguished function is a Lagrangian $L : TQ \to \mathbb{R}$. For Hamiltonian mechanics the phase space is a symplectic or Poisson manifold, the structure is a symplectic form or Poisson bracket, respectively, and the distinguished function is a *Hamiltonian* $H : P \to \mathbb{R}$.

Consider now Lagrangian mechanics. Let Q be a configuration space for a mechanical system and $L : TQ \to \mathbb{R}$ be the *Lagrangian*, i.e. kinetic minus potential energy. Define the *fiber derivative* $\mathbb{F}L : TQ \to T^*Q$ such that for every $q \in Q$ and every $v_q, w_q \in T_qQ$,

$$\langle \mathbb{F}L(v_q), w_q \rangle = \left. \frac{d}{dt} \right|_{t=0} L(v_q + tw_q).$$

For each of the Lagrangian systems considered in this work, there is a Riemannian metric g on Q and a function $V : Q \to \mathbb{R}$ such that the Lagrangian takes the form

$$L(v_q) = \frac{1}{2} g(v_q, v_q) - V(q). \tag{4}$$

Then the triple (Q, g, L) is referred to as a *simple mechanical system*. In this case, it

may be shown that if $v_q = (q, \dot{q})$ in tangent-lifted coordinates, then

$$\mathbb{F}L(v_q) = g_{ij}\dot{q}^j \, \mathbf{d}q^i = \frac{\partial L}{\partial \dot{q}^i} \, \mathbf{d}q^i = p_i \, \mathbf{d}q^i, \tag{5}$$

where the components $p_i = \frac{\partial L}{\partial \dot{q}^i}$ of the fiber derivative are known classicaly as *conjugate momenta*. Hence the fiber derivative and the metric carry the same information in the sense that

$$\langle \mathbb{F}L(v_q), w_q \rangle = g(v_q, w_q). \tag{6}$$

Turning to dynamics, let $\gamma : [a, b] \to Q$ be a curve in Q. A *variation* of γ is a C^2 map $\theta : [-\epsilon, \epsilon] \times [a, b] \to Q$ such that $\theta(0, t) = \gamma(t)$ for all $t \in [a, b]$. It is said to have *fixed endpoints* if $\theta(s, a) = \gamma(a)$ and $\theta(s, b) = \gamma(b)$ for all $s \in [-\epsilon, \epsilon]$. The *virtual displacement* is the map $\delta\gamma : [a, b] \to TQ$ defined by $\delta\gamma(t) \coloneqq \frac{\partial}{\partial s}\big|_{s=0} \theta(s, t)$.[2] The curve γ is said to obey *Hamilton's principle* if for every fixed-endpoint every variation θ of γ, we have

$$0 = \delta \int_a^b L(\gamma(t), \dot{\gamma}(t)) \, dt \coloneqq \left. \frac{d}{ds} \right|_{s=0} \int_a^b L(\theta(s, t), \dot{\theta}(s, t)) \, dt. \tag{7}$$

Assuming that Q is finite dimensional, say $\dim Q = n$, then arguments from the calculus of variations show that a curve γ obeys Hamilton's principle if and only the *Euler-Lagrange* equations

$$\frac{d}{dt}\frac{\partial L}{\partial \dot{q}^i} - \frac{\partial L}{\partial q^i} = 0, \qquad (i = 1, \ldots, n), \tag{8}$$

hold along the trajectory in every chart that meets the image of γ, and where $(q, \dot{q})$ are

[2] I think "virtual velocity" is more fitting since $\delta\gamma(t)$ is a velocity vector, but I yield to tradition.

the chart's tangent-lifted coordinates. It is experimentally observed that a trajectory taken by an unconstrained Lagrangian system obeys Hamilton's principle and hence the Euler-Lagrange equations.

Mechanical systems often exhibit symmetry that may be exploited for insight or to simplify the dynamics. A symmetry of a simple mechanical system is the smooth action of a Lie group G on configuration space Q such that for every $g \in G$ and every $v_q \in TQ$,

$$L(T_q\Phi_g \cdot v_q) = L(v_q). \tag{9}$$

Corresponding to this symmetry is a *momentum map* $\mathbf{J} : TQ \to \mathfrak{g}^*$, taking values in the dual $\mathfrak{g}^*$ of the Lie algebra $\mathfrak{g}$ of G, defined such that for every velocity vector $v_q \in TQ$ and for every Lie algebra element $\xi \in \mathfrak{g}$,

$$\langle \mathbf{J}(v_q), \xi \rangle = \langle \mathbb{F}L(v_q), \xi_Q(q) \rangle . \tag{10}$$

Here ξ_Q is the *infinitesimal generator* corresponding to ξ, i.e. the vector field on Q defined by

$$\xi_Q(q) \coloneqq \left. \frac{d}{dt} \right|_{t=0} \Phi(\exp(t\xi), q), \tag{11}$$

where $\exp : \mathfrak{g} \to G$ is the Lie exponential map, defined such that $\exp(\xi)$ is the point in G obtained by starting at the identity $e \in G$ and flowing for one unit of time along the left-invariant vector field X_ξ of G defined by $X_\xi(g) \coloneqq T_eL_g \cdot \xi$. The pairings on the left and right sides of (10) are the natural ones between $\mathfrak{g}^*$ and $\mathfrak{g}$, and between

T^*Q and TQ, respectively. When the Lagrangian is of the form (4), then (6) gives

$$\langle \mathbf{J}(v_q), \xi \rangle = g(v_q, \xi_Q(q)) = g_{ij} v_q^i \xi_Q^j(q),$$

which is an explicit formula for the component of the momentum map that corresponds to the Lie algebra element ξ. The importance of the momentum map stems from *Noether's theorem*, which asserts that if the Lagrangian is invariant in the sense of (9), then the momentum map is conserved along solutions of the Euler-Lagrange equations; i.e. if $\phi_t : Q \to Q$ is the time-t flow of the Euler-Lagrange equations and $q \in Q$, then $\frac{d}{dt}\mathbf{J}(\phi_t(q)) = 0$. A proof may be found in [7].

Consider now Hamiltonian mechanics. A (finite-dimensional) *symplectic manifold* comprises a manifold P endowed with a *symplectic form*, i.e. a closed and *nondegenerate* 2-form Ω on P; that is, $\mathbf{d}\Omega = 0$ and the map $X \mapsto X \lrcorner \Omega \coloneqq \Omega(X, \cdot)$ gives an isomorphism from vector fields to 1-forms on P. Every cotangent bundle $P = T^*Q$ is a symplectic manifold in a natural way. Define the *Liouville 1-form* Θ on T^*Q such that whenever $\mu \in T^*Q$ and $v \in T_\mu T^*Q$ then $\langle \Theta(\mu), v \rangle = \mu(T_\mu \pi \cdot v)$, where $\pi : T^*Q \to Q$ is the projection. The *canonical symplectic form* is then $\Omega \coloneqq -\mathbf{d}\Theta$. If $\dim T^*Q = 2n$ and (q, p) are cotangent-lifted local coordinates, then $\Omega = \mathbf{d}q^1 \wedge \mathbf{d}p_1 + \cdots + \mathbf{d}q^n \wedge \mathbf{d}p_n$. Turning to dynamics, the *Hamiltonian vector field* associated to a smooth function $H : P \to \mathbb{R}$ is that vector field X_H on P such that $X_H \lrcorner \Omega = \mathbf{d}H$. *Hamilton's equations* are the evolution equations $\dot{z}(t) = X_H(z(t))$ for a curve $t \mapsto z(t) \in P$. In cotangent-lifted coordinates (q, p), these are

$$\dot{q}^i = \frac{\partial H}{\partial p_i}, \quad \dot{p}_i = -\frac{\partial H}{\partial q^i}. \tag{12}$$

Meanwhile, a *Poisson manifold* is a smooth manifold P endowed with a *Poisson bracket* operation $\{\cdot,\cdot\} : C^\infty(P) \times C^\infty(P) \to C^\infty(P)$ that makes $C^\infty(P)$ into a Lie algebra and obeys the *Leibniz rule*, $\{fg, h\} = f\{g, h\} + g\{f, h\}$. The *Hamiltonian vector field* associated with $H : P \to \mathbb{R}$ is the unique vector field X_H on P such that $X_H f = \{f, H\}$ for every $f \in C^\infty(P)$. This is well defined, because the Leibniz rule implies that $f \mapsto \{f, H\}$ is a derivation, and there is a one-to-one correspondence between derivations of the algebra $C^\infty(P)$ and vector fields on P. Every symplectic manifold (Ω, P) is also a Poisson manifold because Ω induces the Poisson bracket $\{f, g\} \coloneqq \Omega(X_f, X_g)$. In cotangent-lifted coordinates (q, p), *Hamilton's equations* are the evolution equations

$$\dot{q}^i = \{q^i, H\}, \quad \dot{p}_i = \{p_i, H\}. \tag{13}$$

If the Poisson bracket is induced by the canonical symplectic form on a cotangent bundle, this reproduces the symplectic form of Hamilton's equations (12).

Turning to constraints, in the most basic formulation a *constraint* is an equation on phase space that must be satisfied along system trajectories. I will only be interested in linear velocity constraints. By linearity, such a constraint is represented by a 1-form $\omega \in \Omega^1(Q)$ such that a velocity vector $v_q \in TQ$ satisfies the constraint if and only if $\omega_q(v_q) = 0$, i.e. if and only if $v_q \in \ker(\omega_q)$. Assume now that k linearly independent such constraints are present, represented by 1-forms $\omega^1, \ldots, \omega^k$. The resulting *constraint distribution* $\mathcal{D} \subset TQ$ is the codimension-k distribution defined

by

$$\mathcal{D} = \ker(\omega^1) \cap \cdots \cap \ker(\omega^k).$$

Such a system of constraints is said to be *holonomic* or *nonholonomic* according as to whether the induced constraint distribution is integrable or not in the sense of Frobenius. That is, the constraints are holonomic if and only if whenever X, Y are vector fields in $\mathcal{D}$ then $[X, Y] \in \mathcal{D}$. To accommodate the constraints in the dynamics, Hamilton's principle is modified as follows — a trajectory $\gamma : [a, b] \to Q$ obeys the *Lagrange d'Alembert principle* if (7) holds for every fixed-endpoint variation θ of γ whose virtual displacements satisfy the constraints in the sense that $\delta\gamma(t) \in \mathcal{D}_{\gamma(t)}$ for all $t \in [a, b]$. A detailed discussion may be found in [40] and [7].

2.3 Geometry of Locomotion

A recurring theme in this work is the geometry of locomotion, and I now discuss the relevance of the foregoing geometric machinery — bundles, connections, parallel transport, and geometric phases — in understanding locomotion. Most of the systems I consider have configuration spaces that may be factored as a product of two manifolds, $Q = M \times G$, where points of M encode the internal shape of the system, and where G is a Lie group whose points encode the system's position and orientation in ambient space. Accordingly, in this context M is called the *shape manifold* or *shape space*. When endowed with the canonical projection $\pi : Q \to M$, the configuration space naturally has the structure of a principal G-bundle (defined in §3.2) in two different ways, via left or right multiplication by G in the second factor of Q. It turns

out that for problems in rigid body mechanics it is the left multiplication that leads to symmetry, whereas for fluid mechanics right multiplication does so. The systems I consider will be endowed with left multiplication.

Now suppose that, in addition to having the aforementioned structure of a left principal G-bundle, Q is also a simple mechanical system; that is, it is endowed with a Riemannian metric g such that the Lagrangian is given by (4). Then the bundle has a metric connection defined by (3), and I prove in §A.4 that the resulting connection — known as the *mechanical connection* — is a principal connection on this bundle. This principal connnection is represented by a 1-form $\Gamma : TQ \to \mathfrak{g}$, taking values in the Lie algebra $\mathfrak{g}$ of the symmetry group G, defined such that $\Gamma(v_q)$ returns the unique Lie algebra element ξ such that $\xi_Q(q)$ is the vertical part of v_q. If we define the *local connection form* $A : TM \to \mathfrak{g}$ by $A(r, \dot{r}) \coloneqq \Gamma(r, e, \dot{r}, 0)$, then it is proved in §A.3 that the horizontal lift $t \mapsto (r(t), g(t))$ passing through g_0 of a given curve $r : [0, T] \to M$ is determined by the initial-value problem

$$\dot{g}(t) = g(t)A(r(t), \dot{r}(t)),$$

$$g(0) = g_0.$$

Since $r(t)$ and hence $A(r(t), \dot{r}(t))$ are known, this initial-value problem may be integrated in order to *reconstruct* the evolution of the group variables $g(t)$, which encode the system's position and orientation in its environment, from the known initial conditions and the evolution of the shape variables $r(t)$. What's more, if G is an abelian

Lie group an explicit solution is given by

$$g(t) = g_0 \exp\left(-\int_0^t A(r(s), \dot{r}(s))\, ds\right),$$

where $\exp : \mathfrak{g} \to G$ is the Lie exponential map. As a special case, if the path in shape space is a closed loop to which Stokes' theorem applies, the preceding display equals

$$g(T) = g_0 \exp\left(-\iint_S \mathbf{d}A\right),$$

where S is any oriented submanifold of M whose boundary coincides with the given loop in shape space; this formula is called the *area rule for abelian bundles*, and — since it is manifestly independent of the time parameterization — it gives the geometric phase associated with the closed loop in shape space.

CHAPTER 3: ON THE DEFINITION OF A PRINCIPAL BUNDLE

In this chapter I prove the mutual equivalence of three seemingly different definitions of a principal bundle that appear in the literature, and I introduce another definition with certain simplifications and prove its equivalence as well. I also give an elementary proof of a theorem that relates the vertical spaces to the tangent spaces of the group orbits and to the infinitesimal generators induced by the Lie algebra of the bundle's structure group.

3.1 Introduction

Bundles and connections, and principal bundles and connections in particular, are of central importance in differential geometry ([32], [58]), in geometric mechanics and the theory of geometric phases ([36], [42], [37], [11], [8], [7], [27]), and in theoretical physics ([54], [6], [22], [5]) in which a field (e.g. the electromagnetic field) is a section of a bundle over spacetime, a gauge potential is a connection, a choice of gauge is a local trivialization, and field strength corresponds to the curvature of a connection.

Principal bundles arise in mechanics in at least two ways, both of which appear in this dissertation. First, the configuration space of a mechanical system has the structure of a trivial principal G-bundle $\pi : M \times G \to M$, where M is a manifold, G is a Lie group, and π is the projection. Not only do the systems I consider in Chapter 4 and Chapter 5 have this structure, for example, but so do many examples

appearing in the mechanics literature (e.g. [29], [44], and [49]). Second, mechanical systems frequently exhibit *symmetry* in the sense of the action of a Lie group on the system's configuration manifold Q whose lift to phase space leaves invariant some important structure — such as a Lagrangian, or a Hamiltonian, or a variational principle — and under suitable technical conditions discussed in this chapter, the canonical projection from Q onto the quotient Q/G comprising orbits of the action forms a principal G-bundle.

Principal bundles are ubiquitous in differential geometry and mechanics, and it is therefore quite profitable to study them in some detail. To this end, there appear in the literature several definitions of a principal bundle so different from one another that it is not at all obvious if they are equivalent, much less how to move between them if they are ([32], [35], [43]). In this chapter I elucidate the relationship between these definitions, I introduce a new definition that is a simpler version of the one appearing in [32], and I prove their mutual equivalence.

Because powerful machinery is associated with the theory of bundles and connections — for example parallel transport, geometric phase, holonomy, and curvature — it is beneficial to have a means of constructing, or at least recognizing when present, the structure of a principal bundle. The theorems in this chapter provide some progress in that direction.

3.2 On the Definition of a Principal Bundle

Consider the following definitions, in which M is a manifold and G is a Lie group.

1. [32] defines a right principal-G bundle over M as a manifold P together with

a smooth, free right action $P \times G \to P : (u, g) \mapsto ug$ such that P/G is diffeomorphic to M, the canonical projection $\pi : P \to P/G \cong M$ is a submersion, and such that every point in $p \in M$ belongs to an open set $U \subset M$ for which there is a diffeomorphism $\phi : \pi^{-1}(U) \to U \times G : u \mapsto (\pi(u), \tilde{\phi}(u))$ where $\tilde{\phi} : \pi^{-1}(U) \to U \times G$ satisfies $\tilde{\phi}(ug) = \tilde{\phi}(u)g$ for all $u \in \pi^{-1}(U)$ and all $g \in G$.

2. [35] defines a right principal G-bundle as a bundle $\pi : P \to P/G$ arising from the quotient of a manifold P by a smooth, free, proper right action $P \times G \to P$, and where $\pi : P \to P/G$ is the canonical projection onto the orbit space.

3. [43] defines a right principal G-bundle over M as a fiber bundle over M with model fiber G and whose structure group, as defined in §2.1, is G in the sense that every transition function is left multiplication by a group element.

A few questions immediately arise. First, are these definitions equivalent? If so, how does one move between them? Why does the last definition of a *right* bundle require transition functions to be *left* multiplication? Finally, are there any ineffeciencies or redundancies in the definitions? For example, the first definition seems to demand a lot when compared to the other two. I begin to address these questions — and the claims made in the chapter's opening paragraph — by introducing the following definition, which emphasizes the concept of *equivariance* due to its usefulness in applications.

Definition 5. *If G is a Lie group, a* right principal G-bundle *is a fiber bundle (P, π, M, G) together with a smooth right action $R : P \times G \to P : (u, g) \mapsto ug$ such that every local trivialization (U, ϕ) is* equivariant*, meaning that that $\tilde{\phi}(ug) = \tilde{\phi}(u)g$*

for every $u \in \pi^{-1}(U)$ and every $g \in G$.

The equivariance condition means that for every $g \in G$ the diagram

$$\begin{array}{ccc} \pi^{-1}(U) & \xrightarrow{\phi} & U \times G \\ {\scriptstyle R_g}\downarrow & & \downarrow{\scriptstyle \tilde{R}_g} \\ \pi^{-1}(U) & \xrightarrow[\phi]{} & U \times G \end{array}$$

commutes, where $\tilde{R}_g : U \times G \to U \times G$ is right multiplication in the second factor, i.e. $\tilde{R}_g(r, h) = (r, hg)$. That is, equivariance says that if $u \in \pi^{-1}(U)$ and $g \in G$ then

$$\phi(u) = (r, h) \Rightarrow \phi(ug) = (r, hg), \quad \text{or equivalently,} \quad \tilde{\phi}(ug) = \tilde{\phi}(u)g.$$

This is illustrated in Figure 4.

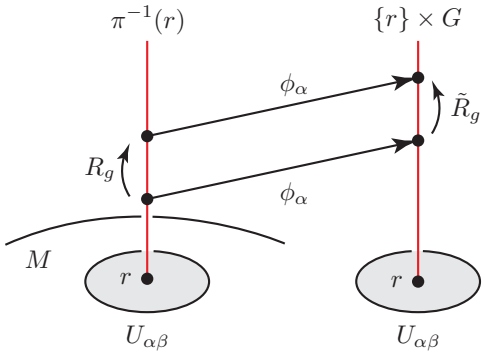

Figure 4: Equivariance of the local trivializations in a principal bundle.

I now turn to the consequences of Definition 5. The following proposition shows that equivariance severely restricts the action. At the same time, it shows that the definition of [32] has certain redundances; for example, freeness of the action is a *consequence* of equivariance.

PROPOSITION 6. *The action of a principal bundle is fiber-preserving, free, and proper, and its restriction to each fiber is transitive.*

Proof. Let $\pi : P \to M$ be a right principal G-bundle. Let $u \in P$, let $g \in G$, choose a local trivialization (U, ϕ) such that $r \coloneqq \pi(u) \in U$, and write $\phi(u) = (r, h)$. By equivariance, $\phi(ug) = (r, hg)$. Then $ug = \phi^{-1}(r, hg) \in \pi^{-1}(r)$ because ϕ, and hence ϕ^{-1}, is fiber-preserving. Therefore, the action is fiber preserving. To prove the action is free, assume $u = ug$. Since ϕ is bijective, $(r, h) = (r, hg)$, which implies $g = e$, so the action is free. To see that it acts transitively on each fiber, let u' also belong to the fiber $\pi^{-1}(r)$ and write $\phi(u') = (r, h')$. Let g be the unique element of G such that $h' = hg$. By equivariance, $\phi(ug) = (r, hg) = (r, h')$, which implies $ug = \phi^{-1}(r, h') = u'$, hence the action is transitive on each fiber.

Finally, to prove the action is proper, let $\Phi : P \times G \to P \times P : (u, g) \mapsto (u, ug)$, and let $K \subset P \times P$ be compact. It must be shown that $\Phi^{-1}(K)$ is compact. Since manifolds are metrizable, compactness and sequential compactness are equivalent. Thus let (u_n, g_n) be a sequence in $\Phi^{-1}(K)$. Then $\Phi(u_n, g_n) = (u_n, u_n g_n)$ is a sequence in the compact set K, hence it has a convergent subsequence, say $(u_{n_k}, u_{n_k} g_{n_k}) \to (u, u')$. This implies $u_{n_k} \to u$, $u_{n_k} g_{n_k} \to u'$, and $\pi(u_{n_k}) \to \pi(u)$ because π is continuous. Let (U, ϕ) be a local trivialization such that $\pi(u) \in U$. Since $u_{n_k} \to u \in \pi^{-1}(U)$, by throwing away finitely many leading terms it may be assumed that all $u_{n_k} \in \pi^{-1}(U)$. Continuity of π implies $\pi(u_{n_k} g_{n_k}) \to \pi(u')$. Since the action preserves fibers, it is also true that $\pi(u_{n_k} g_{n_k}) = \pi(u_{n_k}) \to \pi(u)$. Since limits are unique in a Hausdorff space, $\pi(u') = \pi(u)$. Because the action is free and transitive on the fibers and u, u' belong to the same fiber, there is a unique $g \in G$ such that $u' = ug$. Taken together, $u_{n_k} g_{n_k} \to ug$ and $u_{n_k} \to u$ imply that $g_{n_k} \to g$. Hence $(u_{n_k}, g_{n_k}) \to (u, g)$, which proves that $\Phi^{-1}(K)$ is sequentially compact, hence compact, and so Φ is proper. $\square$

COROLLARY 7. *In a principal bundle, the group orbit through any point coincides with the fiber through that point. That is, for every point q in the total space, $\pi^{-1}(\pi(q)) = \mathcal{O}_q$.*

For a principal bundle there is a nice correspondence between local sections and local trivializations in the sense that choosing one determines the other:

PROPOSITION 8. *Let $\pi : P \to M$ be a principal G-bundle. If (U, ϕ) is a local trivialization, then $\sigma : U \to P : r \mapsto \phi^{-1}(r, e)$ is a local section. Conversely, if $\sigma : U \to P$ is a local section then $\phi : \pi^{-1}(U) \to U \times G : u \mapsto (\pi(u), g)$, where g is the unique element in G such that $\sigma(\pi(u))g = u$, defines a local trivialization.*

Proof. The first part is clear. To prove the second part, let $\sigma : U \to P$ be a local section, and let $u \in \pi^{-1}(U)$. By Proposition 6, the action is free and transitive on the fibers, so there is a unique $g \in G$ such that $\sigma(\pi(u))g = u$. Since $\sigma \circ \pi$ and the action are smooth, the implicit function theorem implies that the solution g to the equation $\sigma(\pi(u))g = u$ depends smoothly on u. Therefore ϕ is smooth. Since the inverse $\phi^{-1} : U \times G \to \pi^{-1}(U) : (r, g) \mapsto \sigma(r)g$ is also smooth, ϕ is a diffeomorphism. □

COROLLARY 9. *A principal bundle is trivial if and only if it admits a global section.*

I now demonstrate the equivalence of the various definitions of a principal bundle and show how the quotient of a manifold by a smooth, free, and proper Lie group action induces a principal bundle.

THEOREM 10. *If $\pi : P \to M$ is a right principal G-bundle, then the quotient space P/G comprising orbits of the bundle action is a manifold diffeomorphic to the base M. Conversely, a smooth, free, proper right action of a Lie group G on a manifold*

P makes the canonical projection $\pi : P \to P/G$ into a right principal G-bundle.

Proof. Let $\pi : P \to M$ be a principal G-bundle with smooth action $P \times G \to P : (u, g) \mapsto ug$. By Proposition 6 this action is free and proper. Hence the quotient manifold theorem implies P/G is a smooth manifold and the natural projection $\pi_G : P \to P/G : u \mapsto [u]$ is a submersion. To show that P/G is diffeomorphic to M, consider the following diagram, in which $f : P/G \to M : [u] \mapsto \pi(u)$.

$$\begin{array}{ccc} P & & \\ {\scriptstyle \pi_G}\downarrow & \searrow^{\pi} & \\ P/G & \xrightarrow[f]{} & M \end{array}$$

To prove f is well defined, let $u' \in [u]$. Then $u' = ug$ for some $g \in G$, and

$$f([u']) = \pi(u') = \pi(ug) = \pi(u) = f([u]),$$

where the third equality holds because Proposition 6 says the action preserves the fibers of π. Hence f is well defined. Moreover, the definition of f implies that $f \circ \pi_G = \pi$. Now apply both parts of Theorem 2: that the lift $f \circ \pi_G = \pi$ is smooth implies f is smooth, and since f is bijective and π is a submersion it follows that f is a diffeomorphism.

Conversely, assume $P \times G \to P$ is a smooth, free, proper right action. The quotient manifold theorem asserts that P/G is a smooth manifold, and that the natural projection $\pi : P \to P/G$ is a submersion. We construct a smooth structure of equivariant local trivializations for P. Because π is a submersion, Theorem 1 implies that for any $u \in P$ there is an open set $U \subset P/G$ and a local section $\sigma : U \to \pi^{-1}(U) \subset P$ such that $\pi(u) \in U$. Define $\phi : \pi^{-1}(U) \to U \times G$ by $\phi(u) = (\pi(u), g)$ where g is

the unique element in G such that $\sigma(\pi(u))g = u$. There is such a g because $\pi(u)$ is (by definition) the orbit through u, and g is unique because the action is free. Both $\sigma \circ \pi$ and the action are smooth, so the implicit function theorem implies that the solution g to $\sigma(\pi(u))g = u$ depends smoothly on u, so ϕ is smooth. Its inverse $\phi^{-1} : U \times G : (r, g) \mapsto \sigma(r)g$ is also smooth, so ϕ is a diffeomorphism. The family of all such (U, ϕ) is a smooth structure for P. It remains to prove equivariance. To do so, let (U, ϕ) be one of the local trivializations just constructed. Let $u \in \pi^{-1}(U)$ and write $\phi(u) = (r, h)$, where by definition of ϕ we have $r = \pi(u)$ and $\sigma(\pi(u))h = u$. If $g \in G$, then $ug = \sigma(\pi(u))hg = \sigma(\pi(ug))hg$ because $\pi(u) = \pi(ug)$, and so $\phi(ug) = (r, hg)$ by definition of ϕ. Therefore, ϕ is equivariant. □

Consider now the third definition of a principal bundle, in terms of the structure group. Recall that if G is a Lie group and $a \in G$, then $L_a : G \to G$ denotes the left multiplication diffeomorphism, i.e. $L_a g = ag$ for every $g \in G$.

THEOREM 11. *If G is a Lie group, then a bundle (P, π, M, G) admits $\{L_a : a \in G\} \subset \mathcal{D}(G)$ as a structure group if and only if there is a smooth right action relative to which every local trivialization is equivariant.*

The idea for the first half of the proof is due to [43].

Proof. Assume the first statement and define $P \times G \to P : (u, g) \mapsto ug$ as follows. Given $u \in P$ and $g \in G$, choose a local trivialization (U_α, ϕ_α) such that $r \coloneqq \pi(u) \in U_\alpha$, write $\phi_\alpha(u) = (r, h)$, and define

$$ug \coloneqq \phi_\alpha^{-1}(r, hg). \tag{14}$$

To prove this is well defined, let (U_β, ϕ_β) be another local trivialization such that $\phi_\beta(u) = (r, h')$. Then $\phi_\beta^{-1}(r, h'g) = \phi_\alpha^{-1}(r, hg)$ if and only if $(r, h'g) = (\phi_\beta \circ \phi_\alpha^{-1})(r, hg)$, if and only if $h'g = g_{\beta\alpha}(r)(hg)$. Let $a \in G$ be such that $g_{\beta\alpha}(r) = L_a$. By definition of $g_{\beta\alpha}(r)$ and associativity of group multiplication, $h'g = (g_{\beta\alpha}(r)h)g = (ah)g = a(hg) = g_{\beta\alpha}(r)(hg)$. Therefore, the action is well defined, and it is smooth because the local trivializations by which it is defined are smooth. The equivariance property follows from (14).

Conversely, assume $P \times G \to P : (u, g) \mapsto ug$ is a smooth, right action relative to which the local trivializations are equivariant. Suppose (U, ϕ_α) and (U_β, ϕ_β) are overlapping trivializations, and let $r \in U_{\alpha\beta}$. We will find $a \in G$ such that $g_{\beta\alpha}(r) = L_a$. To do so, let $f_\alpha : \pi^{-1}(r) \to G$ and $f_\beta : \pi^{-1}(r) \to G$ be the restrictions of the principal parts $\tilde{\phi}_\alpha$ and $\tilde{\phi}_\beta$ to $\pi^{-1}(r)$. Then f_α and f_β are diffeomorphisms, $g_{\beta\alpha}(r) = f_\beta \circ f_\alpha^{-1}$ by definition, and for all $u \in \pi^{-1}(r)$ and all $h, g \in G$ equivariance implies $f_\alpha(ug) = f_\alpha(u)g$ and $f_\alpha^{-1}(hg) = f_\alpha^{-1}(h)g$, and similarly for f_β. Choose $u \in \pi^{-1}(r)$. Put $h_\alpha \coloneqq f_\alpha(u)$ and let a be the unique element of G such that $f_\beta(f_\alpha^{-1}(h_\alpha)) = ah_\alpha$. We claim that $g_{\beta\alpha}(r) = L_a$. To prove this, let $h'_\alpha \in G$ be arbitrary, and let g be the unique element of G such that $h_\alpha g = h'_\alpha$. Applying equivariance twice and then associativity gives $g_{\beta\alpha}(r)(h'_\alpha) = f_\beta(f_\alpha^{-1}(h_\alpha g)) = f_\beta(f_\alpha^{-1}(h_\alpha)g) = f_\beta(f_\alpha^{-1}(h_\alpha))g = (ah_\alpha)g = a(h_\alpha g) = ah'_\alpha = L_a h'_\alpha$. Since h'_α was arbitrary, $g_{\beta\alpha}(r) = L_a$ as claimed. □

The proof explains the left-right distinction as follows: the Lie group of a principal bundle need not be abelian, but in every group (abelian or not) left and right multiplication commute. Each part of the proof involved a string of equations where

two group elements flanked a third element in the middle, and associativity was used in an essential way. Had we considered $\{R_a : a \in G\}$ as a structure group instead, commutativity rather than mere associativity would have been necessary; since the group was not assumed to be commutative, the conclusion would not have followed.

Looking back on the preceding results, I now make the following remarks.

1. There is nothing special about right bundles. All of the preceding development applies equally well with "left" and "right" interchanged, obtaining the notion of a *left principal G-bundle*, where the action is $L : G \times P \to P : (g, u) \mapsto gu$ and the equivariance condition for a local trivialization $\phi : \pi^{-1}(U) \to U \times G$ becomes $\phi(u) = (r, h) \Rightarrow \phi(gu) = (r, gh)$.

2. Many situations are described in terms of principal bundles, and others in terms of vector bundles. It is natural to wonder how they are related. It turns out that every vector bundle induces in a natural manner a principal bundle known as the frame bundle associated with the given vector bundle. Conversely, a principal bundle leads to various vector bundles, for example the adjoint bundle. These constructions are standard and will not be given here (see [32]). However, principal bundles are more general than vector bundles because while a vector bundle must have a general linear group as its structure group, any Lie transformation group of the fiber may serve as the structure group of a principal bundle. This generality partially explains why so much attention is given to principal bundles, e.g. in [32].

3. Since a principal bundle is equivalent to the quotient of a smooth, free, proper

action of a Lie group G on a manifold Q, it will often be denoted by $Q \to Q/G$, especially when it is unnecessary to emphasize the distinction between left and right, or when a statement applies equally well to both cases. For the same reasons, the group action will be denoted Φ rather than R or L.

3.3 Vertical Spaces in a Principal Bundle

In any bundle, vertical vectors are tangent to the fibers. In a principal bundle $Q \to Q/G$ with action Φ, the fiber through any point q is the orbit $\mathcal{O}_q = \{\Phi_g q : g \in G\}$ through q because the action is fiber-preserving and transitive according to Proposition 6. Therefore, it might be hoped that the vertical spaces in a principal bundle may be characterized in terms of the group action. This is indeed the case. Although a version of the theorem below appears in §4.1 of [1], it does not emphasize the principal bundle setting. Furthermore, I will make significant use of this theorem in Chapter 4, by way of Theorem 14 and (23). Therefore, I present here an elementary proof, different from the one given in [1].

THEOREM 12. *For any point q in a principal bundle $Q \to Q/G$,*

$$V_q = T_q \mathcal{O}_q = \{\xi_Q(q) : \xi \in \mathfrak{g}\}.$$

Proof. Let $\xi \in \mathfrak{g}$, let $q \in Q$, and let $t \in \mathbb{R}$. Then $\pi(\Phi_{\exp(t\xi)}q) = \pi(q)$ because the action preserves fibers. Therefore, $T_q\pi \cdot \xi_Q(q) = \frac{d}{dt}\big|_{t=0} \pi(\Phi_{\exp(t\xi)}q) = \frac{d}{dt}\big|_{t=0} \pi(q) = 0$. Hence $\{\xi_Q(q) : \xi \in \mathfrak{g}\} \subset V_q \coloneqq \ker(T_q\pi)$. I will show that equality obtains. Indeed, $\lambda : \mathfrak{g} \mapsto V_q : \xi \mapsto \xi_Q(q)$ is a linear map of vector spaces whose kernel is $\{0\}$ by freeness of the action. Since the kernel is trivial, λ is injective. Meanwhile, Theorem 4 implies

that $\pi : Q \to Q/G$ is a submersion and that $\dim Q = \dim Q/G + \dim G$. Because π is a submersion, $T_q\pi : T_qQ \to T_{\pi(q)}Q/G$ is surjective, which implies $\operatorname{rank}(T_q\pi) = \dim Q/G$. It now follows by the rank+nullity theorem that $\dim V_q = \dim(\ker T_q\pi) = \dim Q - \dim Q/G = \dim G = \dim \mathfrak{g}$. Since $\mathfrak{g}$ and V_q are equidimensional and λ is a linear injection, λ is an isomorphism, so $V_q = \{\xi_Q(q) : \xi \in \mathfrak{g}\}$.

To obtain the characterization $V_q = T_q\,\mathcal{O}_q$, note that for each $\xi \in \mathfrak{g}$ the image of the curve $t \mapsto \Phi_{\exp(t\xi)}q$ is contained in $\mathcal{O}_q$. Hence $\xi_Q(q) \coloneqq \frac{d}{dt}\big|_{t=0} \Phi_{\exp(t\xi)}q \in T_q\,\mathcal{O}_q$, so that $V_q = \{\xi_Q(q) : \xi \in \mathfrak{g}\} \subset T_q\,\mathcal{O}_q$. For the same reasons as above, the map $\mu : \mathfrak{g} \mapsto T_q\,\mathcal{O}_q : \xi \mapsto \xi_Q(q)$ is linear and injective. Now the orbit $\mathcal{O}_q$ is the fiber over $\pi(q) \in Q/G$, and so $\mathcal{O}_q$ is diffeomorphic to G by Theorem 4. Therefore, $\dim T_q\,\mathcal{O}_q = \dim \mathcal{O}_q = \dim G = \dim \mathfrak{g}$. By the same dimension argument as above, μ is a an isomorphism, so $V_q = T_q\,\mathcal{O}_q$. □

3.4 Summary

In this chapter, I elucidated the relationship between different definitions of a principal G-bundle appearing in the literature. I introduced a new definition that emphasizes equivariance and eliminates some unnecessary assumptions appearing in [32], and I gave explicit proofs of the equivalences between the definitions according to the following diagram.

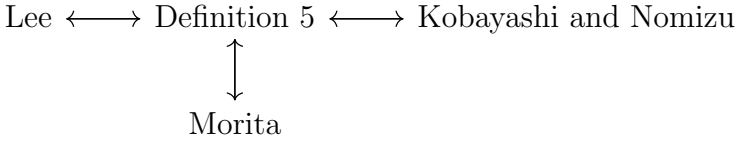

Finally, I gave an elementary proof of the known theorem that the vertical spaces of a principal bundle $Q \to Q/G$ coincide with the tangent spaces of the group orbits

and with the set of infinitesimal generators induced by elements in the Lie algebra of the structure group.

CHAPTER 4: CHAPLYGIN CONTROL SYSTEMS

In this chapter I introduce a general class of nonholonomic mechanical control systems, which I call *Chaplygin control systems*, obtained by enlarging the configuration space of the classical Chaplygin sleigh to allow for internal degrees of freedom. The resulting systems have the structure of a principal $SE(2)$-bundle in a natural way, and symmetry will be exploited in deriving the dynamics. Next, I analyze those parts of the geometry, dynamics, and constraints that are relevant to the entire class. I then show that by considering the Chaplygin sleigh as a trivial Chaplygin control system, the known equations of motion for the sleigh are recovered. Finally, I introduce two new systems, the Chaplygin beanie and the Chaplygin pendulum. The former is a synthesis of Elroy's beanie (discussed in Appendix A) and the Chaplygin sleigh, and the latter is a combination of the inverted pendulum on a cart (treated in [7]) and Chaplygin's sleigh. The resulting dynamics and control of these two systems exhibit a number of interesting phenomena — such as locomotion generation and asymptotic underactuated control — which arise from complicated nonlinear interactions between nonholonomic constraints, symmetry, and control inputs. For the Chaplygin beanie, I prove a rigorous control result, to the effect that both heading and speed may be asymptotically controlled with a single input, and a similar result is verified numerically for the Chaplygin pendulum.

4.1 Introduction

The Chaplygin sleigh was introduced in [12] and studied extensively in [45]. Modified versions of the Chaplygin sleigh have been the subject of persistent interest in the literature, including many recent papers. For example, a discrete version of the system is analyzed in [21], a hydrodynamic version is treated in [19] and [20], and a sleigh with two control inputs was considered in [48]. Among these, the latter work is closest in its considerations and approach to this work, but it differs in two important ways. First, that paper considers only the balanced sleigh, whereas I consider the more general unbalanced sleigh (definitions to appear in the sequel). Second, I am concerned with underactuated single-input controls rather than multi-input controls. The reason is that control is generally harder to achieve with fewer inputs, and this makes for a more challenging analysis. The material in this chapter is a synthesis and generalization of my two recent papers [17] and [28], which build upon a large body of earlier work.

4.2 Chaplygin Control Systems

The *Chaplygin sleigh* comprises a rigid body moving in the Euclidean plane and subject to a nonholonomic constraint that permits forward motion but disallows sideslip. The constraint is represented by a blade, or skate, such that the sleigh may translate parallel to the blade or pivot about the *contact point* of the blade with the ground. The allowed motions of the system are akin to those of a one-legged ice skater.

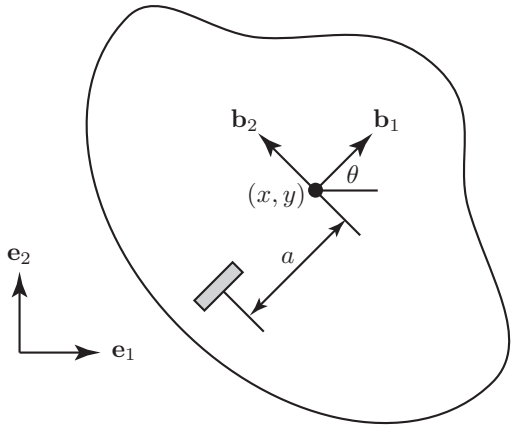

Figure 5: The Chaplygin sleigh, a nonholonomic mechanical system.

The Chaplygin sleigh is depicted in Figure 5, in which the shaded box illustrates the blade, $\{\mathbf{e}_1, \mathbf{e}_2\}$ is a fixed inertial coordinate system relative to which (x, y) are the coordinates of the center of mass, and $\{\mathbf{b}_1, \mathbf{b}_2\}$ is a noninertial *body coordinate system* that moves with the sleigh and is oriented such that $\mathbf{b}_1$ is parallel to the blade. Let a be the distance from the center of the blade (its contact point) to the center of mass. I assume the center of mass lies along the line through the blade. Let θ denote the angle between $\mathbf{b}_1$ and $\mathbf{e}_1$. The inertial and body coordinate systems are related by

$$\begin{aligned} \mathbf{b}_1 &= \cos\theta\, \mathbf{e}_1 + \sin\theta\, \mathbf{e}_2, \\ \mathbf{b}_2 &= -\sin\theta\, \mathbf{e}_1 + \cos\theta\, \mathbf{e}_2. \end{aligned} \tag{15}$$

The configuration space of the Chaplygin sleigh is the Lie group $G = SE(2)$ of rigid Euclidean motions of the plane with local coordinates (x, y, θ). Let M be the mass of the sleigh, and let J be the moment of inerta of the sleigh about the vertical axis through its center of mass. There are two distinct cases which exhibit very different dynamics: the *balanced* case, where the contact point coincides with the sleigh's center

of mass, and the *unbalanced* case otherwise. These two cases correspond to $a = 0$ and $a \neq 0$, respectively, and it will be seen that the unbalanced case exhibits much richer dynamics than the balanced one.

I now enlarge the Chaplygin sleigh by allowing for internal degrees of freedom — such as momentum wheels, movable masses, and the like — so that the configuration space becomes $Q = M \times G$, where M is a manifold whose points encode the internal configuration.[3] Such a system will be referred to as a *Chaplygin control system* when the internal variables are interpreted as control inputs, as throughout the remainder of this chapter. The coordinates on M will be denoted $(r^1, \ldots, r^k)$. Local coordinates on Q are therefore $(r^1, \ldots, r^k, x, y, \theta)$. The dynamic coupling between the system's internal configuration and its position and orientation is encoded in the Lagrangian.

Consider now a typical configuration $q = (r^1, \ldots, r^k, x, y, \theta) \in Q$. Since pivoting about the blade is permitted but sideslip is not, it follows from Figure 5 that the component of the sleigh's translational velocity in the $\mathbf{b}_2$ direction must coincide with circular motion of angular velocity $\dot{\theta}$ and of radius a; that is, $(\dot{x}, \dot{y}) \cdot \mathbf{b}_2 = a\dot{\theta}$. Referring to (15), the constraint is therefore represented by the equation

$$-\dot{x} \sin\theta + \dot{y} \cos\theta = a\dot{\theta}. \tag{16}$$

This is a linear velocity constraint, so as disucssed in §2.2 there is a 1-form $\omega \in \Omega^1(Q)$ such that a velocity vector $v_q \in TQ$ satisfies the constraint if and only if $\omega_q(v_q) = 0$.

[3]It should not cause confusion that the symbol M is used to denote both a manifold and the mass of the sleigh.

This 1-form is

$$\omega_q \coloneqq -\sin\theta\,\mathbf{d}x + \cos\theta\,\mathbf{d}y - a\,\mathbf{d}\theta. \tag{17}$$

Let $q \mapsto \mathcal{D}_q \coloneqq \ker(\omega_q)$ be the resulting constraint distribution. Since $\dim Q = 3 + k$ and there is one constraint, it follows that $\dim \mathcal{D}_q = 2 + k$. To find a basis of vector fields that span $\mathcal{D}$, begin by noting that $\frac{\partial}{\partial r^1}, \ldots, \frac{\partial}{\partial r^k}$ are k linearly independent vector fields in $\mathcal{D}$. Two more independent vector fields that lie in $\mathcal{D}$ may be found either by linear algebra, or — what is easier — by physical considerations. In particular, two motion primitives that satisfy the constraint are forward motion along the blade and pivoting motion about the contact point. These are represented, respectively, by the linearly independent vector fields

$$\begin{aligned} X_1 &\coloneqq \cos\theta\frac{\partial}{\partial x} + \sin\theta\frac{\partial}{\partial y}, \\ X_2 &\coloneqq -a\sin\theta\frac{\partial}{\partial x} + a\cos\theta\frac{\partial}{\partial y} + \frac{\partial}{\partial\theta}. \end{aligned} \tag{18}$$

It follows that for each $q \in Q$,

$$\mathcal{D}_q = \operatorname{Span}\left\{X_1, X_2, \frac{\partial}{\partial r^1}, \ldots, \frac{\partial}{\partial r^k}\right\}. \tag{19}$$

The resulting constraint distribution $\mathcal{D}$ is nonholonomic. In verifying this, it suffices by Frobenius' theorem to show that $[X_1, X_2] \notin \mathcal{D}$. Note that $[X_1, X_2] \subset \operatorname{Span}\{\frac{\partial}{\partial x}, \frac{\partial}{\partial y}, \frac{\partial}{\partial\theta}\}$, and this justifies omission of $\frac{\partial}{\partial r^1}, \ldots, \frac{\partial}{\partial r^k}$ in the following computa-

tion:

$$
\begin{aligned}
[X_1, X_2] &= DX_2 \cdot X_1 - DX_1 \cdot X_2 \\
&= \begin{bmatrix} 0 & 0 & -a\cos\theta \\ 0 & 0 & -a\sin\theta \\ 0 & 0 & 0 \end{bmatrix} \begin{bmatrix} \cos\theta \\ \sin\theta \\ 0 \end{bmatrix} - \begin{bmatrix} 0 & 0 & -\sin\theta \\ 0 & 0 & \cos\theta \\ 0 & 0 & 0 \end{bmatrix} \begin{bmatrix} -a\sin\theta \\ a\cos\theta \\ 1 \end{bmatrix} \\
&= \begin{bmatrix} \sin\theta \\ -\cos\theta \\ 0 \end{bmatrix}.
\end{aligned}
$$

If $[X_1, X_2] \in \mathcal{D}$, then there exist scalars α, β such that $[X_1, X_2] = \alpha X_1 + \beta X_2$, which in coordinates amounts to the matrix equation

$$
\begin{bmatrix} \cos\theta & -a\sin\theta \\ \sin\theta & a\cos\theta \\ 0 & 1 \end{bmatrix} \begin{bmatrix} \alpha \\ \beta \end{bmatrix} = \begin{bmatrix} \sin\theta \\ -\cos\theta \\ 0 \end{bmatrix},
$$

which has no solution. Therefore $[X_1, X_2] \notin \mathcal{D}$, and the constraint is nonholonomic according to the definition given in §2.2.

For Chaplygin control systems there is a natural Lie group action, $\Phi : G \times Q \to Q$ given by left multiplication in the group factor of Q. It is defined such that an element $h = (u, v, \phi) \in G$ acts on Q according to

$$
\Phi_h(r^1, \ldots, r^k, x, y, \theta) = (r^1, \ldots, r^k, u + x\cos\phi - y\sin\phi, v + x\sin\phi + y\cos\phi, \theta + \phi). \quad (20)
$$

In local coordinates, the derivative of the action is represented by the matrix

$$T_q\Phi_{(u,v,\phi)} = \left(\begin{array}{c|ccc} \mathbf{I}_{k\times k} & \multicolumn{3}{c}{\mathbf{0}_{k\times 3}} \\ \hline & \cos\phi & -\sin\phi & 0 \\ \mathbf{0}_{3\times k} & \sin\phi & \cos\phi & 0 \\ & 0 & 0 & 1 \end{array}\right). \tag{21}$$

It follows that if $\dot{q} = \dot{r}^i\frac{\partial}{\partial r^i} + \dot{x}\frac{\partial}{\partial x} + \dot{y}\frac{\partial}{\partial y} + \dot{\theta}\frac{\partial}{\partial\theta} \in T_qQ$, then

$$T_q\Phi_{(u,v,\phi)}\cdot\dot{q} = \dot{r}^i\frac{\partial}{\partial r^i} + (\dot{x}\cos\phi - \dot{y}\sin\phi)\frac{\partial}{\partial x} + (\dot{x}\sin\phi + \dot{y}\cos\phi)\frac{\partial}{\partial y} + \dot{\theta}\frac{\partial}{\partial\theta}. \tag{22}$$

In preparation for a subsequent use of Theorem 14, I now show that the constraint is symmetric with respect to the group action.

Lemma 13. *The action leaves the constraint 1-form ω invariant in the sense that $\Phi_h^*\omega = \omega$ for all $h \in G$.*

Proof. The constraint 1-form ω is invariant if $\Phi_h^*\omega = \omega$ for every $h \in G$. In local coordinates, write $h = (u, v, \phi)$, $q = (r^1, \ldots, r^k, x, y, \theta)$, and $X = \dot{r}^i\frac{\partial}{\partial r^i} + \dot{x}\frac{\partial}{\partial x} + \dot{y}\frac{\partial}{\partial y} + \dot{\theta}\frac{\partial}{\partial\theta}$. Then (17), (20), (22), and the addition formulas for sine and cosine give

$$\begin{aligned} \omega_{\Phi_h q}(T_q\Phi_h\cdot X_q) = & -\sin(\theta+\phi)(\dot{x}\cos\phi - \dot{y}\sin\phi) \\ & + \cos(\theta+\phi)(\dot{x}\sin\phi + \dot{y}\cos\phi) - a\dot{\theta} \\ = & -(\cos\theta\sin\phi + \sin\theta\cos\phi)(\dot{x}\cos\phi - \dot{y}\sin\phi) \\ & + (\cos\theta\cos\phi - \sin\theta\sin\phi)(\dot{x}\sin\phi + \dot{y}\cos\phi) - a\dot{\theta} \\ = & -\dot{x}\sin\theta + \dot{y}\cos\theta - a\dot{\theta} \\ = & \,\omega_q(X_q). \end{aligned}$$

□

It follows that the constraint distribution is *invariant* with respect to the action in the sense that $\mathcal{D}_{\Phi_g q} = T_q \Phi_g \cdot \mathcal{D}_q$ for every $q \in Q$ and every $g \in G$. Furthermore, in the particular examples that follow I will also verify that the Lagrangian is invarant under the tanent-lifted action in the sense of (9). Hence the Chaplygin control systems considered here exhibit both constraints and symmetry. To determine the dynamics of this class of systems, for each $q \in Q$ define

$$S_q \coloneqq T_q \mathcal{O}_q \cap \mathcal{D}_q, \tag{23}$$

and let $\mathfrak{g}^{\mathcal{D}}$ be the bundle over Q whose fiber through q comprises those Lie algebra elements $\xi \in \mathfrak{g}$ whose infinitesimal generators at q belong to S_q, i.e.

$$\mathfrak{g}^{\mathcal{D}} \coloneqq \{(q, \xi) \in Q \times \mathfrak{g} : q \in Q, \xi_Q(q) \in \mathcal{S}_q\}.$$

Define the *nonholonomic momentum map* $\mathbf{J}^{\mathrm{nh}} : TQ \to (\mathfrak{g}^{\mathcal{D}})^*$ such that for every section $q \mapsto \xi^q$ of the bundle $\mathfrak{g}^{\mathcal{D}}$,

$$\left\langle \mathbf{J}^{\mathrm{nh}}(v_q), \xi^q \right\rangle = \left\langle \mathbb{F}L(v_q), \xi_Q^q(q) \right\rangle. \tag{24}$$

The pairing on the left is the natural one between $(\mathfrak{g}^{\mathcal{D}})^*$ and $\mathfrak{g}^{\mathcal{D}}$, namely $\langle (q, \mu), (q, \xi) \rangle \coloneqq \mu(\xi)$, whereas the pairing on the right is the natural one between the cotangent bundle T^*Q and the tangent bundle TQ. This definition mirrors the one given in §2.2 for a system without constraints, but it is bundle-valued rather than Lie-algebra valued. The reason it cannot simply be Lie-algebra valued is that the Lie algebra elements whose infinitesimal generators are consistent with the constraints may vary from point

to point. The physical interpretation of $\mathbf{J}^{\mathrm{nh}}$ is that it gives the components of the ordinary momentum map $\mathbf{J}$ that satisfy the constraints. The following theorem appears in [8].

THEOREM 14. *If a Lie group G acts on a simple mechanical system (Q, g, L) endowed with a nonholonomic constraint distribution $\mathcal{D}$ such that the Lagrangian and constraint distribution are invariant, then any path $t \mapsto q(t) \in Q$ satisfying the Lagrange d'Alembert principle must, in addition to satisfying the given constraints, also satisfy*

$$\frac{d}{dt}\left\langle \mathbf{J}^{nh}(q(t),\dot{q}(t)), \xi^{q(t)} \right\rangle = \left\langle \mathbb{F}L(q(t),\dot{q}(t)), \left(\frac{d}{dt}\xi^q(t)\right)_Q \right\rangle \tag{25}$$

for every section $q \mapsto \xi^q$ of $\mathfrak{g}^{\mathcal{D}}$. Furthermore, if $\xi_Q(q(t)) \in \mathcal{D}_{q(t)}$ for all t, then

$$\frac{d}{dt}\left\langle \mathbf{J}^{nh}(q(t),\dot{q}(t)), \xi^{q(t)} \right\rangle = 0.$$

(Actually, the hypothesis of invariance may be weakened to infinitesimal invariance as discussed in [8], but this more general statement will not be needed in the sequel.) We refer to (25) as the *nonholonomic momentum equation*, or just the *momentum equation*. A key distinction between the ordinary momentum map and the nonholonomic momentum map is that while the former is conserved along Euler-Lagrange trajectories, the latter is generally *not* conserved. Indeed, according to the theorem the nonholonomic momentum map $\mathbf{J}^{\mathrm{nh}}$, rather than being conserved, evolves according to the momentum equation (25). It follows that *for systems with nonholonomic constraints, momentum is not necessarily conserved.*

I now compute (23) for the class of Chaplygin control systems. First, it may be

shown that the infinitesimal generator ξ_Q corresponding to a Lie algebra element $\xi \in \mathfrak{g}$ is

$$\xi_Q = (\xi^1 - y\xi^3)\frac{\partial}{\partial x} + (\xi^2 + x\xi^3)\frac{\partial}{\partial y} + \xi^3\frac{\partial}{\partial \theta}. \tag{26}$$

Now recall from Theorem 12 that the tangent space $T_q\,\mathcal{O}_q$ to the group orbit through $q \in Q$ is

$$T_q\,\mathcal{O}_q = \{\xi_Q(q) : \xi \in \mathfrak{g}\}.$$

To compute this explicitly, use linearity of the map $\xi \mapsto \xi_Q$, the fact that $\{(1,0,0),(0,1,0),(0,0,1)\}$ is a basis for $\mathfrak{g} \cong \mathbb{R}^3$, and (26) to obtain

$$\begin{aligned} T_q\,\mathcal{O}_q &= \mathrm{Span}\{(1,0,0)_Q,(0,1,0)_Q,(0,0,1)_Q\} \\ &= \mathrm{Span}\left\{\frac{\partial}{\partial x},\ \frac{\partial}{\partial y},\ -y\frac{\partial}{\partial x} + x\frac{\partial}{\partial y} + \frac{\partial}{\partial \theta}\right\} \\ &= \mathrm{Span}\left\{\frac{\partial}{\partial x}, \frac{\partial}{\partial y}, \frac{\partial}{\partial \theta}\right\}. \end{aligned} \tag{27}$$

It now follows from (18), (19), and (27) that

$$S_q = \mathcal{D}_q \cap T_q\,\mathcal{O}_q = \mathrm{Span}\{X_1, X_2\}.$$

Since for each $q \in Q$ the vectors $\{X_1(q), X_2(q)\}$ form a basis for S_q, there are two sections of $\mathfrak{g}^{\mathcal{D}}$, say $q \mapsto \zeta^q$ and $q \mapsto \eta^q$, such that for every $q \in Q$,

$$\begin{aligned} \zeta^q_Q(q) &= X_1(q), \\ \eta^q_Q(q) &= X_2(q). \end{aligned} \tag{28}$$

Finding these sections is a matter of linear algebra. Let $q = (r^1, \ldots, r^k, x, y, \theta)$ and

write $\zeta^q = (\zeta^1, \zeta^2, \zeta^3)$ and $\eta^q = (\eta^1, \eta^2, \eta^3)$. Then (28) becomes

$$(\zeta^1 - y\zeta^3)\frac{\partial}{\partial x} + (\zeta^2 + x\zeta^3)\frac{\partial}{\partial y} + \zeta^3\frac{\partial}{\partial \theta} = \cos\theta\frac{\partial}{\partial x} + \sin\theta\frac{\partial}{\partial y},$$
$$(\eta^1 - y\eta^3)\frac{\partial}{\partial x} + (\eta^2 + x\eta^3)\frac{\partial}{\partial y} + \eta^3\frac{\partial}{\partial \theta} = -a\sin\theta\frac{\partial}{\partial x} + a\cos\theta\frac{\partial}{\partial y} + \frac{\partial}{\partial \theta}.$$

Comparing like coefficients on each side of these equations leads to the two linear systems

$$\begin{bmatrix} 1 & 0 & -y \\ 0 & 1 & x \\ 0 & 0 & 1 \end{bmatrix} \begin{bmatrix} \zeta^1 \\ \zeta^2 \\ \zeta^3 \end{bmatrix} = \begin{bmatrix} \cos\theta \\ \sin\theta \\ 0 \end{bmatrix},$$

and

$$\begin{bmatrix} 1 & 0 & -y \\ 0 & 1 & x \\ 0 & 0 & 1 \end{bmatrix} \begin{bmatrix} \eta^1 \\ \eta^2 \\ \eta^3 \end{bmatrix} = \begin{bmatrix} -a\sin\theta \\ a\cos\theta \\ 1 \end{bmatrix}.$$

The solutions to these systems of equations are found to be

$$\zeta^q = (\cos\theta, \sin\theta, 0),$$

$$\eta^q = (y - a\sin\theta, -x + a\cos\theta, 1).$$

I now calculate some additional quantities that will be needed later when computing the nonholonomic momentum equations. First,

$$\frac{d\zeta^q}{dt} = (-\dot{\theta}\sin\theta, \dot{\theta}\cos\theta, 0),$$
$$\frac{d\eta^q}{dt} = (\dot{y} - a\dot{\theta}\cos\theta, -\dot{x} - a\dot{\theta}\sin\theta, 0).$$

It follows from (26) that

$$\begin{aligned}\left(\frac{d\zeta^q}{dt}\right)_Q &= -\dot\theta\sin\theta\frac{\partial}{\partial x}+\dot\theta\cos\theta\frac{\partial}{\partial y},\\ \left(\frac{d\eta^q}{dt}\right)_Q &= (\dot y-a\dot\theta\cos\theta)\frac{\partial}{\partial x}+(-\dot x-a\dot\theta\sin\theta)\frac{\partial}{\partial y}.\end{aligned} \tag{29}$$

Since $\mathfrak{g}^{\mathcal{D}}$ has two-dimensional fibers, there are two scalar components of the nonholonomic momentum map defined in (24). I denote these two components by J_ζ and J_η, chosen so that J_ζ corresponds with the section $q\mapsto\zeta^q$ and J_η corresponds to the section $q\mapsto\eta^q$. (In turn, these correspond to the forward and pivoting motions, respectively.) Then

$$\begin{aligned}J_\zeta(v_q) &\coloneqq \left\langle \mathbf{J}^{\mathrm{nh}}(v_q),\zeta_Q^q(q)\right\rangle = \left\langle \mathbb{F}L(v_q),\zeta_Q^q(q)\right\rangle,\\ J_\eta(v_q) &\coloneqq \left\langle \mathbf{J}^{\mathrm{nh}}(v_q),\eta_Q^q(q)\right\rangle = \left\langle \mathbb{F}L(v_q),\eta_Q^q(q)\right\rangle.\end{aligned} \tag{30}$$

Meanwhile, according to Theorem 14 the two sections $q\mapsto\zeta^q$ and $q\mapsto\eta^q$ induce the following two scalar evolution equations that are satisfied along trajectories of the system.

$$\begin{aligned}\frac{d}{dt}J_\zeta(v_{q(t)}) &= \left\langle \mathbb{F}L(v_{q(t)}),\left(\frac{d\zeta^{q(t)}}{dt}\right)_Q(q(t))\right\rangle,\\ \frac{d}{dt}J_\eta(v_{q(t)}) &= \left\langle \mathbb{F}L(v_{q(t)}),\left(\frac{d\eta^{q(t)}}{dt}\right)_Q(q(t))\right\rangle.\end{aligned} \tag{31}$$

The details of the nonholonomic momentum and its dynamics depend on the particular Lagrangian, and the remainder of this chapter is dedicated to the analysis of three specific examples in this class of systems.

4.3 The Chaplygin Sleigh

The Chaplygin sleigh is the degenerate case of a Chaplygin control system in which there are no internal degrees of freedom. The configuration space is merely $Q = G = SE(2)$. For $v_q \in TQ$, write $v_q = \dot{x}\frac{\partial}{\partial x} + \dot{y}\frac{\partial}{\partial y} + \dot{\theta}\frac{\partial}{\partial \theta}$. Then the Lagrangian $L : TQ \to \mathbb{R}$ is given by

$$L(v_q) = \frac{1}{2}M(\dot{x}^2 + \dot{y}^2) + \frac{1}{2}J\dot{\theta}^2, \tag{32}$$

which corresponds to the Riemannian metric g given in local coordinates by

$$g = \begin{pmatrix} M & 0 & 0 \\ 0 & M & 0 \\ 0 & 0 & J \end{pmatrix}.$$

From (5) the fiber derivative is given in local coordinates by

$$\begin{aligned} \mathbb{F}L &= g_{ij}\dot{q}^j \, \mathbf{d}q^i \\ &= M\dot{x} \, \mathbf{d}x + M\dot{y} \, \mathbf{d}y + J\dot{\theta} \, \mathbf{d}\theta. \end{aligned} \tag{33}$$

To see that the Lagrangian is invariant under the group action (20), begin by noting that (21) simplifies in this case to

$$T_q\Phi_g = \begin{pmatrix} \cos\phi & -\sin\phi & 0 \\ \sin\phi & \cos\phi & 0 \\ 0 & 0 & 1 \end{pmatrix}.$$

Hence if $v_q = \dot{x}\frac{\partial}{\partial x} + \dot{y}\frac{\partial}{\partial y} + \dot{\theta}\frac{\partial}{\partial \theta}$ and $h = (u, v, \phi) \in G$, then

$$T_q\Phi_h \cdot v_q = (\dot{x}\cos\phi - \dot{y}\sin\phi)\frac{\partial}{\partial x} + (\dot{x}\sin\phi + \dot{y}\cos\phi)\frac{\partial}{\partial y} + \dot{\theta}\frac{\partial}{\partial \theta}. \tag{34}$$

Since (32) depends only on $\dot{q}$, and since $T_q\Phi_h$ preserves $\dot{\theta}$, I need only check that the term $\dot{x}^2 + \dot{y}^2$ in the Lagrangian is preserved. To do so, note that $T_q\Phi_h$ maps $\dot{x} \mapsto \dot{x}\cos\phi - \dot{y}\sin\phi$, and it maps $\dot{y} \mapsto \dot{x}\sin\phi + \dot{y}\cos\phi$. Then

$$(\dot{x}\cos\phi - \dot{y}\sin\phi)^2 = \dot{x}^2\cos^2\phi - 2\dot{x}\dot{y}\cos\phi\sin\phi + \dot{y}^2\sin^2\phi,$$

$$(\dot{x}\sin\phi + \dot{y}\cos\phi)^2 = \dot{x}^2\sin^2\phi + 2\dot{x}\dot{y}\sin\phi\cos\phi + \dot{y}^2\cos^2\phi.$$

Adding these two equations gives

$$(\dot{x}\cos\phi - \dot{y}\sin\phi)^2 + (\dot{x}\sin\phi + \dot{y}\cos\phi)^2 = \dot{x}^2 + \dot{y}^2,$$

so the Lagrangian is invariant under the tangent-lifted action.

The scalar components J_ζ, J_η of the nonholonomic momentum map are given by (30),

$$\begin{aligned} J_\zeta(v_q) &= \left\langle \mathbb{F}L(v_q), \zeta_Q^q(q) \right\rangle \\ &= (M\dot{x}\,\mathbf{d}x + M\dot{y}\,\mathbf{d}y + J\dot{\theta}\,\mathbf{d}\theta)\left(\cos\theta\frac{\partial}{\partial x} + \sin\theta\frac{\partial}{\partial y}\right) \\ &= M(\dot{x}\cos\theta + \dot{y}\sin\theta), \end{aligned}$$

and

$$\begin{aligned} J_\eta(v_q) &= \left\langle \mathbb{F}L(v_q), \eta_Q^q(q) \right\rangle \\ &= (M\dot{x}\,\mathbf{d}x + M\dot{y}\,\mathbf{d}y + J\dot{\theta}\,\mathbf{d}\theta)\left(-a\sin\theta\frac{\partial}{\partial x} + a\cos\theta\frac{\partial}{\partial y} + \frac{\partial}{\partial\theta}\right) \\ &= M\dot{x}(-a\sin\theta) + M\dot{y}(a\cos\theta) + J\dot{\theta} \\ &= Ma(-\dot{x}\sin\theta + \dot{y}\cos\theta) + J\dot{\theta} \\ &= (J + Ma^2)\dot{\theta}, \end{aligned}$$

where the constraint (16) was used in the last step. Summarizing, the nonholonomic momenta for the Chaplygin sleigh are defined by

$$\begin{aligned} J_\zeta &= M(\dot{x}\cos\theta + \dot{y}\sin\theta), \\ J_\eta &= (J + Ma^2)\dot{\theta}. \end{aligned} \tag{35}$$

I now make the following observations. First, note that $J_\eta = (J + Ma^2)$ is simply the angular momentum of the system as it pivots about a vertical axis through the blade. Second, it follows by writing $J_\zeta = M(\dot{x}, \dot{y}) \cdot (\cos\theta, \sin\theta) = M(\dot{x}, \dot{y}) \cdot \mathbf{b}_1$ that J_ζ is the projection of the system's linear momentum along the sleigh's heading. Hence J_ζ and J_η may be interpreted as the components of the ordinary linear and angular momentum that are consistent with the constraints. (In subsequent and more complicated examples the physical interpretation of the components of the nonholonomic momentum map will not be quite so immediate.) Third it follows by taking norms that $||(\dot{x}, \dot{y})|| = \frac{|J_\zeta|}{M}$, and so $\frac{J_\zeta}{M}$ is the sleigh's translational speed — positive or negative according as to whether its translation motion is parallel or antiparallel to the blade.

There are two contributions to the system's motion — one due to translational motion and the other due to rotational motion. For pure translation, note that if at some instant the sleigh's heading and forward speed are θ and $\frac{J_\zeta}{M}$, then after a small time Δt has elapsed, the sleigh's position has changed by the amounts $\Delta x = (\frac{J_\zeta}{M}\cos\theta)\Delta t$ and $\Delta y = (\frac{J_\zeta}{M}\sin\theta)\Delta t$. For pure rotation, note that if the sleigh is rotating with angular velocity $\dot{\theta}$, then in a small time Δt the position has changed by the amounts $\Delta x = (-a\dot{\theta}\sin\theta)\Delta t$ and $\Delta y = (a\dot{\theta}\cos\theta)\Delta t$. Adding these contributions, dividing through by Δt, and taking the limit $\Delta t \to 0$ gives the *reconstruction equations*,

$$\begin{aligned} \dot{x} &= \frac{J_\zeta}{M}\cos\theta - \frac{aJ_\eta \sin\theta}{J + Ma^2}, \\ \dot{y} &= \frac{J_\zeta}{M}\sin\theta + \frac{aJ_\eta \cos\theta}{J + Ma^2}, \\ \dot{\theta} &= \frac{J_\eta}{J + Ma^2}, \end{aligned} \tag{36}$$

where the last equation is a consequence of (35). Once the momentum equations governing J_ζ and J_η have been solved, the reconstruction equations may be integrated to find the system trajectory in configuration space.

I turn now to a derivation of the nonholonomic momentum equations. Using (33)

and (29), the momentum equations (31) become

$$\begin{aligned}
\dot{J}_\zeta &= \left\langle \mathbb{F}L, \left(\tfrac{d\zeta^q}{dt}\right)_Q \right\rangle \\
&= (M\dot{x}\,\mathbf{d}x + M\dot{y}\,\mathbf{d}y + J\dot{\theta}\,\mathbf{d}\theta)\left(-\dot{\theta}\sin\theta\frac{\partial}{\partial x} + \dot{\theta}\cos\theta\frac{\partial}{\partial y}\right) \\
&= M\dot{x}(-\dot{\theta}\sin\theta) + M\dot{y}(\dot{\theta}\cos\theta) \\
&= M\dot{\theta}(-\dot{x}\sin\theta + \dot{y}\cos\theta) \\
&= Ma\dot{\theta}^2 \\
&= \frac{MaJ_\eta^2}{(J+ma^2)^2},
\end{aligned}$$

on account of (16) and (35). Meanwhile,

$$\begin{aligned}
\dot{J}_\eta &= \left\langle \mathbb{F}L, \left(\tfrac{d\eta^q}{dt}\right)_Q \right\rangle \\
&= (M\dot{x}\,\mathbf{d}x + M\dot{y}\,\mathbf{d}y + J\dot{\theta}\,\mathbf{d}\theta)\left((\dot{y} - a\dot{\theta}\cos\theta)\frac{\partial}{\partial x} + (-\dot{x} - a\dot{\theta}\sin\theta)\frac{\partial}{\partial y}\right) \\
&= M\dot{x}(\dot{y} - a\dot{\theta}\cos\theta) + M\dot{y}(-\dot{x} - a\dot{\theta}\sin\theta) \\
&= -Ma\dot{\theta}(\dot{x}\cos\theta + \dot{y}\sin\theta) \\
&= -aJ_\zeta\dot{\theta} \\
&= \frac{-aJ_\zeta J_\eta}{J+Ma^2},
\end{aligned}$$

by using (35). Summarizing, the nonholonomic momenta evolve according to the following coupled, nonlinear system of equations.

$$\begin{aligned}
\dot{J}_\zeta &= \frac{MaJ_\eta^2}{(J+Ma^2)^2}, \\
\dot{J}_\eta &= \frac{-aJ_\zeta J_\eta}{J+Ma^2}.
\end{aligned} \tag{37}$$

These are the same nonholonomic momentum equations for the Chaplygin sleigh

that appear in [21], despite the fact that the configuration variables in that paper are defined somewhat differently, thus emphasizing the intrinsic nature of the momentum equations.

I now make a few remarks on the dynamics of the Chaplygin sleigh. In the balanced case ($a = 0$), the momentum equations (37) yield $\dot{J}_\zeta = \dot{J}_\eta = 0$, so that both nonholonomic linear momentum and nonholonomic angular momentum are conserved. In the unbalanced case however, this is not so. Indeed, when $a \neq 0$ the system (37) has a one-dimensional manifold of equilibria, namely the line $J_\eta = 0$. These equilibria correspond to the straight-line motions where the sleigh is not rotating but is translating along the line parallel to the blade with speed $\frac{J_\zeta}{M}$. Generically, however, $J_\eta \neq 0$, in which case neither linear nor angular momenta are conserved. The phase portrait in the J_ζ-J_η plane, shown in Figure 6, is foliated by heteroclinic connections described by elliptic arcs joining the unstable fixed points along the negative J_ζ axis and the stable fixed points situated along the positive J_ζ axis.

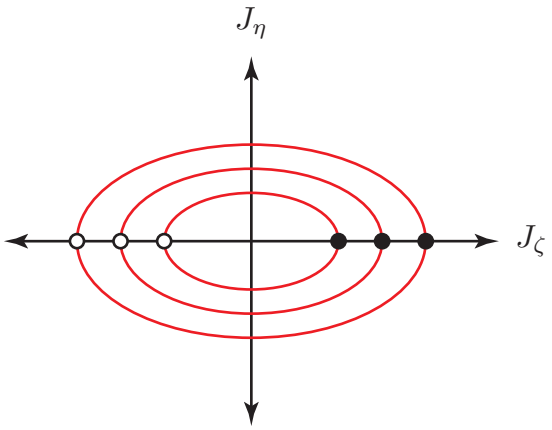

Figure 6: The phase portrait for the nonholonomic momenta J_ζ, J_η of the Chaplygin sleigh, a degenerate Chaplygin control system.

Furthermore, note that $\dot{J}_\zeta \geq 0$, so that even if $J_\zeta = 0$ initially, so long as $J_\eta \neq 0$

then $J_\zeta > 0$ after a small time. This means that in the unbalanced case, a pivoting motion of the sleigh about its blade directly induces a component of linear motion along the blade. This phenomenon is called *locomotion generation*, and it will be exploited in the sequel.

The dynamics of a Chaplygin sleigh with a typical set of parameters and initial conditions is shown in Figure 7. The corresonding trajectory of the blade's contact point is shown in Figure 8.

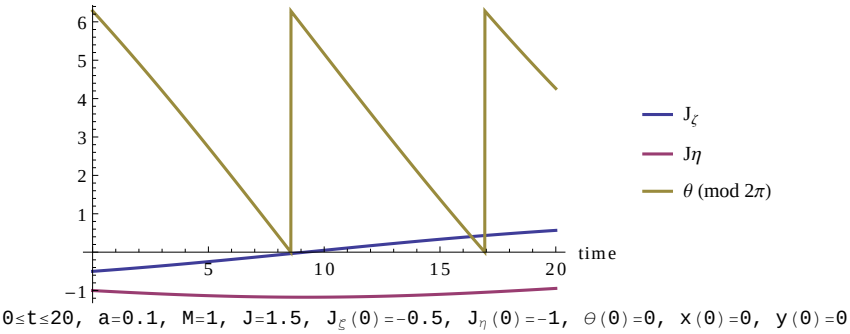

Figure 7: Dynamics of the Chaplygin sleigh for a typical set of parameters and initial conditions.

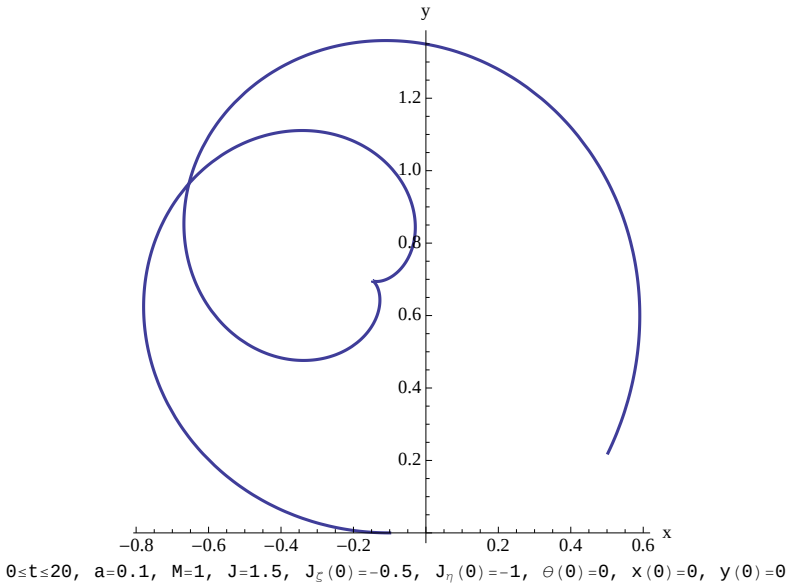

Figure 8: The trajectory of the blade's contact point for the Chaplygin sleigh in Figure 7.

4.4 The Chaplygin Beanie

I now introduce the *Chaplygin beanie* as a nontrivial Chaplygin control system that synthesizes the Chaplygin sleigh and Elroy's beanie.[4] The system is depicted in Figure 9. Elroy's beanie, discussed in Appendix A, is a simple mechanical system comprising two planar rigid bodies pinned together and free to rotate about their common joint by exertion of an internal torque, and it is perhaps the simplest system that exhibits the phenomena of geometric phase discussed in §2.2 — whereby a change in the internal shape of a system results in a net reorientation in the ambient environment in a manner that is independent of time parameterization.

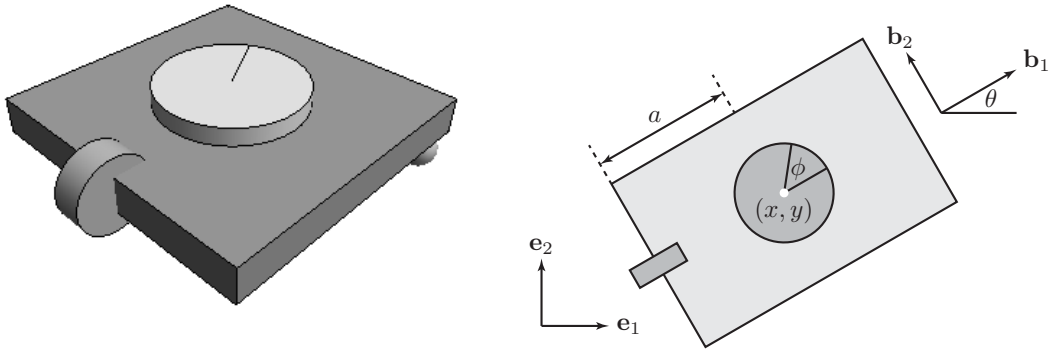

Figure 9: The *Chaplygin beanie* is depicted at left, and a top view showing the model parameters is shown at right.

Referring to Figure 9, the Chaplygin beanie is constructed by affixing a momentum wheel — also called the beanie — to the center of mass of the Chaplygin sleigh. Let m denote the beanie's mass and let B denote its moment of inertia about a vertical axis through its center. The configuration space of the resulting system is the product $Q = M \times G$, where $M = S^1$ and $G = SE(2)$, with coordinates (ϕ, x, y, θ). Here ϕ

[4]This resulting system might also have been called *Elroy's sleigh*, but as Elroy is a fictional character whereas Chaplygin is not, I give deference to the latter.

denotes the angle a fixed line in the momentum wheel makes with $\mathbf{b}_1$. The kinetic energy of the sleigh is $\frac{1}{2}M(\dot{x}^2+\dot{y}^2)+\frac{1}{2}J\dot{\theta}^2$ and that of the momentum wheel is $\frac{1}{2}m(\dot{x}^2+\dot{y}^2)+\frac{1}{2}B(\dot{\theta}+\dot{\phi})^2$. The Lagrangian $L:TQ\to\mathbb{R}$ is the total kinetic energy,

$$\begin{aligned} L &= \frac{1}{2}(M+m)(\dot{x}^2+\dot{y}^2)+\frac{1}{2}J\dot{\theta}^2+\frac{1}{2}B(\dot{\theta}+\dot{\phi})^2 \\ &= \frac{1}{2}(M+m)(\dot{x}^2+\dot{y}^2)+\frac{1}{2}(J+B)\dot{\theta}^2+B\dot{\theta}\dot{\phi}+\frac{1}{2}B\dot{\phi}^2. \end{aligned} \tag{38}$$

This corresponds to the nondiagonal Riemannian metric

$$g=\begin{pmatrix} B & 0 & 0 & B \\ 0 & M+m & 0 & 0 \\ 0 & 0 & M+m & 0 \\ B & 0 & 0 & J+B \end{pmatrix}.$$

By (21), the tangent lift of the group action leaves $\dot{\theta}$ and $\dot{\phi}$ unchanged, so to verify invariance of the Lagrangian I need only check that $\frac{1}{2}(M+m)(\dot{x}^2+\dot{y}^2)$ is invariant. The calculation is much the same as was given for the Chaplygin sleigh and is omitted. The fiber derivative is

$$\begin{aligned} \mathbb{F}L &= g_{ij}\dot{q}^j\,\mathbf{d}q^i \\ &= B(\dot{\theta}+\dot{\phi})\,\mathbf{d}\phi+(M+m)\dot{x}\,\mathbf{d}x+(M+m)\dot{y}\,\mathbf{d}y+[(J+B)\dot{\theta}+B\dot{\phi}]\,\mathbf{d}\theta. \end{aligned}$$

The nonholonomic momenta (30) are

$$\begin{aligned} J_\zeta &= \left\langle \mathbb{F}L, \zeta_Q^q \right\rangle \\ &= (M+m)\dot{x}(\cos\theta)+(M+m)\dot{y}(\sin\theta) \\ &= (M+m)(\dot{x}\cos\theta+\dot{y}\sin\theta), \end{aligned}$$

and

$$\begin{aligned} J_\eta &= \left\langle \mathbb{F}L, \eta_Q^q \right\rangle \\ &= (M+m)\dot{x}(-a\sin\theta) + (M+m)\dot{y}(a\cos\theta) + (J+B)\dot{\theta} + B\dot{\phi} \\ &= (M+m)a(-\dot{x}\sin\theta + \dot{y}\cos\theta) + (J+B)\dot{\theta} + B\dot{\phi} \\ &= (M+m)a^2\dot{\theta} + (J+B)\dot{\theta} + B\dot{\phi} \\ &= (J+B+(M+m)a^2)\dot{\theta} + B\dot{\phi}, \end{aligned}$$

where in the penultimate equality the constraint (16) was used.

As in the Chaplygin sleigh, note that $J_\zeta = (M+m)(\dot{x},\dot{y})\cdot\mathbf{b}_1$ is the projection of the system's linear momentum along the sleigh's heading $\mathbf{b}_1$, and that $\frac{J_\zeta}{M+m}$ gives the translational speed of the system. Similarly, J_η encodes angular momentum of the system. By the same argument as given for the sleigh, the reconstruction equations for the Chaplygin beanie take the form

$$\begin{aligned} \dot{x} &= \frac{J_\zeta}{M+m}\cos\theta - \frac{a(J_\eta - B\dot{\phi})\sin\theta}{J+B+(M+m)a^2}, \\ \dot{y} &= \frac{J_\zeta}{M+m}\sin\theta + \frac{a(J_\eta - B\dot{\phi})\cos\theta}{J+B+(M+m)a^2}, \\ \dot{\theta} &= \frac{J_\eta - B\dot{\phi}}{J+B+(M+m)a^2}. \end{aligned} \tag{39}$$

Once the nonholonomic momentum equations have been solved, the reconstruction equations may be integrated to yield the evolution of the group variables of the

Chaplygin beanie. The nonholonomic momentum equations (31) are

$$\begin{aligned}
\dot{J}_\zeta &= \left\langle \mathbb{F}L, \left(\tfrac{d\zeta^q}{dt}\right)_Q \right\rangle \\
&= (M+m)\dot{x}(-\dot{\theta}\sin\theta) + (M+m)\dot{y}(\dot{\theta}\cos\theta) \\
&= (M+m)\dot{\theta}(-\dot{x}\sin\theta + \dot{y}\cos\theta) \\
&= (M+m)a\dot{\theta}^2 \\
&= \frac{(M+m)a}{(J+B+(M+m)a^2)^2}(J_\eta - B\dot{\phi})^2
\end{aligned}$$

and

$$\begin{aligned}
\dot{J}_\eta &= \left\langle \mathbb{F}L, \left(\tfrac{d\eta^q}{dt}\right)_Q \right\rangle \\
&= (M+m)\dot{x}(\dot{y} - a\dot{\theta}\cos\theta) + (M+m)\dot{y}(-\dot{x} - a\dot{\theta}\sin\theta) \\
&= -a\dot{\theta}(M+m)(\dot{x}\cos\theta + \dot{y}\sin\theta) \\
&= -a\dot{\theta}J_\zeta \\
&= \frac{-aJ_\zeta}{J+B+(M+m)a^2}(J_\eta - B\dot{\phi})
\end{aligned}$$

Summarizing, the nonholonomic equations of motion for the Chaplygin beanie are given by

$$\begin{aligned}
\dot{J}_\zeta &= \frac{(M+m)a}{(J+B+(M+m)a^2)^2}(J_\eta - B\dot{\phi})^2, \\
\dot{J}_\eta &= \frac{-aJ_\zeta}{J+B+(M+m)a^2}(J_\eta - B\dot{\phi}).
\end{aligned} \tag{40}$$

These equations, together with (39) and a control law for the momentum wheel, comprise the equations of motion for the system in momentum form. Note that if $m = B = 0$ then the Lagrangian, the nonholonomic momenta, and the nonholonomic

momentum equations each simplify to recover the corresponding quantities for the Chaplygin sleigh, thus providing a check of the computations above.

Before turning to control of the Chaplygin beanie, I consider its unforced dynamics, whereby the momentum wheel is rotating about its center with a constant angular velocity. To highlight differences between the unforced Chaplygin beanie and the Chaplygin sleigh that are attributed to the system dynamics rather than the choice of parameters or initial conditions, I consider an example of the former with exactly the same base parameters as given for the Chaplygin sleigh in Figure 8. After adjoining to these base parameters a typical choice for the mass m, moment of inertia B, and constant angular velocity $\dot{\phi} \coloneqq \alpha$ of the momentum wheel, the resulting trajectory of the blade's contact point for the unforced system is shown in Figure 10. Notice that the trajectory is qualitatively the same as for the Chaplygin sleigh in Figure 8, but the system executes its reversal (i.e. reaches the cusp in its trajectory) faster than the sleigh. The trajectory in the J_ζ-J_η plane for the unforced beanie is shown in Figure 11; note the resemblance to a portion of one of the heteroclinic connections of the Chaplygin sleigh from Figure 6.

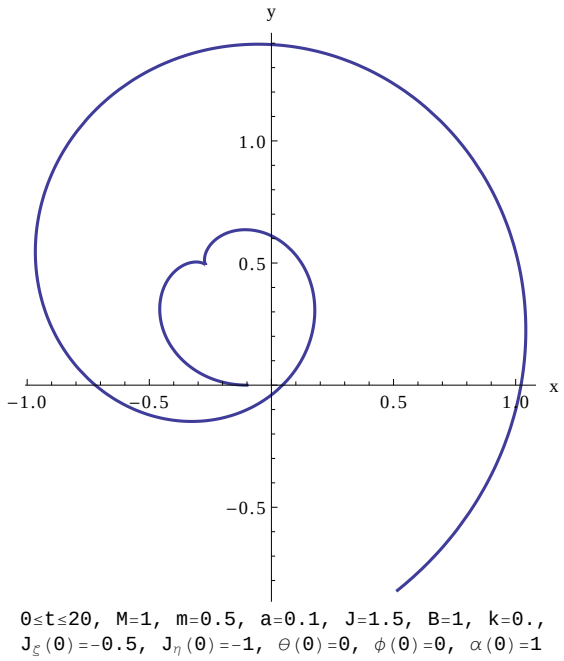

Figure 10: Trajectory of the blade's contact point for the unforced Chaplygin beanie. The parameters and initial conditions for the underlying sleigh are the same as those appearing in Figure 8.

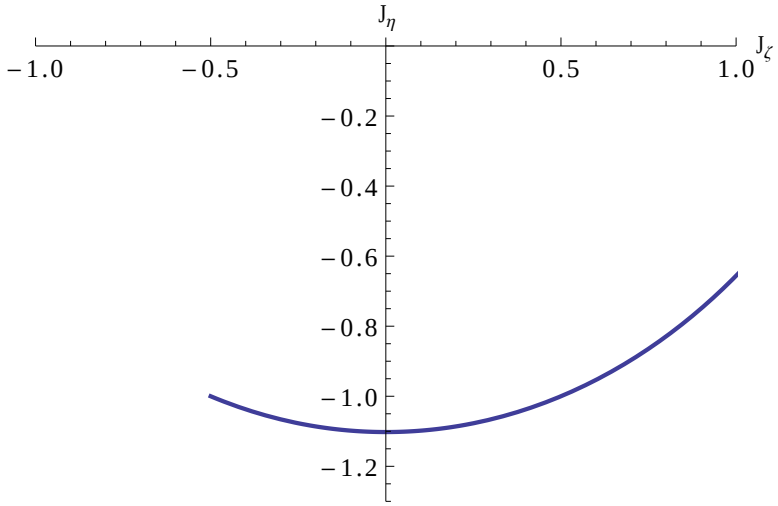

Figure 11: The trajectory in nonholonomic momentum space for the unforced Chaplygin beanie of Figure 10.

I now turn to control of the Chaplygin beanie. The objective is to steer the system — at least asymptotically — along a specified heading and with a specified speed.

To do so, I assume that a control torque may be applied to the momentum wheel. Without loss of generality, choose the inertial coordinate system so that the target heading is $\theta = 0$. Since there are two demands — heading and speed — in the presence of a single control parameter, this is a form of underactuated control. If the momentum wheel is given an impulsive counterclockwise rotation with $\ddot{\phi} > 0$, then the sleigh will tend to rotate clockwise, and vice versa. By analogy with a mass-spring system, I therefore suggest the feedback control law that the applied torque is proportional to the error in the heading, i.e.

$$\ddot{\phi} = k\theta, \tag{41}$$

for a tunable gain constant k. I demand $k > 0$ so that the system corrects, rather than reinforces, an error in heading. I will prove that every choice of gain $k > 0$ causes the system to asymptotically limit on the desired heading. I also prove that given any target speed greater than a particular value (depending on initial conditions), there is a gain k such that the target speed is approached asymptotically from below.

To begin the analysis, make the change of variables

$$u \coloneqq J_\zeta, \quad v \coloneqq J_\eta - B\dot{\phi}, \quad w \coloneqq \theta$$

and define the nonzero constants

$$\begin{aligned} C_1 &\coloneqq \frac{(M+m)a}{(J+B+(M+m)a^2)^2}, \\ C_2 &\coloneqq \frac{-a}{J+B+(M+m)a^2}, \\ C_3 &\coloneqq \frac{1}{J+B+(M+m)a^2}. \end{aligned} \tag{42}$$

Note that $C_1, C_3 > 0$ and $C_2 < 0$. Then equations (39), (40), and (41) become

$$\begin{aligned} \dot{u} &= C_1 v^2, \\ \dot{v} &= C_2 uv - Bkw, \\ \dot{w} &= C_3 v. \end{aligned} \tag{43}$$

together with the equations

$$\begin{aligned} \dot{\phi} &= \alpha, \\ \dot{\alpha} &= kw. \end{aligned} \tag{44}$$

governing control of the momentum wheel. With the equations of motion in this form, I can make some immediate observations. First, $\dot{u} = C_1 v^2 \geq 0$ implies u is monotonically increasing. Because J_ζ is the projection of the linear momentum along the sleigh's heading, the translational speed of the system is monotonically increasing. Therefore, the Chaplygin beanie has *drift* in the sense that a cessation of the beanie's actuation does not result in a cessation of the sleigh's motion through its environment. Furthermore, like the Chaplygin sleigh, any actuation of the momentum wheel imparts forward momentum to the system, even from rest. Indeed, $\dot{w} \neq 0$ implies $v \neq 0$, which then implies $\dot{u} = \dot{J}_\zeta > 0$. Finally, the system (43) has a one-dimensional manifold of equilibria, namely the u-axis $\{(u, v, w) : v = w = 0\}$, and the fixed points on this axis correspond to uniform motion along a straight line in the desired heading.

I am going to use the LaSalle invariance principle, stated below, to establish some facts about the controller. (This theorem is found on page 93 of [13].)

THEOREM 15 (LaSalle Invariance Principle). *Suppose that the differential equation* $\dot{x} = f(x)$ *with flow* ϕ_t *has a compact invariant set* K*, and* $V : K \to \mathbb{R}$ *is a* C^1

function such that $\dot{V}(x) \leq 0$ *for all* $x \in K$. *If* Ω *is the largest invariant set in* $\{x \in K : \dot{V}(x) = 0\}$, *then every solution in* K *approaches* Ω *as* $t \to \infty$.

THEOREM 16. *Assume the initial condition* $x_0 = (u_0, v_0, w_0) \in \mathbb{R}^3$ *is not a fixed point of* (43). *Then for any* $k > 0$, *the forward orbit of the trajectory through* x_0 *limits on the point* $(u_*, 0, 0)$, *where*

$$u_* = \sqrt{u_0^2 + (M+m)\left(\frac{v_0^2}{J + B + (M+m)a^2} + Bkw_0^2\right)}.$$

Equivalently, as $t \to \infty$ *then*

$$J_\zeta \to u_*, \quad J_\eta \to B\dot{\phi}, \quad \theta \to 0.$$

On the other hand, given any real number $J_\zeta^\infty > \sqrt{u_0^2 + \frac{(M+m)v_0^2}{J+B+(M+m)a^2}}$, *it may be arranged that* $\lim_{t\to\infty} J_\zeta(t) = J_\zeta^\infty$ *by choosing*

$$k = \frac{1}{Bw_0^2}\left(\frac{(J_\zeta^\infty)^2 - u_0^2}{M+m} - \frac{v_0^2}{J + B + (M+m)a^2}\right).$$

Proof. To use LaSasalle's theorem, I begin by seeking a first integral of the motion, because the level sets of a first integral are invariant sets. A first integral of (43) is a scalar-valued function $G : \mathbb{R}^3 \to \mathbb{R}$ whose orbital derivative $\frac{d}{dt}G(\phi_t(q))$ vanishes. Here $\phi_t : Q \to Q$ denotes the time-t flow of the system. Consider the trial function

$$G(u, v, w) = \frac{1}{2}(\lambda_1 u^2 + \lambda_2 v^2 + \lambda_3 w^2)$$

for some unknown constants $\lambda_1, \lambda_2, \lambda_3$. The chain rule gives

$$\begin{aligned} DG \cdot (\dot{u}, \dot{v}, \dot{w}) &= \left(\frac{\partial G}{\partial u}, \frac{\partial G}{\partial v}, \frac{\partial G}{\partial w} \right) \cdot (C_1 v^2, C_2 uv - Bkw, C_3 v) \\ &= C_1 v^2 \frac{\partial G}{\partial u} + (C_2 uv - Bkw) \frac{\partial G}{\partial v} + C_3 v \frac{\partial G}{\partial w} \\ &= (\lambda_1 C_1 + \lambda_2 C_2) uv^2 + (\lambda_3 C_3 - \lambda_2 Bk) vw. \end{aligned}$$

It follows that if $\lambda_1, \lambda_2, \lambda_3$ are chosen to satisfy the system

$$\lambda_1 C_1 + \lambda_2 C_2 = 0,$$

$$\lambda_3 C_3 - \lambda_2 Bk = 0,$$

then G will be a first integral of (43). There are three degrees of freedom and only two equations, so I make an arbitrary choice by setting $\lambda_1 = \frac{1}{M+m}$ in order that G has units of energy. Solving this system by hand, and using (42), it follows that $\lambda_2 = \frac{-C_1}{(M+m)C_2} = C_3$, and $\lambda_3 = \frac{\lambda_2 Bk}{C_3} = Bk$. Therefore, the function

$$G(u, v, w) \coloneqq \frac{1}{2} \left(\frac{1}{M+m} u^2 + C_3 v^2 + Bkw^2 \right) \tag{45}$$

is a first integral. Note that since $\frac{1}{M+m}, C_3$, and Bk are all positive, the level sets of (45) are compact invariant ellipsoids centered at the origin in (u, v, w) space. These ellipsoids foliate all of $\mathbb{R}^3$.

Since the level sets of G foliate all of $\mathbb{R}^3$, the initial condition $(u_0, v_0, w_0) \in \mathbb{R}^3$ lies on one of these level sets K, namely

$$K \coloneqq \{(u, v, w) \in \mathbb{R}^3 : G(u, v, w) = G(u_0, v_0, w_0)\}.$$

It was already observed that this is a compact invariant set for the flow. Define

$V : K \to \mathbb{R} : (u, v, w) \mapsto -u$. Then

$$\dot{V} = -\dot{u} = -C_1 v^2 \leq 0,$$

so $\dot{V} = 0$ exactly when $v = 0$. Therefore, $\{x \in K : \dot{V} = 0\} = K \cap \{v = 0\}$, which is the equator of the ellipse K shown in Figure 12. The hypotheses of LaSalle's invariance principle hold, so the forward orbit limits on the largest invariant set Ω inside this equator. I claim that $\Omega = \{(\pm(u_*, 0, 0)\}$, where u_* is given in the statement of the theorem.

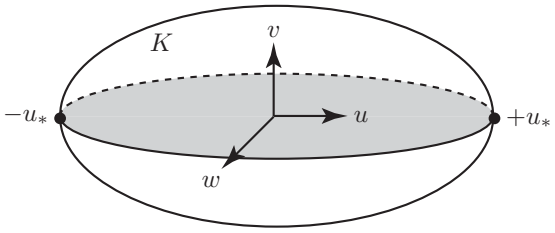

Figure 12: The initial condition (u_0, v_0, w_0) determines the level set $K = \{G(u, v, w) = G(u_0, v_0, w_0)\}$ of the first integral G, defined in (45). This level set is a compact invariant ellipsoid.

To prove this, consider an arbitrary point $p = (u, 0, w)$ on the equator. Then $(\dot{u}, \dot{v}, \dot{w})|_p = (0, -Bkw, 0)$, which is transverse to the equator (and hence not part Ω) unless $w = 0$. It follows that the only points in Ω are the antipodal fixed points $(\pm u_*, 0, 0)$ in $K \cap \{v = 0\}$, where u_* is determined from initial conditions according to $G(u_*, 0, 0) = G(u_0, v_0, w_0)$. Using (45), this is

$$\frac{1}{2}\left(\frac{u_*^2}{M+m}\right) = \frac{1}{2}\left(\frac{1}{M+m}u_0^2 + C_3 v_0^2 + Bkw_0^2\right),$$

which by using (42) may be rearranged to yield

$$\begin{aligned} u_* &= \pm\sqrt{u_0^2 + (M+m)(C_3 v_0^2 + Bkw_0^2)} \\ &= \pm\sqrt{u_0^2 + (M+m)\left(\frac{v_0^2}{J+B+(M+m)a^2} + Bkw_0^2\right)}. \end{aligned}$$

The negative branch of this square root may be ruled out as follows. First, by assumption the initial condition (u_0, v_0, w_0) was not the fixed point $(-u_*, 0, 0)$, and so $u_0 > -u_*$. Second, $\dot{u} \geq 0$, so u is monotonically increasing, so $u(t) \geq u_0 > -u_*$ for all time t, so the forward orbit cannot limit on $(-u_*, 0, 0)$. This proves the first part of the theorem.

To prove the second statement of the theorem, set $u_* = J_\zeta^\infty$ into the formula for u_* and solve for k to obtain

$$k = \frac{1}{Bw_0^2}\left(\frac{(J_\zeta^\infty)^2 - u_0^2}{M+m} - \frac{v_0^2}{J+B+(M+m)a^2}\right).$$

This is positive — and hence the first statement of the theorem applies — provided

$$J_\zeta^\infty > \sqrt{u_0^2 + \frac{(M+m)v_0^2}{J+B+(M+m)a^2}},$$

which is true by assumption. This completes the proof. □

The effectiveness of the controller and the details of the preceding theorem will now be verified numerically for two different configurations — one system initially at rest, and another not. Figure 13 depicts the dynamics of a Chaplygin beanie that begins from rest at the origin but which has an initial heading error, in the sense its initial heading is $\theta_0 = 1$, which is not the target heading of zero. With the model parameters and initial conditions shown in the figure, and for the (arbitrary) choice

of asymptotic speed $\lim_{t\to\infty} u(t) = J_\zeta^\infty = \pi$, Theorem 16 implies that if the gain k is set to $\frac{\pi^2}{3} \approx 3.28987$, then $\lim_{t\to\infty} J_\zeta = \pi$. This is numerically verified in the figure. Snapshots of the system at equally spaced times along its trajectory, reconstructed by using (39), are shown in Figure 14.

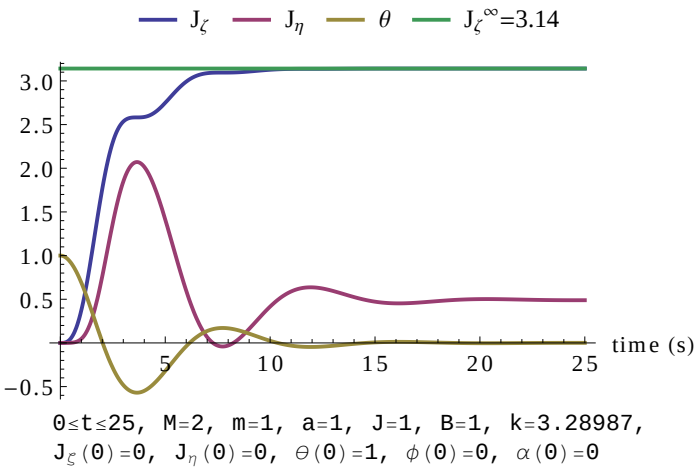

Figure 13: Dynamics of the controlled Chaplygin beanie starting from rest, verifying Theorem 16.

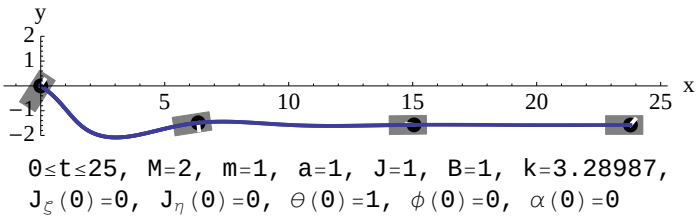

Figure 14: Snapshots at equally spaced times of the controlled Chaplygin beanie characterized in Figure 13.

Now consider a Chaplygin beanie that has nonzero initial momentum. With the (arbitrary) choice of gain $k = 1$, and with the parameters and initial conditions shown in Figure 15, Theorem 16 guarantees that $J_\zeta^\infty = \sqrt{23/5} \approx 2.14$, which is numerically verified in the figure. Snapshots of the system at equally spaced times are shown

in Figure 16, where as before the trajectory was reconstructed from the momentum dynamics by (39).

Finally, the effect of gain constant k is shown in Figure 17. As might be expected, a larger gain increases both the asymptotic speed and the rapidity at which the oscillations about the target heading quiesce.

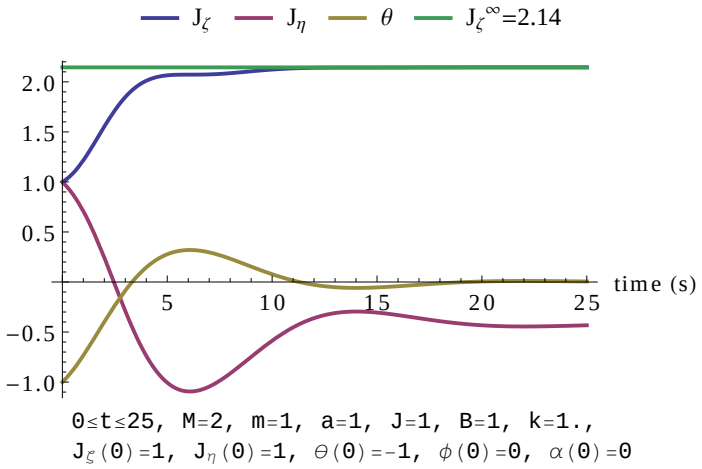

Figure 15: Dynamics of a controlled Chaplygin beanie with nonzero initial momentum, verifying Theorem 16.

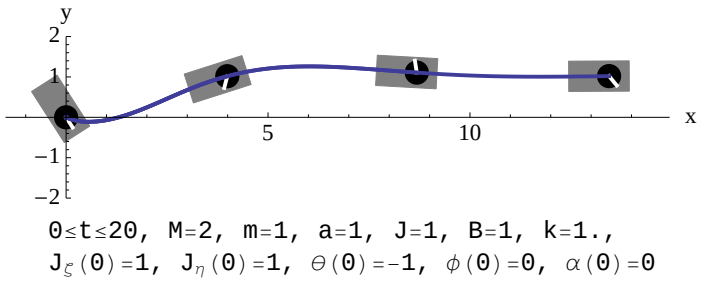

Figure 16: Snapshots at equally spaced times of the controlled Chaplygin beanie characterized in Figure 15.

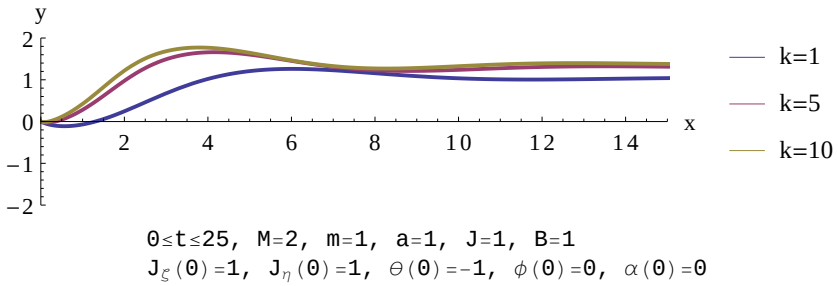

Figure 17: Trajectories of the controlled Chaplygin beanie with various choices of gain k, truncated to the interval $0 \leq x \leq 15$.

4.5 The Chaplygin Pendulum

I now consider another nontrivial Chaplygin control system, the *Chaplygin pendulum*, obtained by combining the Chaplygin sleigh and the inverted pendulum on a cart. This system is shown in Figure 18. The inertial and body coordinate systems, as well as the parameters M, J, and a, are defined as in the Chaplygin sleigh. I simplify matters somewhat by modeling the pendulum as a bob of mass m that slides along a fixed line segment in the sleigh, situated perpendicular to the blade. The distance between this line segment and the sleigh's center of mass is denoted b.

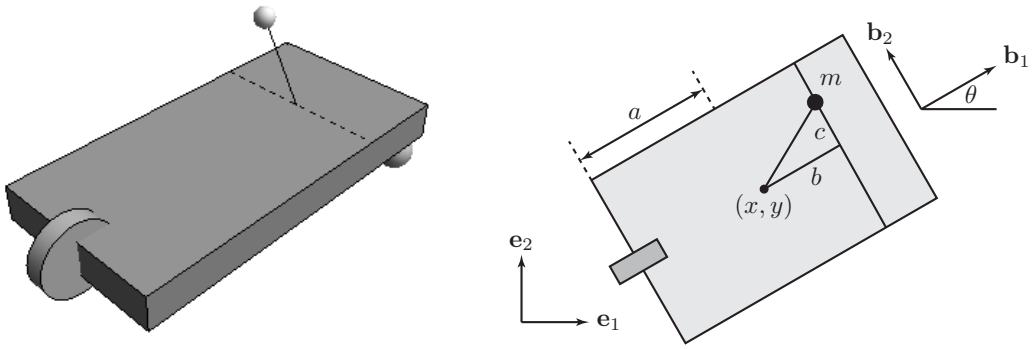

Figure 18: The left panel depicts the *Chaplygin pendulum*. The right panel is a top view showing the model parameters.

The configuration space for the system is $Q = \mathbb{R}\times SE(2)$ with coordinates (c, x, y, θ). It follows from the geometry of Figure 18 that the control mass has position $(x, y) + b\mathbf{b}_1 + c\mathbf{b}_2$. Therefore, the coordinates (x_m, y_m) of the mass are

$$\begin{aligned} x_m &= x + b\cos\theta - c\sin\theta, \\ y_m &= y + b\sin\theta + c\cos\theta. \end{aligned} \tag{46}$$

The Lagrangian $L : TQ \to \mathbb{R}$ is simply the total kinetic energy,

$$L = \frac{1}{2}M(\dot{x}^2 + \dot{y}^2) + \frac{1}{2}J\dot{\theta}^2 + \frac{1}{2}m(\dot{x}_m^2 + \dot{y}_m^2).$$

Using (46) to expand $\dot{x}_m^2$ and $\dot{y}_m^2$ gives

$$\begin{aligned} L =& \frac{1}{2}M(\dot{x}^2 + \dot{y}^2) + \frac{1}{2}J\dot{\theta}^2 \\ &+ \frac{1}{2}m\big[(\dot{x} - b\dot{\theta}\sin\theta - \dot{c}\sin\theta - c\dot{\theta}\cos\theta)^2 + (\dot{y} + b\dot{\theta}\cos\theta + \dot{c}\cos\theta - c\dot{\theta}\sin\theta)^2\big]. \end{aligned} \tag{47}$$

To verify the Lagrangian is invariant under the tangent-lifted action, one must check that it is unchanged under the following substitutions:

$$\begin{aligned} x &\mapsto u + x\cos\phi - y\sin\phi, & \dot{x} &\mapsto \dot{x}\cos\phi - \dot{y}\sin\phi, \\ y &\mapsto v + x\sin\phi + y\cos\phi, & \dot{y} &\mapsto \dot{x}\sin\phi + \dot{y}\cos\phi, \\ \theta &\mapsto \theta + \phi, & \dot{\theta} &\mapsto \dot{\theta}. \end{aligned}$$

This is a tedious computation best suited for a computer algebra system; it was straightforward to verify this result with Mathematica, which I also used to compute

the fiber derivative

$$\mathbb{F}L = p_c\,\mathbf{d}c + p_x\,\mathbf{d}x + p_y\,\mathbf{d}y + p_\theta\,\mathbf{d}\theta,$$

where

$$p_c = m(\dot{c} - \dot{x}\sin\theta + \dot{y}\cos\theta + b\dot{\theta}),$$

$$p_x = -m\dot{c}\sin\theta + (M+m)\dot{x} - m\dot{\theta}(c\cos\theta + b\sin\theta),$$

$$p_y = m\dot{c}\cos\theta + (M+m)\dot{y} + m\dot{\theta}(b\cos\theta - c\sin\theta),$$

$$p_\theta = m\left(b\dot{c} - \dot{x}(c\cos\theta + b\sin\theta) + \dot{y}(b\cos\theta - c\sin\theta)\right) + (J + m(b^2+c^2))\dot{\theta}.$$

By computations similar to those given for the Chaplygin beanie, the nonholonomic momenta (30) are found to be

$$\begin{aligned} J_\zeta &= \left\langle \mathbb{F}L, \zeta_Q^q \right\rangle \\ &= (p_c\,\mathbf{d}c + p_x\,\mathbf{d}x + p_y\,\mathbf{d}y + p_\theta\,\mathbf{d}\theta)\left(\cos\theta\frac{\partial}{\partial x} + \sin\theta\frac{\partial}{\partial y}\right) \\ &= p_x\cos\theta + p_y\sin\theta \\ &= [(M+m)\cos\theta]\dot{x} + [(M+m)\sin\theta]\dot{y} - mc\dot{\theta} \end{aligned}$$

and

$$\begin{aligned}
J_\eta &= \left\langle \mathbb{F}L, \eta_Q^q \right\rangle \\
&= (p_c\,\mathbf{d}c + p_x\,\mathbf{d}x + p_y\,\mathbf{d}y + p_\theta\,\mathbf{d}\theta)\left(-a\sin\theta\frac{\partial}{\partial x} + a\cos\theta\frac{\partial}{\partial y} + \frac{\partial}{\partial\theta}\right) \\
&= a(-p_x\sin\theta + p_y\cos\theta) + p_\theta \\
&= m(a+b)\dot{c} + [-mc\cos\theta - (bm + a(m+M))\sin\theta]\dot{x} \\
&\quad + [(bm + a(m+M))\cos\theta - mc\sin\theta]\dot{y} + [J + mb(a+b) + mc^2]\dot{\theta}
\end{aligned}$$

Unlike the Chaplygin beanie, the equation for $\dot{\theta}$ is more simply recovered from J_ζ rather than J_η,

$$\dot{\theta} = \frac{(M+m)(\dot{x}\cos\theta + \dot{y}\sin\theta) - J_\zeta}{mc}.$$

Next, I found the nonholonomic momentum equations (31) using Mathematica as follows.

$$A = bm + a(m+M),$$

$$B = mcJ_\zeta + (m+M)J_\eta,$$

$$C = m((m+M)(J - abM) + mMc^2)\dot{c}^2$$

$$D = (m+M)((a+b)m\dot{c} - J_\eta) - mcJ_\zeta,$$

$$E = (J + (a+b)^2 m + a^2 M + mc^2)J_\zeta$$

$$F = mc(J_\zeta - (a+b)m\dot{c}),$$

$$G = (J + b^2 m)(m+M) + mMc^2.$$

Then it may be shown that

$$\begin{aligned} \dot{J}_\zeta &= \frac{-D(AB+C)}{G^2}, \\ \dot{J}_\eta &= \frac{-(AB+C)(E+F)}{G^2}. \end{aligned} \tag{48}$$

I checked that when $m = 0$ the preceding nonholonomic momentum equations (48) recover those for the Chaplygin sleigh, (37). Since the right side of (48) depends only on known constants, the control $t \mapsto c(t)$, and the nonholonomic momenta J_ζ, J_η, these equations may be intergrated and then used to reconstruct the group motion according to the reconstruction equations

$$\begin{aligned} \dot{x} &= \frac{J_\zeta + mc\dot{\theta}}{M+m}\cos\theta - \frac{(a\sin\theta)[(M+m)(\dot{x}\cos\theta + \dot{y}\sin\theta) - J_\zeta]}{mc}, \\ \dot{y} &= \frac{J_\zeta + mc\dot{\theta}}{M+m}\sin\theta + \frac{(a\cos\theta)[(M+m)(\dot{x}\cos\theta + \dot{y}\sin\theta) - J_\zeta]}{mc}, \\ \dot{\theta} &= \frac{(M+m)(\dot{x}\cos\theta + \dot{y}\sin\theta) - J_\zeta}{mc}. \end{aligned} \tag{49}$$

The resulting controlled dynamics corresponding to the parameters

$$a = 3, \quad b = 2, \quad M = 1, \quad J = 4, \quad m = 0.5 \tag{50}$$

are shown in the following figures. The first three figures depict the orientation, speed, and lateral displacement of the control mass for the control gain $k = 0.25$, and the next three figures depict the same quantities for the choice of gain $k = 1$. These figures were obtained by numerically integrating (48) and the reconstruction equations (49). However, it must be noted that the controller for the Chaplygin pendulum is not as robust as that for the Chaplygin beanie. Large step changes in the desired heading lead to instability in the control parameter $c(t)$, and even for small changes the initial value of c must be chosen judiciously. Finally, a snapshot of the system's motion is

shown in Figure 25.

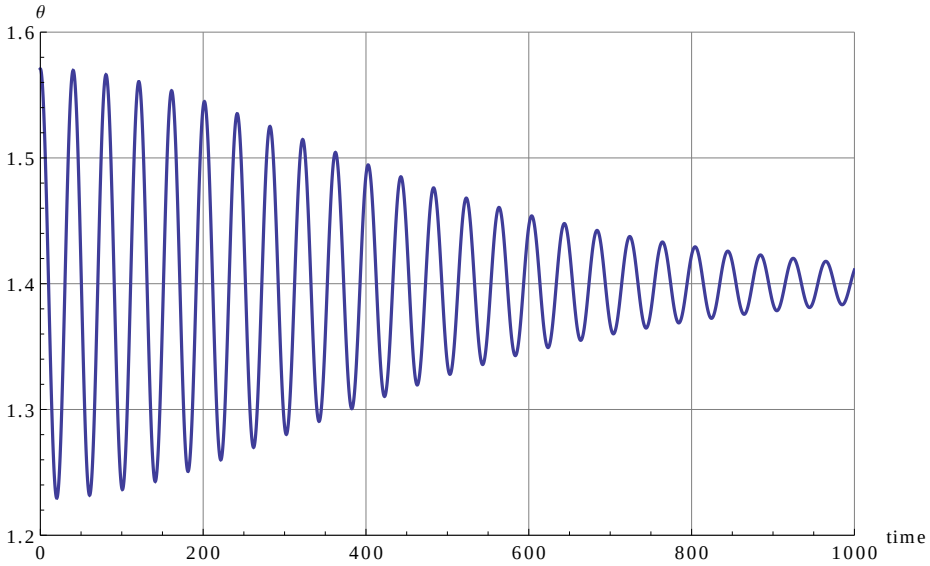

Figure 19: Orientation of the Chaplygin pendulum's sleigh with parameters (50) and control gain $k = 0.25$.

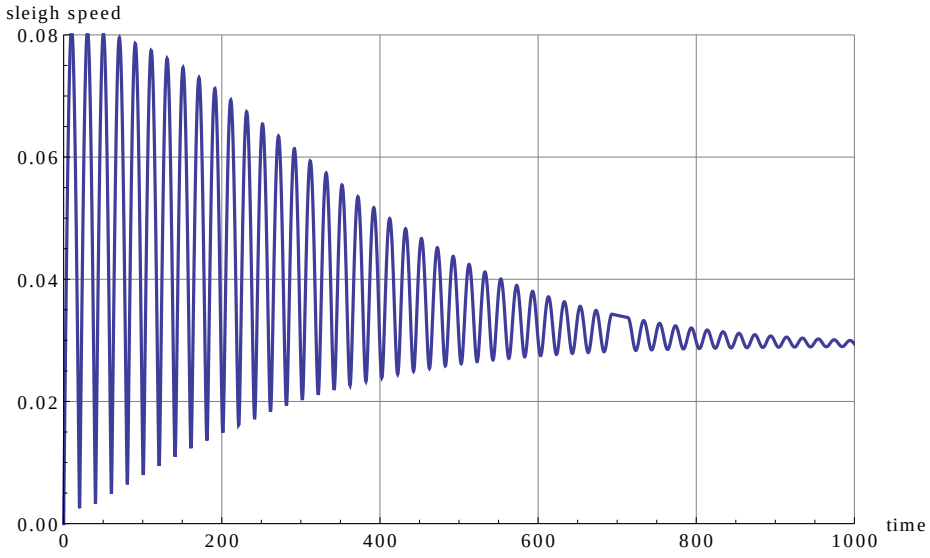

Figure 20: Translational speed of Chaplygin pendulum's sleigh with parameters (50) and control gain $k = 0.25$.

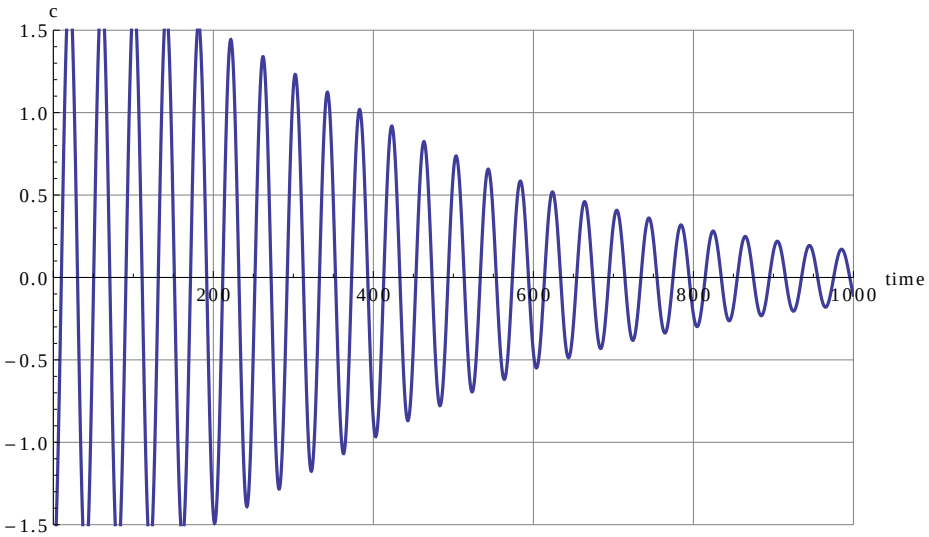

Figure 21: Lateral displacement of the control mass of the Chaplygin pendulum with parameters (50) and control gain $k = 0.25$.

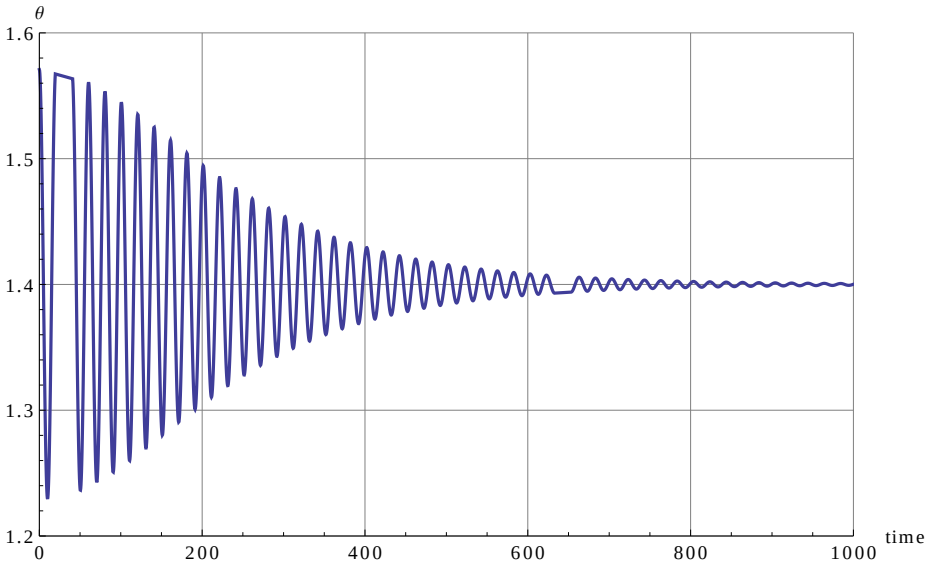

Figure 22: Orientation of the Chaplygin pendulum's sleigh with parameters (50) and control gain $k = 1$.

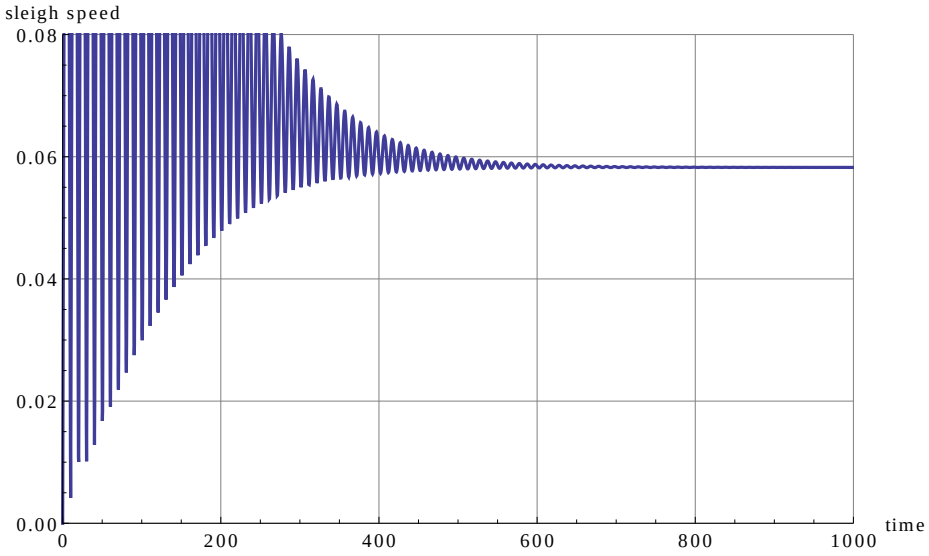

Figure 23: Translational speed of Chaplygin pendulum's sleigh with parameters (50) and control gain $k = 1$.

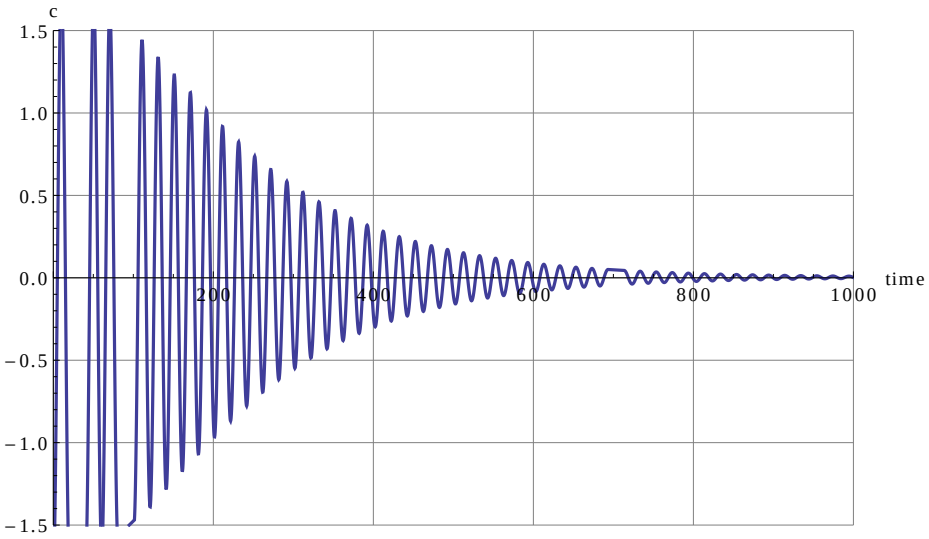

Figure 24: Lateral displacement of the control mass of the Chaplygin pendulum with parameters (50) and control gain $k = 1$.

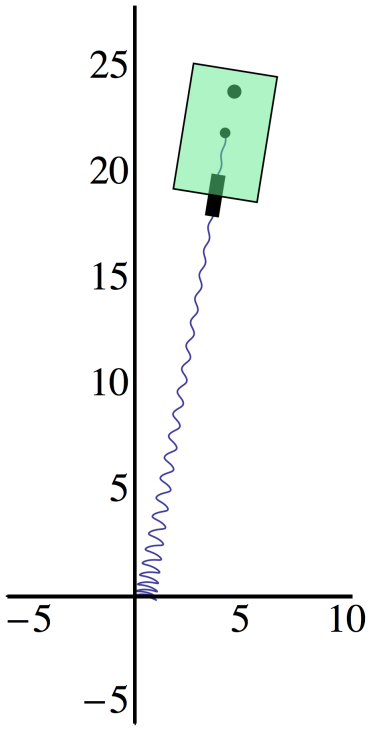

Figure 25: A snapshot of the motion of the controlled Chaplygin pendulum with gain $k = 0.25$.

4.6 Summary

In this chapter I introduced the class of Chaplygin control systems, and after showing that the Chaplygin sleigh may be realized as a special case, I analyzed the nonlinear dynamics and control of two new examples in this class, the Chaplygin beanie and the Chaplygin pendulum. I studied closed-loop controllers for both such systems, where the control input is a torque that is directly proportional to the error in the desired system heading. For the Chaplygin beanie system, I was able to rigorously prove and numerically verify that the controller drives the system asymptotically to the desired heading and with an arbitrary preselected speed. The efficacy of this control strategy for the Chaplygin pendulum, however, was found to be somewhat delicate. Nevertheless, the resulting control strategy provides a basis for single-input

planar navigation of terrestrial vehicles.

CHAPTER 5: LOCOMOTION IN FLUIDS VIA BROKEN SYMMETRY

In this chapter I present a model for the locomotion of swimming microorganisms moving in proximity to a wall in an ideal fluid. The swimmers are modeled by articulated linkages that join several spherical bodies. This differs from previous work in that the bodies are symmetric, thus eliminating any added-mass effects that might arise from an asymmetric inertia tensor. The resulting locomotion stems from a broken symmetry in the fluid boundary — the wall. I consider two examples in detail, the *symmetric scallop* with one internal degree of freedom, and the *articualted swimmer* with two. I show that both swimmers are able to propel themselves towards the wall through cyclic actuation of their internal joint angles. Although the wall breaks the translational symmetry needed for the motion to be governed by a mechanical connection, I present numerical evidence that a geometric phase may be present, thus suggesting the motion is governed by some hidden connection. The material in this chapter is an expanded version of my recent paper [18].

5.1 Introduction

The locomotion of microorganisms swimming in Stokes flow was investigated in [50], where the *scallop theorem* was introduced (emphasis in the original):

> There is a very funny thing about motion at low Reynolds number, which is the following. One special kind of swimming motion is what I call

> reciprocal motion. That is to say, I change my body into a certain shape and then I go back to the original shape by going through the sequence in reverse. At low Reynolds number, everything reverses just fine. Time, in fact, makes no difference — only configuration. If I change quickly or slowly, the pattern of motion is exactly the same ... So, if the animal tries to swim by a reciprocal motion, it *can't go anywhere*. Fast or slow, it exactly retraces its trajectory and it's back where it started. A good example of that is a scallop. You know, a scallop opens its shell slowly and closes its shell fast, squirting out water. The moral of this is that the scallop at low Reynolds number is no good. It can't swim because it only has one hinge, and if you have only one degree of freedom in configuration space, you are bound to make a reciprocal motion. There is nothing else you can do.

In other words, an isolated microorganism enjoying only one internal degree of freedom cannot swim when viscous forces dominate. In this regime, inertial effects are inconsequential, the organism's motion immediately halts when its joint ceases to be activated, and closing the hinge of a scallop exactly undoes whatever motion through the environment the scallop achieved by opening its hinge. As pointed out in [50], Aristotelian mechanics is correct in this regime; it was also remarked that locomotion is possible when two internal degrees of freedom are available, for example by driving two joints in a complementary periodic fashion.

In this chapter I am interested in the analogous locomotion problem for ideal fluids,

by which I mean an inviscid incompressible fluid of constant density. The ideal flow version of Purcell's scallop theorem — that an isolated swimmer in an infinite *ideal* fluid with only one internal degree of freedom cannot swim — holds because of parallels in the mathematical structure of ideal flow and Stokes flow detailed in [30]. As already remarked, however, I will demonstrate that when a wall is introduced into the fluid, the wall breaks the symmetry and enables even the scallop — with only one internal degree of freedom — to locomote in an ideal fluid.

The locomotion of swimmers with multiple internal degrees of freedom has been studied extensively in the literature. For example, [51], [26], and [52] each demonstrated that a planar swimmer comprising multiple links can propel itself in an ideal fluid through a combination of cyclic shape changes and added-mass effects, generating geometric phase relative to a connection on a principal bundle. Meanwhile, [33] showed that a pair of scallops can exploit their hydrodynamic coupling in Stokes flow to propel themselves as a team in a mathematically analogous fashion. However, in each of these cases, the locomotion may ultimately be attributed to shape-dependent added-mass effects arising from the asymmetry in the geometry of the locomoting body.

This chapter is organized as follows. First I give a brief treatment of the motion of Purcell's three-link swimmer for a particular gait by modeling the system as a principal bundle whose motion is governed by geometric phase relative to the mechanical connection. I do this to illustrate the main ideas and also serve as a point of contrast for the subsequent systems I introduce. Then I place a wall into an infinite ideal fluid, and I introduce the *symmetric scallop*. This is Purcell's scallop but swimming

in an ideal fluid and whose body is comprised of spheres rather than ellipses. In the absence of the wall, this system could not locomote. By introduction of the wall, however, I demonstrate that the symmetric scallop *is* able to locomote. I then introduce and analyze the motion of a second system, the *articulated swimmer*, which has two internal joint angles rather than one. In both cases the presence of the wall breaks a symmetry that would otherwise render impossible the locomotion of the swimmers. The locomotion of the swimmers appears, therefore, to be solely accounted for by wall effects.

5.2 Three-Link Swimmer

Consider the *three-link swimmer*, depicted in Figure 26. This is a microorganism moving in an infinite ideal fluid, modeled by a linkage comprising three identical ellipses and two internal joints. It may swim by actuating its two internal joint angles in a periodic fashion.

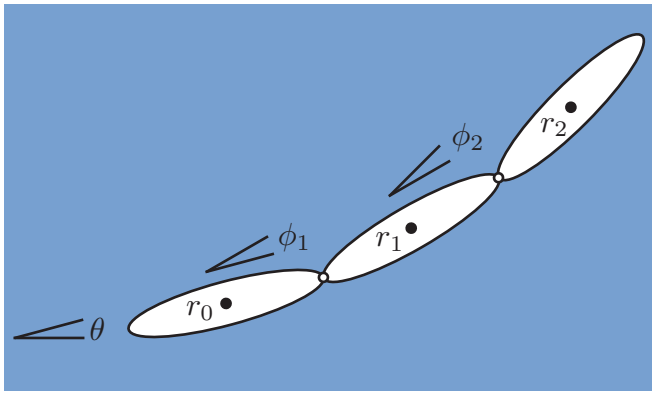

Figure 26: A three-link swimmer in an infinite ideal fluid.

The configuration space is the principal bundle $Q = \mathbb{T}^2 \times SE(2)$ with the canoncial projection $\pi : Q \to \mathbb{T}^2$ and local coordinates $(\phi_1, \phi_2, x, y, \theta)$. The coordinates ϕ_1, ϕ_2 on the torus encode the orientation of the two internal joint angles in the system,

defined so that ϕ_1 is the angle the major axis of the second link makes with the major axis of the first link, and ϕ_2 is the angle the major axis of the third link makes with the second. Let $r_0 = (x, y)$ be the center of the leftmost link, let $r_1 = (x_1, y_1)$ and $r_2 = (x_2, y_2)$ be the centers of the middle and right links, respectively, and let $\theta, \theta_1, \theta_2$ be the angles these links make with the horizontal. Then

$$\begin{aligned} \theta_1 &= \theta + \phi_1, & \theta_2 &= \theta + \phi_1 + \phi_2, \\ x_1 &= x + a\cos\theta + a\cos\theta_1, & x_2 &= x_1 + a\cos\theta_1 + a\cos\theta_2, \\ y_1 &= y + a\sin\theta + a\sin\theta_1, & y_2 &= y_1 + a\sin\theta_1 + a\sin\theta_2. \end{aligned}$$

Let ρ denote the density of the fluid, and let a, b denote the semi-major and semi-minor axes of the ellipse. Here and in the sequel I make use of the commonly employed *hydrodynamic decoupling assumption*, which asserts that each body in an ideal fluid interacts only with the fluid and not with other immersed bodies. Using this assumption and the formula for the kinetic energy of an ellipse in an infinite ideal fluid found in [41], it may be shown that the Lagrangian $L : TQ \to \mathbb{R}$ is

$$L = \frac{1}{2}\sum_{i=1}^{3} \pi\rho(b^2\zeta_i^2 + a^2\eta_i^2) + \frac{\pi(a^2 - b^2)}{8}\dot{\theta}_i^2, \tag{51}$$

where ζ_i, η_i are the projections of the translational velocity $(\dot{x}_i, \dot{y}_i)$ of the ith ellipse along its major and minor axes, respectively, and where $\dot{\theta}_i$ is the angular velocity of the ith ellipse about its center. It may also be shown that the Lagrangian is invariant under the tangent lift of the naturally defined left multiplication of $SE(2)$ on Q. Therefore, as described in §2.2, the principal bundle Q admits the mechanical connection defined such that horizontal is metric orthogonal to vertical, where the

Riemannian metric g on Q is chosen so that (51) takes the form $L(v_q) = \frac{1}{2}g(v_q, v_q)$, and the equations of motion are obtained by demanding that trajectories are horizontal relative to this connection. For the gait shown in Figure 27, the resulting dynamics obtained by integrating the group reconstruction equations (80) are shown Figure 28 and Figure 29, the latter showing snapshots of the system at equally spaced times during the simulation.

The periodic behavior for each of the group variables (x, y, θ) shown in Figure 28 is explained as a geometric phase arising from the periodic behavior of the gait. One full cycle of the gait corresponds to a closed loop in shape space, and this induces corresponding changes in the group variables as described in §2.2. Since the Lie group $SE(2)$ is nonabelian, this geometric phase is not given by (81), but rather may be found by integrating the inital-value problem (80) over one full loop in shape space.

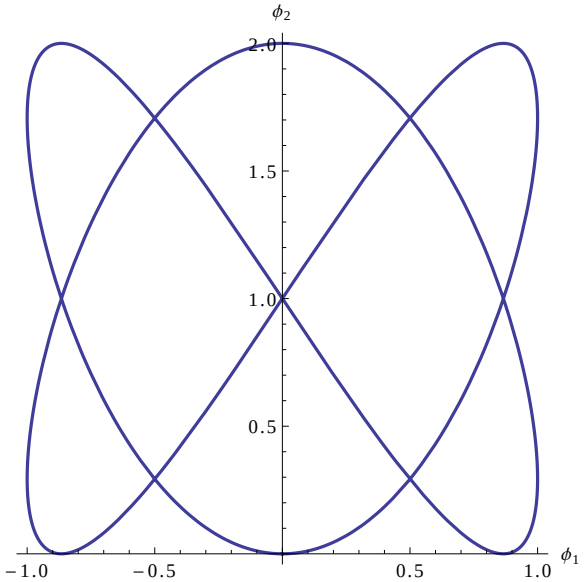

Figure 27: The periodic gait $\phi_1(t) = \sin(2t)$ and $\phi_2(t) = 1 - \cos(3t)$ in shape space $\mathbb{T}^2$ of the three-link swimmer.

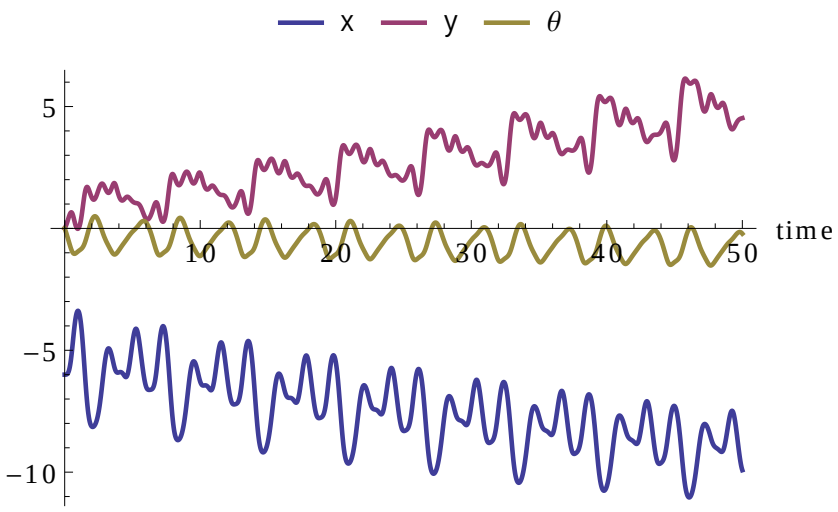

Figure 28: Motion of the three-link swimmer resulting from the gait in Figure 27. The periodic behavior of the group coordinates is explained as a geometric phase arising from closed loops in shape space determined by the periodic gait of Figure 27.

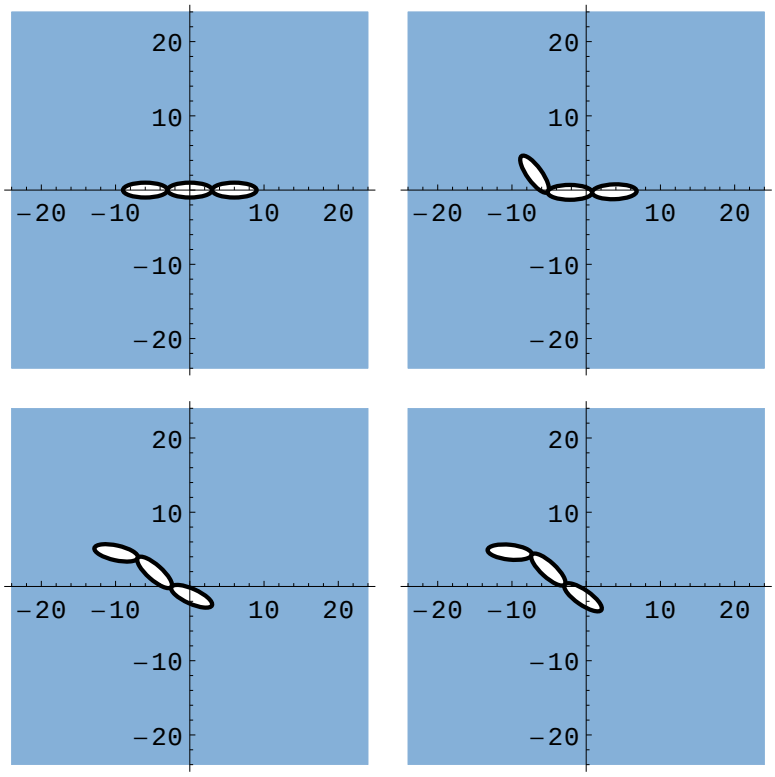

Figure 29: Snapshots at equally spaced times for the three-link swimmer, with gait shown in Figure 27, shown clockwise from top left. As time elapses, the swimmer translates and rotates through its environment.

The ellipses reduce to circles when the semi-axes are equal, $a = b$, in which case the added-mass effects vanish, and the Lagrangian simplifies to $L = \frac{\pi\rho a^2}{2}\sum_{i=1}^{3} \dot{x}_i^2 + \dot{y}_i^2$. Then a net translation of the system is not possible, due to symmetry, no matter how the internal joint angles are actuated. I now add an infinite wall to the fluid and show that even when $a = b$, so that the bodies are spheres rather than ellipses, then both the resulting scallop and three-link spherical swimmers are able to locomote.

5.3 A Symmetric Scallop Near a Wall

Recall that if $\mathbf{u}$ is the steady flow of an inviscid, incompressible fluid without vorticity, there is a velocity potential ϕ such that $\mathbf{u} = \nabla\phi$. That the fluid is incompressible implies $0 = \nabla \cdot \mathbf{u}$, and the velocity potential therefore satisfies the Laplace equation $\nabla^2\phi = 0$, subject to appropriate boundary conditions. For rigid bodies in an infinite ideal fluid, the boundary conditions are of the Neumann type, requiring that the fluid velocity $\nabla\phi$ is everywhere tangent to the boundary. These are supplemented by suitable decay conditions at infinity. An elementary discussion may be found in [2].

Consider now a rigid sphere of radius a and mass m moving in an infinite ideal fluid near an infinite wall. Choose an inertial coordinate system, with coordinates denoted (x, y), such that the wall is described by $y = 0$. The corresponding Laplace problem for the velocity potential is solved in [41] by first considering two spheres moving along their line of centers — in the absence of a wall — and then using the method of images to obtain the result for a single sphere near an infinite wall. From this, a first-order approximation to the kinetic energy of the sphere, located at (x, y),

is derived as

$$T = \frac{1}{2}\left[\left(m + \frac{m_f}{2}\left(1 + \frac{3a^3}{16y^3}\right)\right)\dot{x}^2 + \left(m + \frac{m_f}{2}\left(1 + \frac{3a^3}{8y^3}\right)\right)\dot{y}^2\right], \tag{52}$$

where m_f denotes the mass of the fluid displaced by the sphere. Note that the energy is independent of x, as it must be due to symmetry. Furthermore, it is highly nonlinear in y, and — all else being equal — the energy due to the sphere's vertical motion is larger than that due to its horizontal motion.

This system will serve as a building block for the models in this chapter, so it is worthwhile to investigate its dynamics. With no potential energy in the system, the Lagrangian is simply the total kinetic energy, $L = T$. As in [41], define

$$A(y) = m + \frac{m_f}{2}\left(1 + \frac{3a^3}{16y^3}\right),$$
$$B(y) = m + \frac{m_f}{2}\left(1 + \frac{3a^3}{8y^3}\right).$$

Note that $A(y), B(y) > 0$ because the motion is confined to the half plane $y > 0$. Then the Lagrangian may be written

$$L = \frac{1}{2}\left(A(y)\dot{x}^2 + B(y)\dot{y}^2\right).$$

It follows from Lagrange's equations (8) that

$$0 = \frac{\partial L}{\partial x} = \frac{d}{dt}\frac{\partial L}{\partial \dot{x}} = \frac{d}{dt}\left(A(y)\dot{x}\right) = \frac{\partial A}{\partial y}\dot{x}\dot{y} + A(y)\ddot{x},$$

and

$$\frac{1}{2}\left(\frac{\partial A}{\partial y}\dot{x}^2 + \frac{\partial B}{\partial y}\dot{y}^2\right) = \frac{\partial L}{\partial y} = \frac{d}{dt}\frac{\partial L}{\partial \dot{y}} = \frac{d}{dt}\left(B(y)\dot{y}\right) = \frac{\partial B}{\partial y}\dot{y}^2 + B(y)\ddot{y}.$$

Therefore,

$$\ddot{x} = \frac{-1}{A(y)}\frac{\partial A}{\partial y}\dot{x}\dot{y},$$
$$\ddot{y} = \frac{1}{2B(y)}\left(\dot{x}^2\frac{\partial A}{\partial y} - \dot{y}^2\frac{\partial B}{\partial y}\right).$$

Meanwhile,

$$\frac{\partial A}{\partial y} = \frac{-9m_f a^3}{32y^4} < 0 \quad \text{and} \quad \frac{\partial B}{\partial y} = \frac{-9m_f a^3}{16y^4} < 0.$$

Furthermore, note that $\frac{\partial B}{\partial y} = 2\frac{\partial A}{\partial y}$. Since $\frac{-1}{A(y)}\frac{\partial A}{\partial y} > 0$, it follows that the sphere's horizontal acceleration has the same sign as the product $\dot{x}\dot{y}$. Meanwhile,

$$\ddot{y} = \frac{1}{2B(y)}\frac{\partial A}{\partial y}(\dot{x}^2 - 2\dot{y}^2),$$

and since $\frac{1}{2B(y)}\frac{\partial A}{\partial y} < 0$, it follows that $\ddot{y}$ has the opposite sign as $\dot{x}^2 - 2\dot{y}^2$. Hence $\ddot{y} > 0$ when $\dot{x}^2 < 2\dot{y}^2$, and $\ddot{y} < 0$ when $\dot{x}^2 > 2\dot{y}^2$. That is, the sphere is

repelled from the wall when $\dot{x}^2 < 2\dot{y}^2$,

attracted towards the wall when $\dot{x}^2 > 2\dot{y}^2$.

The resulting dynamics for a typical case are depicted in Figure 30 and Figure 31.

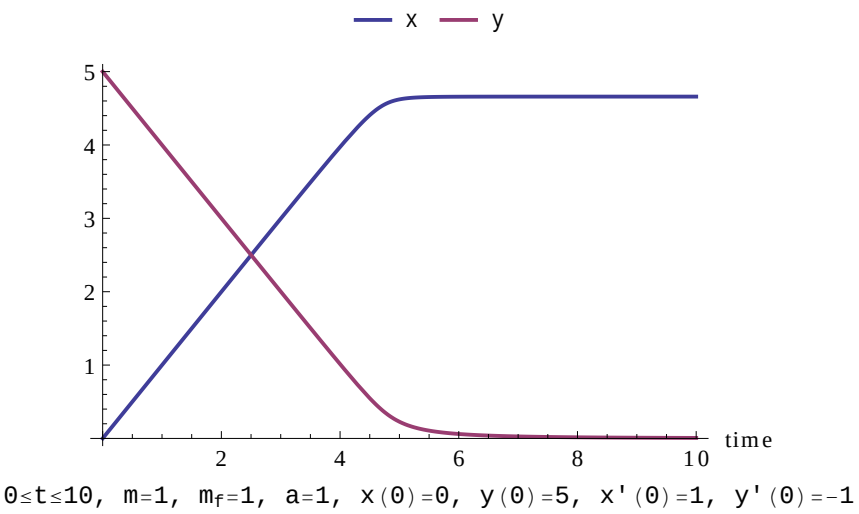

Figure 30: Position of a sphere moving in an ideal fluid near an infinite wall.

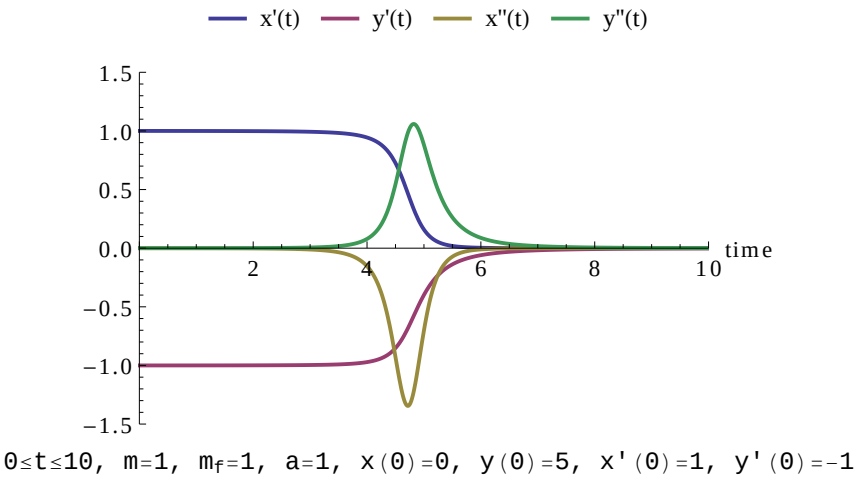

Figure 31: Velocity and acceleration of the sphere of Figure 30.

I now introduce the *symmetric scallop*, a variation of Purcell's hydrodynamic scallop with three important differences:

1. The symmetric scallop swims in ideal flow, rather than Stokes flow.

2. The body of the scallop is comprised of spheres, not anisotropic bodies such as ellipses.

3. There is an infinite wall in the fluid.

It has already been discussed how the last two points are related to one another: the wall introduces an asymmetry, compensating for the asymmetry lost by using spheres rather than ellipses. The symmetric scallop is depicted in Figure 32.

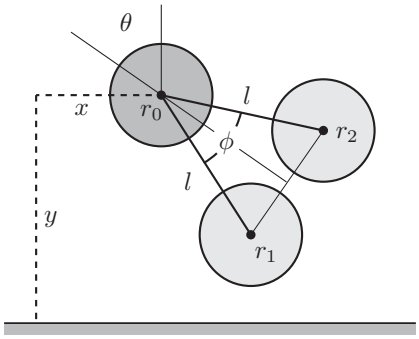

Figure 32: A symmetric scallop in an ideal fluid near an infinite wall.

The three spheres are identical, each with radius a and mass m. Let $r_0 = (x_0, y_0)$ denote the position of the central sphere, and let $r_1 = (x_1, y_1)$ and $r_2 = (x_2, y_2)$ denote those of the distal spheres, which are joined to the central sphere by rigid, infinitesimally thin, near-massless rods of length $l \geq 2a$. I assume the idealized rods, when compared to the bluff spheres, do not make a significant contribution to the system dynamics, and I view them merely as a means of enforcing constraints between the positions of the spheres. The *joint angle* of the scallop is denoted by ϕ, and I assume the ability to control this variable (through the exertion of an internal motor located at r_0, say). The *orientation* of the scallop, denoted θ, is defined to be zero when the vertical line through r_0 is the perpendicular bisector of the line segment

joining r_1 to r_2. Given these parameters, the geometry of Figure 32 implies that

$$\begin{aligned} x_1(t) &= x(t) + l\sin\left(\theta(t) - \frac{\phi(t)}{2}\right), \\ y_1(t) &= y(t) - l\cos\left(\theta(t) - \frac{\phi(t)}{2}\right), \\ x_2(t) &= x(t) + l\sin\left(\theta(t) + \frac{\phi(t)}{2}\right), \\ y_2(t) &= y(t) - l\cos\left(\theta(t) + \frac{\phi(t)}{2}\right). \end{aligned} \tag{53}$$

The configuration space is $Q = S^1 \times SE(2)$ with coordinates (ϕ, x, y, θ). By using (52) and the hydrodynamic decoupling assumption, the Lagrangian $L : TQ \to \mathbb{R}$ for this system is

$$L = \sum_{i=0}^{2} \frac{1}{2}\left[\left(m + \frac{m_f}{2}\left(1 + \frac{3a^3}{16y_i^3}\right)\right)\dot{x}_i^2 + \left(m + \frac{m_f}{2}\left(1 + \frac{3a^3}{8y_i^3}\right)\dot{y}_i^2\right)\right], \tag{54}$$

where x_1, y_1, x_2, y_2 and their derivatives are determined from (53). Note that unlike the three-link swimmer of §5.2, the Lagrangian is not symmetric under vertical translations $y \mapsto y +$ constant, and so the motion is not governed by a mechanical connection on the principal bundle Q. Instead, the dynamics are determined by Lagrange's equations,

$$\frac{d}{dt}\frac{\partial L}{\partial \dot{q}^i} - \frac{\partial L}{\partial q^i} = 0, \qquad q = (\phi, x, y, \theta). \tag{55}$$

Since the Lagrangian is *cyclic* in the x coordinate, i.e. $\partial L/\partial x = 0$, it follows that $\frac{d}{dt}\frac{\partial L}{\partial \dot{x}} = 0$. Hence the conjugate momentum $p_x \coloneqq \frac{\partial L}{\partial \dot{x}}$ is conserved. This observation will be used as a check of the numerical integration.

I now investigate the dynamics that result from controlled actuation of the joint angle ϕ. It follows from the geometry of Figure 32 that the minimum physically

realizable joint angle $\phi_{\min}$, defined as the joint angle when the distal spheres are tangent to one another, is

$$\phi_{\min} = 2 \arcsin\left(\frac{a}{l}\right).$$

By prescribing the open-loop control

$$\phi(t) = \phi_{\min} + \frac{(\pi - \phi_{\min})(1 + \sin t)}{2}, \tag{56}$$

the joint angle undergoes a sinusoidal motion with a minimum value of $\phi_{\min}$ and a maximum value of π, where the joint is "wide open." The resulting dynamics for a typical set of parameters are shown in Figure 33. Since I wish to investigate the locomotion of the system arising solely from actuation of its internal shape and not from any drift momentum that may be present, the initial velocities $\dot{x}(0), \dot{y}(0), \dot{\theta}(0)$ were chosen by requiring that the system's net initial momentum vanishes. This was not done by simply choosing zero initial velocities because even at $t = 0$ the controller is driving the system. Instead, the condition of zero net initial momentum is obtained by solving, after all other parameters are specified, the following system of equations

$$p_x(y, \theta, \dot{x}, \dot{y}, \dot{\theta}) = 0,$$

$$p_y(y, \theta, \dot{x}, \dot{y}, \dot{\theta}) = 0,$$

$$p_\theta(y, \theta, \dot{x}, \dot{y}, \dot{\theta}) = 0,$$

at $t = 0$ for $\dot{x}(0), \dot{y}(0), \dot{\theta}(0)$, given the known values of the parameters and $\dot{\phi}(0)$. Since the system starts with zero net momentum, this means that any net locomotion through the environment must arise solely from the actuation of the internal shape

variable.

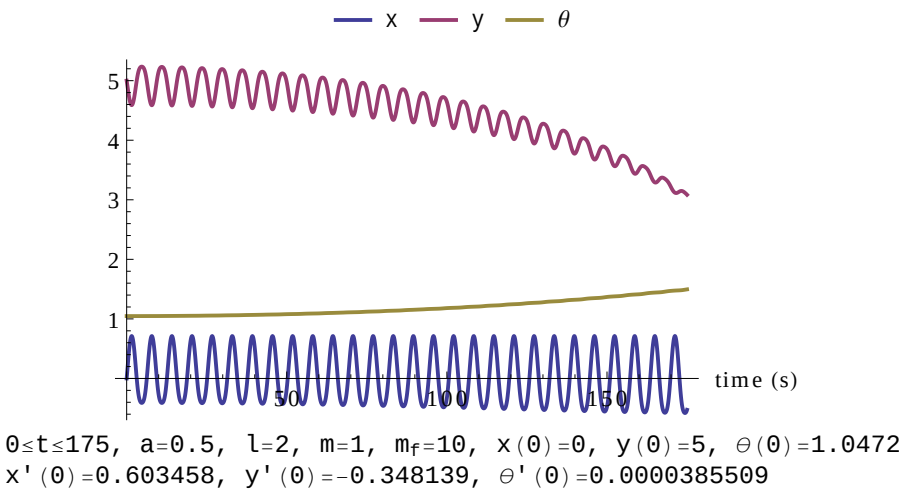

Figure 33: Dynamics of the symmetric scallop in an ideal fluid near an infinite wall and with zero net initial momentum.

Note that the scallop slowly inches its way towards the wall located at $y = 0$, as evidenced by the oscillatory decrease in the y coordinate. The horizontal coordinate of the central sphere oscillates about its initial value, but on average its position is unchanged. This comports with the fact that, due to translational symmetry of the Lagrangian and Noether's theorem, the horizontal component of momentum of the system is conserved; although the central sphere's horizontal position oscillates, there are compensating oscillations of the distal spheres as well, so that i.e. $\frac{\partial L}{\partial \dot{x}}$ is conserved throughout the motion. Evidence for this is presented in Figure 34.

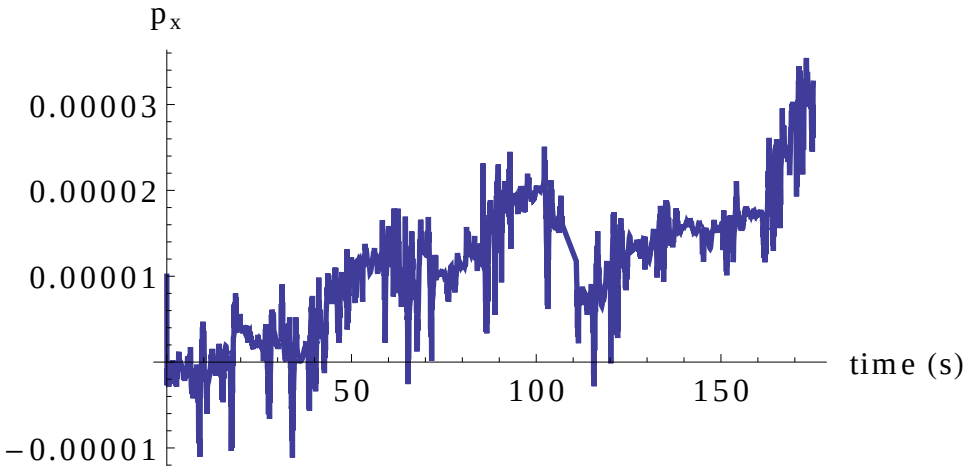

Figure 34: The horizontal component $p_x = \frac{\partial L}{\partial \dot{x}}$ of the total linear momentum for the scallop in Figure 33 is conserved up to 10^{-4} throughout the simulation.

Snapshots of the system's motion at equally spaced times during the motion are presented in Figure 35. A comparison of the first snapshot with the last shows that the scallop is not only moving towards the wall, but is also rotating counterclockwise as it does so, as may also be seen by the plot of $\theta(t)$ in Figure 33.

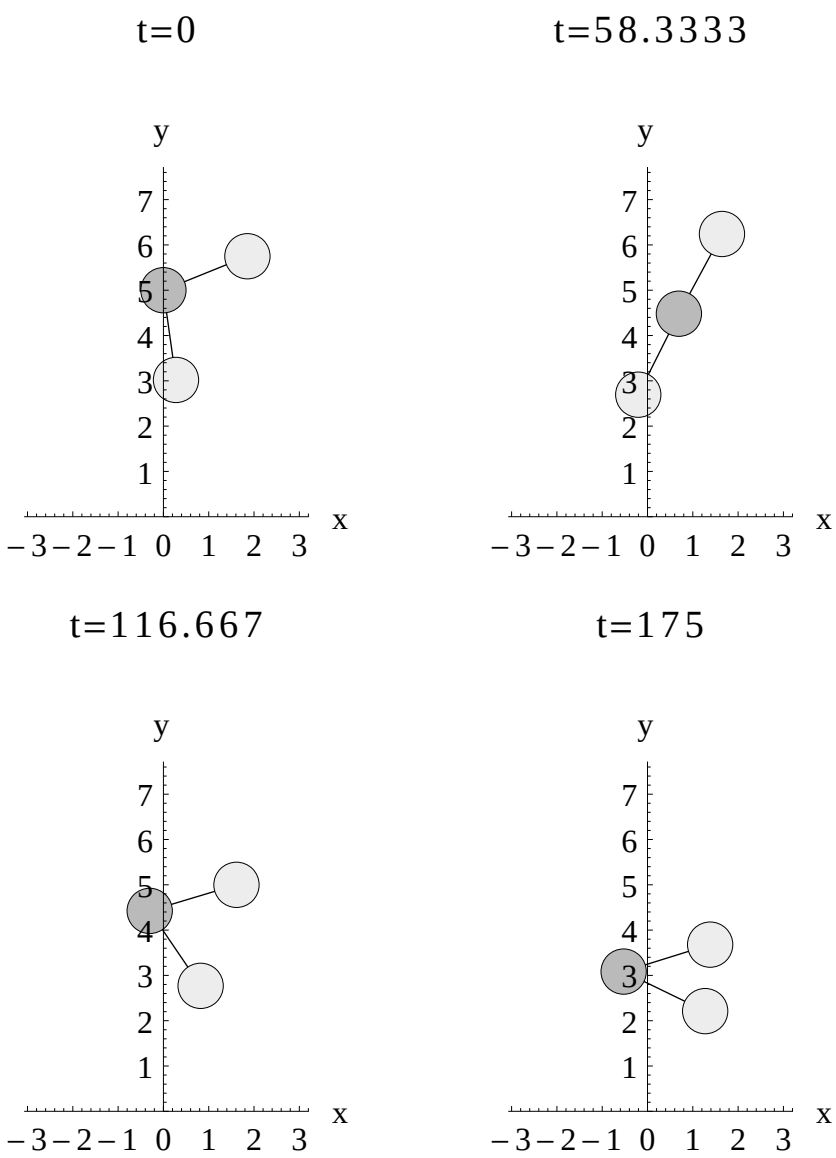

Figure 35: Snapshots at equally spaced times of the symmetric scallop from Figure 33. As time elapses, the swimmer moves towards the wall.

Since the motion of the joint angle is prescribed by (56), to fully understand the motion it is only necessary to know the trajectory of the scallop's central sphere. This is shown in Figure 36. The symmetric scallop is seen to undergo a swinging motion, with a net translation towards the wall and a net positive reorientation.

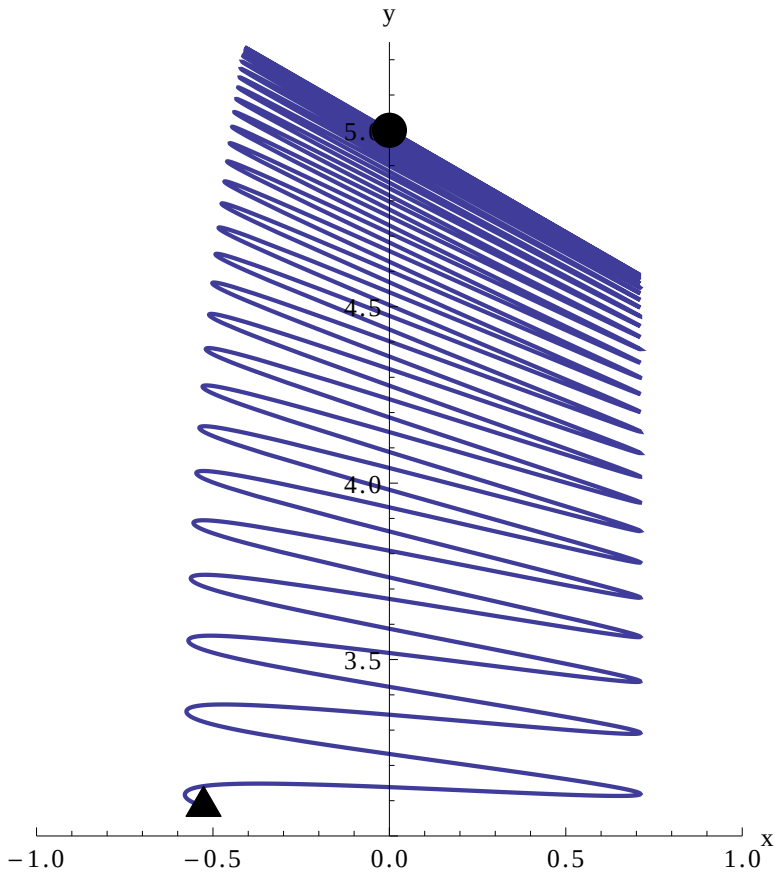

Figure 36: Trajectory of the central sphere for the scallop in Figure 33.

It is natural to ask how the initial orientation θ_0 affects the system's motion. To investigate this, the dynamics were determined for the initial orientations $\theta_0 = 0, \pi/3, 2\pi/3$, and π, all other parameters being left unchanged. By symmetry of the system, there will be corresponding motions for negative values of θ_0. I concentrate attention on the vertical component of the motion, since the horizontal motion is, in the net, trivial. A plot of $y(t)$ for each of these four cases is shown in Figure 37. The case $\theta_0 = \pi/3$ in the upper-right panel of the figure is most successful in generating vertical motion. (In fact, this motivated the choice $\theta_0 = \pi/3$ used throughout the rest of this section.) That this initial orientation leads to more vertical motion than

the other choices may be explained by examining the initial configuration of the system, depicted in the upper-left panel of Figure 35. There, one of the distal spheres hangs low, closer to the wall than any of the spheres would be in the other cases $\theta_0 = 0, 2\pi/3$, or π. Together with the y^{-3} dependence of the energy (54), motion towards the wall is most energetically favorable when y is small since the y^{-3} terms are then comparatively large. Note that in each of the four cases considered in Figure 37, the symmetric scallop locomotes towards the wall.

The symmetric scallop has only one internal degree of freedom. Since its geometry prohobits the joint angle from completing a revolution, there can be no geometric phase associated with a closed loop in shape space. To allow for the possibility of geometric phase I introduce in the next section an analogous swimmer but with two internal degrees of freedom.

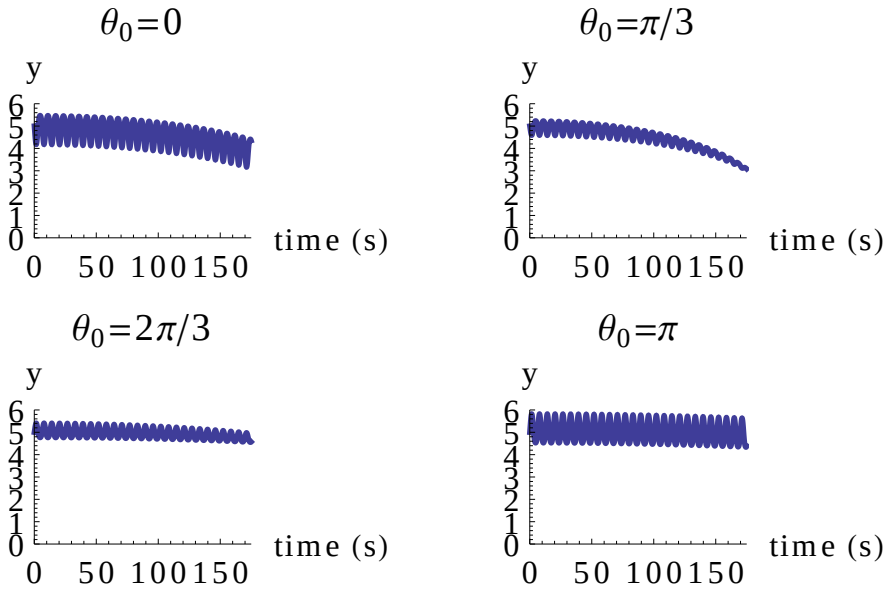

Figure 37: Vertical position of the central sphere of the symmetric scallop. The system parameters are defined as in Figure 33 but with different initial orientations, namely $\theta_0 = 0$, $\pi/3$, $2\pi/3$, and π. In each case, the scallop slowly inches its way towards the wall.

5.4 An Articulated Swimmer Near a Wall

Consider now an *articulated swimmer* comprising three spheres again but now joined by a linkage with two internal joint angles. It will be seen that this system subsumes as a special case the symmetric scallop. On the one hand, with two degrees of freedom it might be hoped that the system's motion through its enviornment is governed by an underlying geometric phase. On the other hand, the Lagrangian is not invariant under vertical translations due to the wall, so the full mechanical connection arising from an $SE(2)$ symmetry, as in the three-link swimmer considered in §5.2, will not be relevant here. Nevertheless, I will show that there does seem to be an underlying geometric phase associated with this system.

As with the symmetric scallop, the spheres are assumed to be identical, each with mass m and radius a. Let l_1, l_2 represent the distances from the central sphere's center to the joints and from the joints to the distal spheres' centers, respectively, and let $r_0 = (x, y)$ and let $r_i = (x_i, y_i)$ for $i = 1, 2$ denote the coordinates of the centers of the spheres.

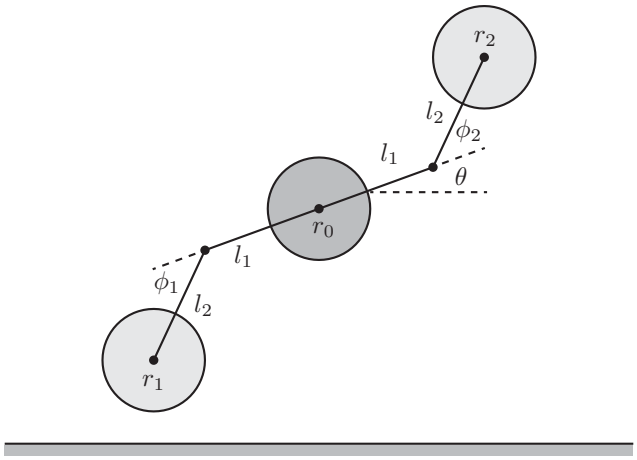

Figure 38: An articulated swimmer near an infinite wall in an ideal fluid.

Then it follows from the geometry of Figure 38 that

$$\begin{aligned} x_1(t) &= x(t) - l_1 \cos\theta(t) - l_2 \cos(\theta(t) + \phi_1(t)), \\ y_1(t) &= y(t) - l_1 \sin\theta(t) - l_2 \sin(\theta(t) + \phi_1(t)), \\ x_2(t) &= x(t) + l_1 \cos\theta(t) + l_2 \cos(\theta(t) + \phi_2(t)), \\ y_2(t) &= y(t) + l_1 \sin\theta(t) + l_2 \sin(\theta(t) + \phi_2(t)), \end{aligned} \tag{57}$$

To permit the distal spheres to rotate freely while rendering self-collisions impossible, the parameters l_1 and l_2 are required to satisfy the inequalities

$$l_1 \geq 2a \quad \text{and} \quad a \leq l_2 \leq l_1 - 2a. \tag{58}$$

(Without these restrictions, the single-jointed scallop considered earlier is recovered as the special case $l_1 = 0$, in which case the single joint angle is $\phi = \pi - \phi_1 + \phi_2$.) The orientation angle θ is now defined relative to the horizontal, and I assume that the internal angles ϕ_1, ϕ_2 may be independently actuated for control.

With the aid of two — rather than one — shape variables, more sophisticated gaits

may be studied. As with the symmetric scallop, the Lagrangian for the articulated swimmer is given by

$$L = \sum_{i=0}^{2} \frac{1}{2} \left[\left(m + \frac{m_f}{2} \left(1 + \frac{3a^3}{16 y_i^3} \right) \right) \dot{x}_i^2 + \left(m + \frac{m_f}{2} \left(1 + \frac{3a^3}{8 y_i^3} \right) \dot{y}_i^2 \right) \right], \tag{59}$$

where $x_1, x_2, \theta_1, \theta_2$ and their derivatives defined by (57). I now drive the system with according to the periodic gait

$$\begin{aligned} \phi_1(t) &:= \sin(t), \\ \phi_2(t) &:= \sin(t)\cos(t), \end{aligned} \tag{60}$$

whose image is a figure eight depicted in Figure 39.

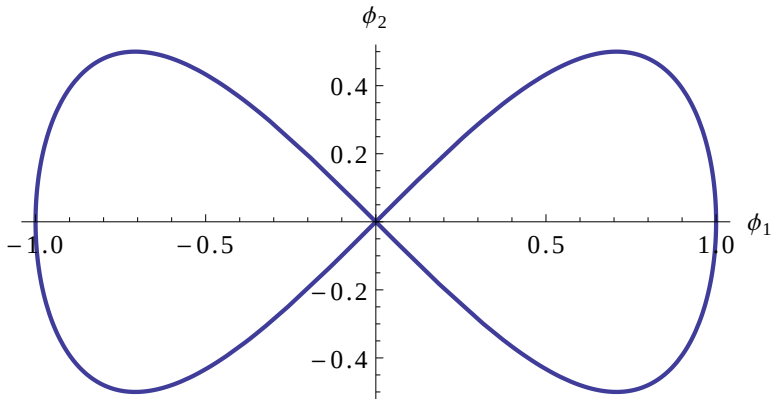

Figure 39: The gait in shape space for the articulated swimmer, defined by (60).

I will now carry out a similar analysis of the resulting dynamics for the articulated swimmer as for the symmetric scallop. In order that the differences in behavior between the two cases be isolated to the dynamics rather than the choice of parameters, the numerical values for the parameters in the new model are chosen to agree, insofar as possible, with those from the symmetric scallop considered in the previous section. For the gait depicted in Figure 39, the resulting vertical motion of the system

is shown in Figure 40. The vertical motion is somewhat less pronounced than that of the symmetric scallop, in part due to the fact that the outermost distal sphere is further from the wall than in the symmetric scallop. Furthermore, the complicated gait of the two-jointed scallop is reflected in the jagged evolution of $y(t)$ in Figure 40. (Contrast this with the smooth oscillations of $y(t)$ in Figure 33.)

The orientation of the articulated swimmer is illustrated in Figure 41. Unlike the symmetric scallop, the orientation of its two-jointed counterpart is primarily oscillatory, although its orientation angle does increase over a longer time scale.

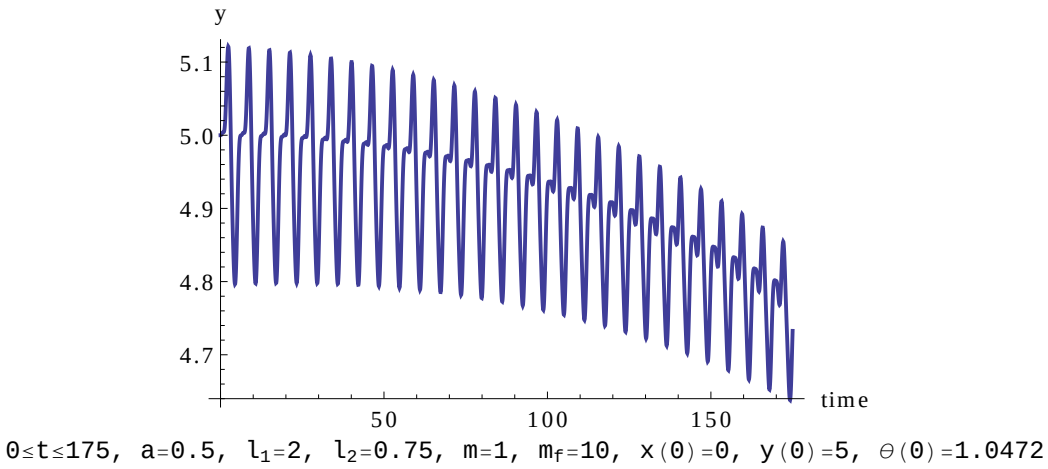

Figure 40: The vertical motion of the articulated swimmer with gait depicted in Figure 39.

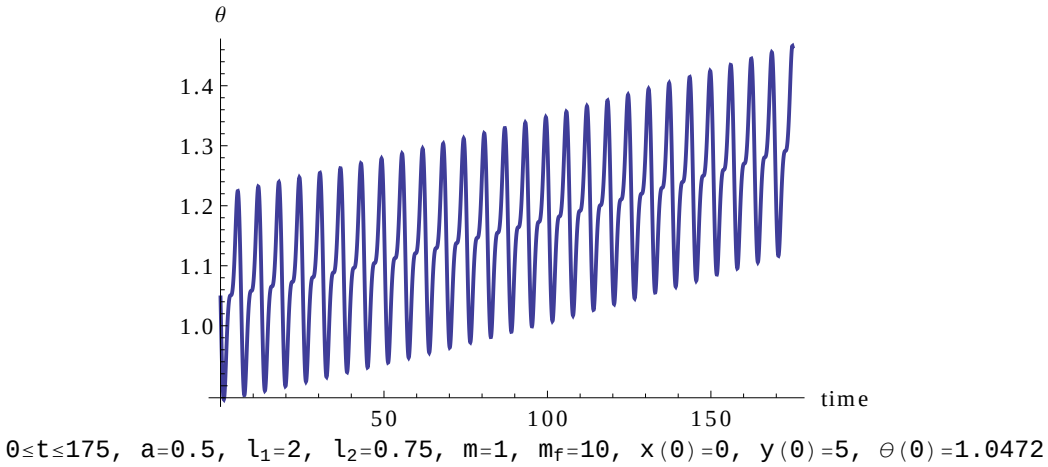

Figure 41: The orientation of the articulated swimmer depicted in Figure 40.

As a check on the numerical integration, the horizontal component $p_x = \frac{\partial L}{\partial \dot{x}}$ of the translational momentum must be conserved by symmetry of the Lagrangian and Noether's theorem. A graph of the horizontal momentum for this system is shown in Figure 42.

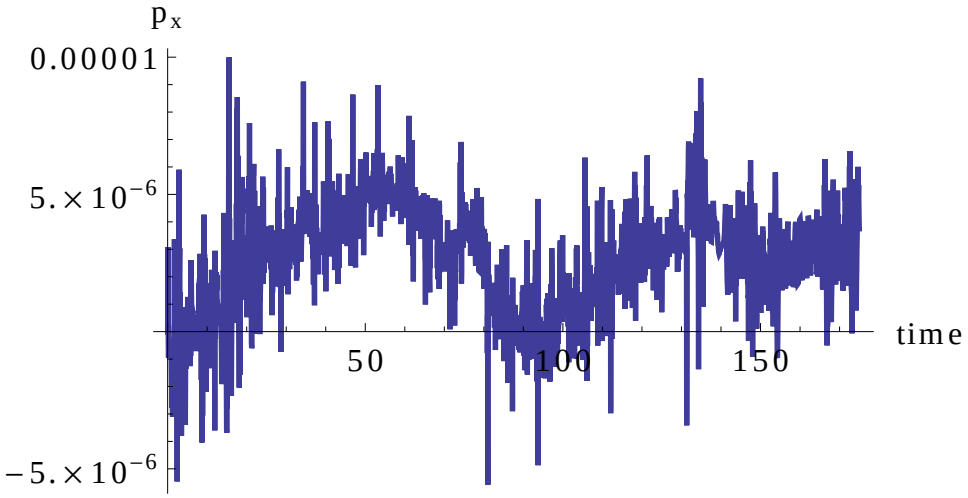

Figure 42: The horizontal component of momentum, $p_x = \frac{\partial L}{\partial \dot{x}}$, for the articulated swimmer in Figure 40 is conserved up through 10^{-5}.

Just like the scallop, the articualted swimmer slowly inches towards the wall while

simultaneously rotating counterclocwise as time evolves. Snapshots at equally spaced times during the motion are shown in Figure 43, while the trajectory of the central sphere is depicted in Figure 44. Compare the two lobes of the resulting trajectory with the lobes appearing in the gait Figure 39.

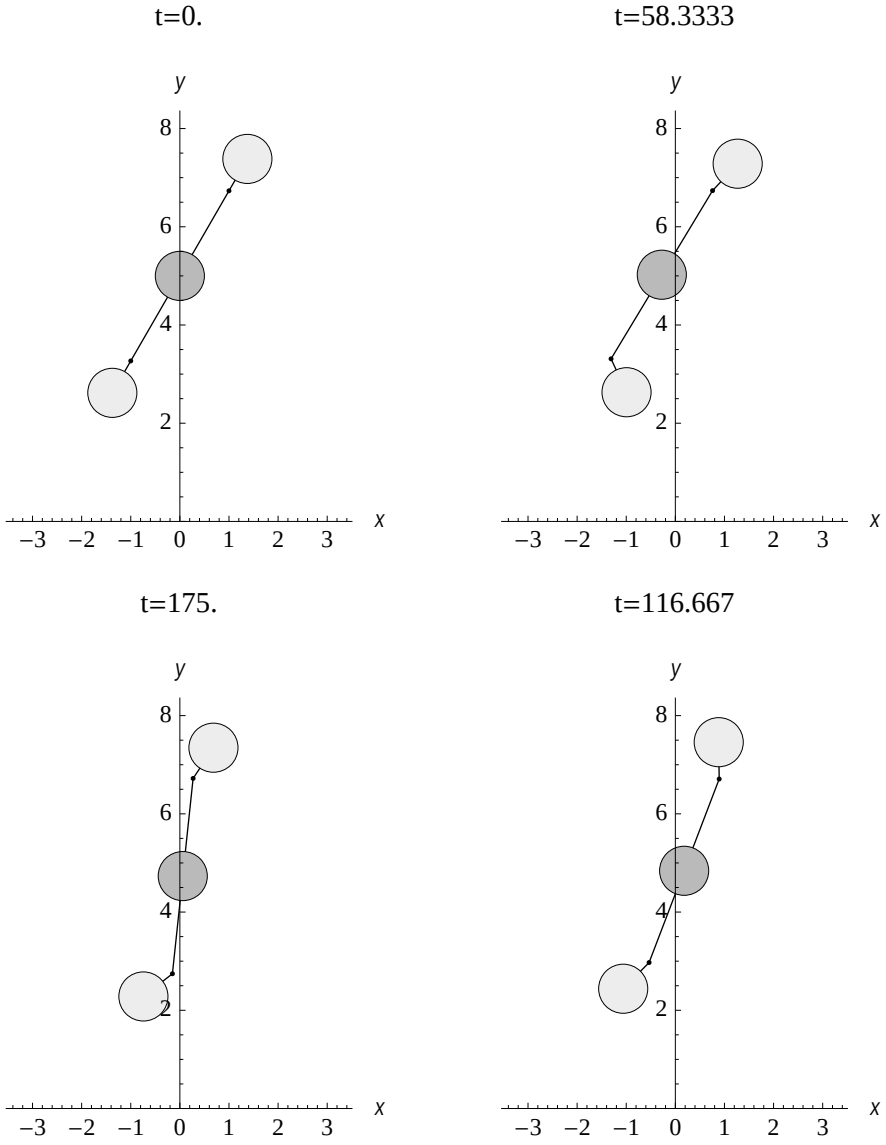

Figure 43: Snapshots at equally spaced times of the articulated swimmer depicted in Figure 40.

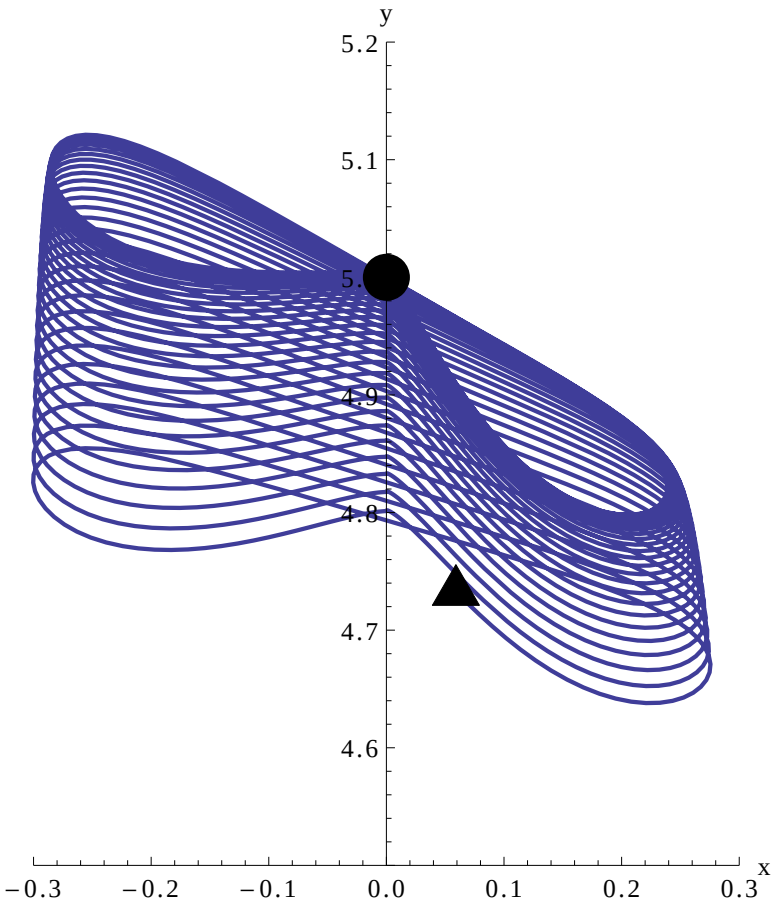

Figure 44: Trajectory of the central sphere in the articulated swimmer from Figure 40.

I now consider the effect of different initial orientations, $\theta_0 = 0, \pi/3, 2\pi/3$ and π on the articulated swimmer. Figure 45 depicts the effect of the initial orientation on the subsequent evolution of $y(t)$, the vertical coordinate of the central sphere. The same reasoning as given for the symmetric scallop explains why the initial angle $\theta_0 = \pi/3$ is most effective of those considered in generating vertical motion.

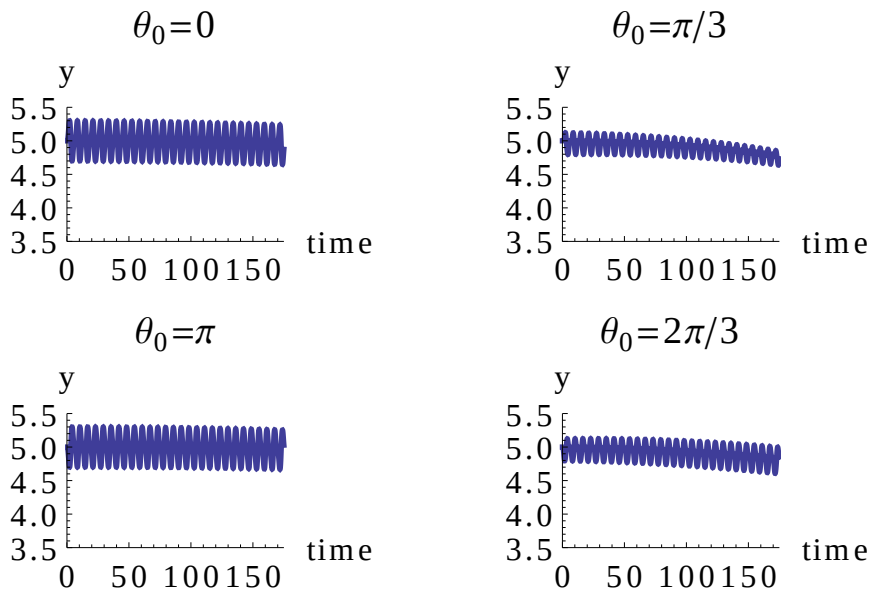

Figure 45: Vertical position of the articulated swimmer for various initial orientations.

Finally, I now consider the possiblity of an underlying geometric phase governing the motion of the articulated swimmer. Recall from §2.2 that a hallmark of geometric phase is that motion in the group variables is related to the gait in shape space in a manner that is independent of the time parameterization. Although the articulated swimmer considered in this section is not governed by a mechanical connection, there may still be some notion of connection that leads to geometric phase. To investigate this possiblity, I modified the gait (60) to the following parameterized version,

$$\begin{aligned} \phi_1(t) &= \sin(t/\tau), \\ \phi_2(t) &= \sin(t/\tau)\cos(t/\tau). \end{aligned} \tag{61}$$

I varied the parameter τ and then adjusted the length of the numerical integration accordingly. For example, when $\tau = 10$ the gait in shape space is traversed one-tenth as fast, and so the length of the numerical integration (when compared to the case

$\tau = 1$) is increased by a factor of ten. Intriguingly, the resulting plots of the system trajectory and orientation angle for $\tau = 1, 10, 100$, shown in Figure 46 and Figure 47, suggests that an underlying geometric phase may be present.

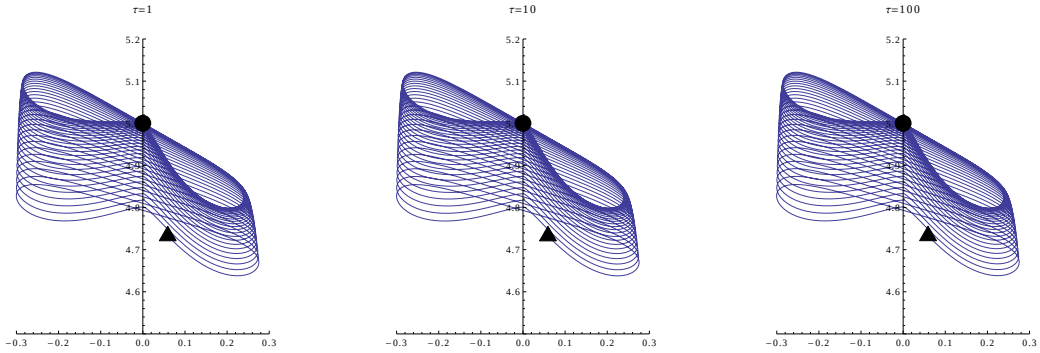

Figure 46: Trajectories (x, y) for the articulated swimmer corresponding to the parameterized gaits $\tau = 1, 10, 100$, from left to right.

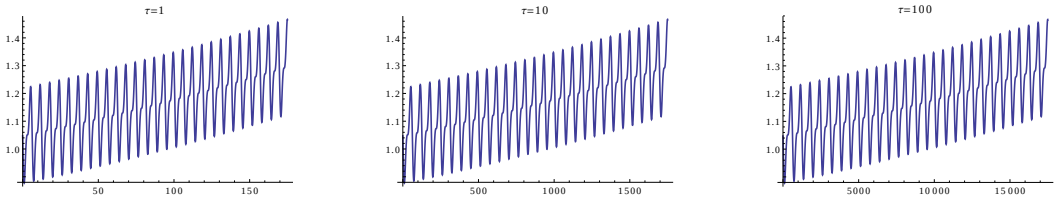

Figure 47: Orientation $\theta(t)$ of the articulated swimmer corresponding to the parameterized gaits $\tau = 1, 10, 100$, from left to right.

5.5 Summary

In this chapter I introduced a new model for the locomotion in an ideal fluid of jointed rigid bodies that do not benefit from shape-dependent added-mass effects. The model was built upon on a first-order approximation for the kinetic energy of a sphere moving near a wall in an ideal fluid. I considered two systems of this type, neither of which would be able to locomote in the absence of the wall. The first was a variant of Purcell's scallop, which — despite having only a single degree of freedom — is able to swim towards the wall. This system cannot be governed by a geometric

phase of any type because it has only one internal variable that cannot complete a closed loop due to steric collisions. I then introduced another example, an articulated swimmer with two joint angles. This system was also shown to swim towards the wall with a particular gait, and although its motion cannot be governed by the mechanical connection, I conjectured on the basis of numerical evidence that there is a hidden connection that governs the motion.

CHAPTER 6: CONSTRAINED VORTEX MOTION

In this chapter I study the dynamics of point vortices in an inviscid incompressible fluid interacting with solid bodies that impose constraints on the fluid flow. The basic idea is to start with the classical N-vortex problem in its Hamiltonian formulation, then express the constraints on the velocity field in terms of the vortex strengths and locations, and finally to apply Dirac's method of constraints. After studying a few examples of this type, I then use this same technique to devise an approximate reduced-order model for the interaction of a vortical fluid with a bluff rigid cylinder.

This chapter is organized as follows. I begin by reviewing the Hamiltonian formulation of the classical N-vortex problem, which is needed in order to apply Dirac's method of constraints. I then use Dirac's method to introduce constraints of three types into the classical N-vortex problem: (i) velocity constraints, which may model a stagnation point, (ii) direction constraints, which may model an infinitesimal fin in the fluid, and (iii) distance constraints, which may model vortex dipoles. The second of these constraints is the hydrodynamic analog of the nonholonomic constraint featured in the Chaplygin control systems of Chapter 4, in that it permits fluid motion along, but not perpendicular to, a given direction. For each of these types of constraints, I analyze the resulting dynamics and the evolution of four quantities — energy, angular impulse, and two components of linear impulse — that are known to be conserved in the unconstrained vortex dynamics. It is found that generally en-

ergy is conserved by the constraints, but that neither linear nor angular impulse are conserved, so the constraints impart momentum but not energy to the fluid. Finally, I use constrained vortex dynamics to devise a reduced-order model for the dynamic interaction of a rigid cylinder with a single external point vortex. For this problem, I use the method of images to introduce artificial point vortices and constrain their motion so as to always satisfy the boundary conditions along the boundary of the moving cylinder if it were present. The dynamics are shown to agree qualititatively, if not quantitatively, with the known exact solution. I delivered a talk about the material in this chapter at the *2015 SIAM Conference on Dynamical Systems* in Snowbird, Utah.

6.1 Introduction

A persistent theme throughout this dissertation has been that of symmetry and constraints in mechanical systems. There is a long and venerable history, and a vast array of techniques, for analyzing systems of particles and rigid bodies subject to constraints. The same cannot be said for constraints in fluid systems. Even a seemingly simple question — such as, in what sense may a stagnation point in a fluid be viewed as a constraint on its phase space? — seems to not have a clear or satisfactory answer. One reason is that fluids are governed by the Navier-Stokes equations, a nonlinear system of partial differential equations, and unlike the ordinary differential equations that arise in rigid body and particle mechanics these equations are *infinite-dimensional* in the sense that the underlying configuration space is an infinite-dimensional space of functions — for inviscid incompressible fluids, for ex-

ample, it is the group of volume-preserving diffeomorphisms from the fluid region to itself (see [4] and [38]).

A very fruitful idea for the analysis of fluid systems is to devise *reduced-order models*, which means a system of finitely many ordinary differential equations that govern the fluid dynamics. Then all of the theory and techniques from ordinary differential equations and dynamical systems may be brought to bear in the analysis. In simple cases, such as the classical N-vortex problem considered below, this can be done to great effect. Devising reduced-order models for any but the simplest fluid systems is generally a very difficult task. For example, it is surprising that a reduced-order model for the interaction of a rigid cylinder and an inviscid incompressible fluid with point vortices was only developed very recently, in [55] and [10]. Previous attempts at devising reduced-order models for this system omitted essential physics and did not produce the correct dynamics of the true nonlinear system, as explained in [55]. The problem of finding reduced-order models for more complicated interactions of fluids and solids has so far eluded solution.

The technique introduced in this chapter is found to have application to both of the research questions above.

6.2 The Classical N-Vortex Problem

The N-vortex problem is to solve the dynamics of N mutually interacting vortices in an infinite, inviscid, incompressible fluid. It is the hydromechanical analog of the gravitational N-body problem. The N-vortex problem was studied by Helmholtz ([24]), Lord Kelvin ([60]), and Kirchhoff ([31]). Research today continues along many lines,

including vortex motion on curved manifolds with applications to geophysical flows, vortex motion in bounded domains and in periphractic (i.e. non-simply-connected) domains, numerical methods such as Lie group integrators, reduced dynamics and stability of relative equilibria, statistical point vortex and equilibrium theories, geometrization of vortex motion, and the dynamical interaction of vortices with rigid bodies. The reader is referred to [46] for details and an extensive survey of the literature, as well as to [2], [34], [41], and [53] for elementary treatments of point vortex dynamics. The N-vortex problem exhibits a wide range of behavior depending on the number of vortices. When $N \leq 3$, the motion is known to be completely integrable, but for $N \geq 4$ nonintegrable examples exist in which the phase space simultaneously admits regions with periodic, quasiperiodic, and chaotic orbits ([46]). The different mathematical techniques relevant to the problem are so varied that the N-vortex problem has more than earned its appellation as a "classical mathematics playground," given to it by Aref in his influential review paper [3].

Let an inviscid, incompressible fluid of constant density fill the unbounded plane $\mathbb{R}^2$. Let $\mathbf{u}$ be the vector field on $\mathbb{R}^2$ such that $\mathbf{u}(\mathbf{x}, t)$ is the velocity of a fluid parcel at position $\mathbf{x}$ and time t. The *vorticity* of the fluid is $\boldsymbol{\omega} \coloneqq \nabla \times \mathbf{u}$, and it measures the local rate of rotation of the fluid. By the Helmholtz-Hodge theorem, there exists a scalar potential ϕ and a vector potential $\boldsymbol{\Psi}$ such that the velocity field may be decomposed as

$$\mathbf{u} = \nabla\phi + \nabla \times \boldsymbol{\Psi}, \tag{62}$$

where $\nabla\phi$ is the irrotational part of the fluid velocity and $\nabla \times \boldsymbol{\Psi}$ is the vortical

part. Since the motion is in the plane, one may write $\boldsymbol{\omega} = \omega\,\hat{\mathbf{n}}$ and $\boldsymbol{\Psi} = \psi\,\hat{\mathbf{n}}$ for two scalar functions ω and ψ, with $\hat{\mathbf{n}}$ denoting the unit normal vector to the plane, so that $\omega = \boldsymbol{\omega}\cdot\hat{\mathbf{n}}$ and $\psi = \boldsymbol{\Psi}\cdot\hat{\mathbf{n}}$. Taking the divergence of (62) and using the incompressibility condition $\nabla\cdot\mathbf{u} = 0$ gives the Laplace problem $\Delta\phi = 0$. Meanwhile, taking the curl of (62) and applying some vector identities leads to the Poisson problem

$$-\Delta\psi = \omega. \tag{63}$$

The point vortices are modeled as singularities in the vorticity field; that is, I assume the vorticity field may be written as the linear combination

$$\omega = \sum_i \Gamma_i\,\delta(\mathbf{x}_i), \tag{64}$$

where δ is the Dirac-delta distribution. The weight Γ_i is called the *strength* of the ith vortex, and it represents the circulation $\oint \mathbf{u}\cdot d\mathbf{l}$ of the fluid around a small loop enclosing only that vortex. To see this, let D denote a small disk centered at $\mathbf{x}_i$ enclosing no other vortices. Green's theorem gives

$$\oint_{\partial D} \mathbf{u}\cdot d\mathbf{l} = \int_D (\nabla\times\mathbf{u})\cdot\hat{\mathbf{n}}\,dA = \int_D \omega\,dA = \sum_i \int_D \Gamma_i\delta(\mathbf{x}_i)\,dA = \Gamma_i,$$

and since the left side is exactly the circulation around the ith vortex, the assertion is proved. To solve the Poisson problem (63), recall the Green's function for the Laplace operator in $\mathbb{R}^2$,

$$G(\mathbf{x};\mathbf{y}) = \frac{1}{2\pi}\log||\mathbf{x}-\mathbf{y}||.$$

Then for a single vortex of strength Γ_i at $\mathbf{x}_i$,

$$\psi(\mathbf{x}) = \int_{\mathbb{R}^2} G(\mathbf{x};\mathbf{y})\,\omega(\mathbf{y})\,d\mathbf{y} = \frac{-\Gamma_i}{2\pi}\log||\mathbf{x}-\mathbf{x}_i||, \tag{65}$$

and for N point vortices superposition gives

$$\psi(\mathbf{x}) = \frac{-1}{2\pi}\sum_{i=1}^{N}\Gamma_i \log||\mathbf{x}-\mathbf{x}_i||.$$

By direct computation,[5] the velocity field is

$$\mathbf{u} = \nabla\times\mathbf{\Psi} = \frac{-1}{2\pi}\sum_{i=1}^{N}\Gamma_i\frac{(y-y^i,-(x-x^i))}{||\mathbf{x}-\mathbf{x}_i||^2}. \tag{66}$$

Of course this velocity field has singularities at each vortex location — which may be interpreted as vortex self-energy as in [39] — and we *regularize* by asserting that the velocity of each vortex is the sum of the velocity contributions from vortices *other than itself*, thus arriving at the well known *point vortex equations*,

$$\begin{aligned}\dot{x}^i &= \frac{-1}{2\pi}\sum_{j\neq i}\Gamma_j\frac{y^i-y^j}{||\mathbf{x}_i-\mathbf{x}_j||^2},\\ \dot{y}^i &= \frac{1}{2\pi}\sum_{j\neq i}\Gamma_j\frac{x^i-x^j}{||\mathbf{x}_i-\mathbf{x}_j||^2}.\end{aligned} \tag{67}$$

As pointed out in [34], this regularization procedure is completely standard and goes back at least to Kirchhoff [31].

In studying the constrained N-vortex problem I will apply Dirac's method of constraints, so I need to get the (67) into Hamiltonian form. With no potential energy, the Hamiltonian H is simply the kinetic energy of the fluid,

$$H = \frac{1}{2}\int_{\mathbb{R}^2}||\mathbf{u}(\mathbf{x})||^2\,d\mathbf{x}.$$

[5] Subscripts denote vortex labels, and superscripts denote components; thus $\mathbf{x}_1 = (x^1, y^1)$, etc.

It can be shown (see [53]) that $\int ||\mathbf{u}||^2 = \int \omega\, \psi$, so that by using (64) and (65),

$$H = \frac{1}{2}\int_{\mathbb{R}^2} \left(\sum_i \Gamma_i \delta(\mathbf{x}_i) \right) \psi(\mathbf{x})\, d\mathbf{x} = \frac{1}{2}\sum_i \Gamma_i \psi(\mathbf{x}_i) = \frac{-1}{4\pi}\sum_{j>i} \Gamma_i \Gamma_j \log ||\mathbf{x}_i - \mathbf{x}_j||^2. \tag{68}$$

By introducing the (noncanonical) Poisson bracket

$$\{f, g\} \coloneqq \sum_i \frac{1}{\Gamma_i} \left(\frac{\partial f}{\partial x^i}\frac{\partial g}{\partial y^i} - \frac{\partial f}{\partial y^i}\frac{\partial g}{\partial x^i} \right), \tag{69}$$

one may verify that Hamilton's equations (13)

$$\begin{aligned} \dot{x}^i &= \{x^i, H\}, \\ \dot{y}^i &= \{y^i, H\}, \end{aligned} \tag{70}$$

relative to (69) and (68) reproduce the point vortex equations (67). (This is rather unusual in that a position coordinate, y, is playing the role of conjugate momenta.)

6.3 The Constrained N-Vortex Problem

I now introduce constraints into the N-vortex problem. I consider the following four concrete examples, the first three of which are illustrated in Figure 48.

1. A velocity constraint, in which the fluid velocity at a point is required to maintain its initial velocity at that point for all time. The case of zero initial velocity gives a stagnation-point constraint, modeling an infinitesimally small cylinder immersed in the fluid.

2. A direction constraint, in which the fluid velocity at a specified point is tangent to a fixed direction for all time, modeling an infinitesimally small rigid fin immersed in the fluid.

3. A distance constraint, in which a pair of vortices must maintain a fixed distance from one another at all times, modeling a vortex dipole.

4. A position constraint, in which one or more vortices are forced to move so as to satisfy a given condition, to be used in modeling certain fluid-solid interactions.

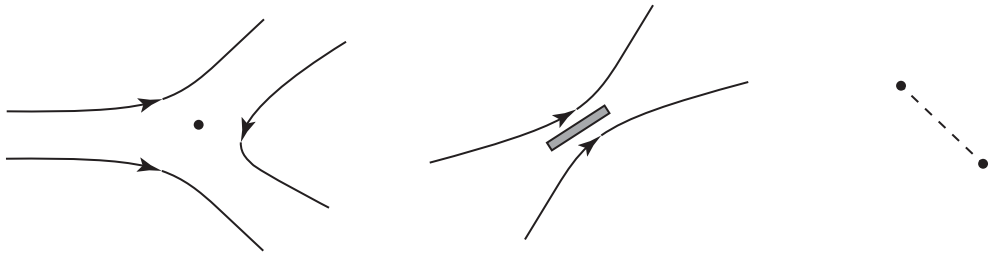

Figure 48: A (zero) velocity constraint (left), a direction constraint (center), and a distance constraint (right).

In Lagrangian mechanics constraints may be treated with Lagrange multipliers. However, the N-vortex dynamics encoded in (70) are in Hamiltonian form. One way of treating constraints in Hamiltonian mechanics is by Dirac's method of constraints, first introduced in [14] and further expounded upon in [15] and [38], the latter of which I take as my primary reference. When a constraint is present, trajectories evolve on a constraint submanifold, and the essence of Dirac's method is that the ordinary Poisson bracket $\{f, g\}$ may contain terms representing derivatives of f and g along directions pointing out of the constraint submanifold. Since the motion is confined to the constraint submanifold, however, the offending terms must be subtracted off; doing so produces a new bracket, called the Dirac bracket, relative to which the equations of motion are in Hamiltonian form.

Before stating the relevant theorem, recall that an embedded submanifold S of a symplectic manifold (P, Ω) is a symplectic submanifold if $\omega \coloneqq i^*\Omega$ is a symplectic

form on S, where $i : S \hookrightarrow P$ is the inclusion map. The submanifold inherits a Poisson bracket that is related to the bracket on P by the following modern formulation of Dirac's theorem. The reader is referred to [38] for more details on this theorem, including a coordinate-free version, and its proof.

THEOREM 17 (Dirac). *Let (P, Ω) be a symplectic manifold of dimension $2n$, and let $S \subset P$ be an embedded, symplectic submanifold of dimension $2k$ with $k < n$. Endow P with the induced Poisson bracket $\{f, g\} \coloneqq \Omega(X_f, X_g)$. Assume (U, z^i) is a chart for P on which*

$$S \cap U = \{z \in U : z^{2k+1} = \cdots = z^{2n} = 0\}.$$

Let (C_{ij}) be the inverse of the matrix (C^{ij}), where $C^{ij} \coloneqq \{z^i, z^j\}$ for $i, j = 2k + 1, \ldots, 2n$. If $f|_S$ and $g|_S$ denote the restrictions of $f, g : P \to \mathbb{R}$ to S, then

$$\{f|_S, g|_S\} = \{f, g\} - \sum_{i,j=2k+1}^{2n} \{f, z^i\} C_{ij} \{z^j, g\},$$

and

$$X_{f|_S} = X_f - \sum_{i,j=2k+1}^{2n} \{f, z^i\} C_{ij} X_{z^j}.$$

Define the *Dirac bracket* $[\cdot, \cdot]$ by

$$[f, g] \coloneqq \{f|_S, g|_S\} = \{f, g\} - \sum_{i,j=2k+1}^{2n} \{f, z^i\} C_{ij} \{z^j, g\}. \tag{71}$$

The time evolution of a function f along a trajectory of the constrained system is

$$\dot{f} = [f, H].$$

A concrete example of Dirac's method appears in Appendix B.

To explain how this method may be used to handle the constraints above, recall that the velocity field of the fluid may be expressed via (66) in terms of the locations and strengths of the point vortices. Therefore, provided a constraint or system of constraints can be expressed in terms of the fluid flow at finitely many points, then it may be recast in terms of the locations and strengths of the point vortices. The remaining sections in this chapter apply this technique to the hydrodynamic constraints listed above.

6.4 Velocity Constraint

For this constraint, the fluid velocity at a specified point must maintain its initial value for all time. This initial velocity can be made arbitrary by judiciously choosing initial placement of the vortices. Without loss of generality, I assume the point in question to be the origin. The constraint, therefore, is that $\mathbf{u}(\mathbf{0}, t) = \mathbf{u}(\mathbf{0}, 0)$ for all $t \geq 0$.

To keep the complexity somewhat under control, I take $N = 3$ in this example. With three vortices the phase space is twelve-dimensional: there are 6 phase space variables encoding the positions of the three vortices and six encoding their momenta. Let the vortex strengths be $\Gamma_1 = \Gamma_2 = \Gamma_3 = 1$ and write their locations as $\mathbf{x}_1 = (x^1, y^1)$, $\mathbf{x}_2 = (x^2, y^2)$, and $\mathbf{x}_3 = (x^3, y^3)$. If u, v are the components of the fluid velocity, i.e. $\mathbf{u} = (u, v)$, then (66) gives the velocity field due to these three unit-

strength vortices as

$$u(x,y) = \frac{-1}{2\pi}\left(\frac{y-y^1}{(x-x^1)^2+(y-y^1)^2} + \frac{y-y^2}{(x-x^2)^2+(y-y^2)^2} + \frac{y-y^3}{(x-x^3)^2+(y-y^3)^2}\right),$$
$$v(x,y) = \frac{-1}{2\pi}\left(\frac{x^1-x}{(x-x^1)^2+(y-y^1)^2} + \frac{x^2-x}{(x-x^2)^2+(y-y^2)^2} + \frac{x^3-x}{(x-x^3)^2+(y-y^3)^2}\right). \tag{72}$$

Since the velocity field $\mathbf{u} = (u, v)$ is now expressed solely in terms of the point vortex locations, the constraint may be expressed in terms of the phase space variables, and Dirac's method of constraints may be applied. In particular, define $(u_0, v_0) \coloneqq \mathbf{u}(\mathbf{0}, 0)$. Then the constraint $\mathbf{u}(\mathbf{0}, t) = \mathbf{u}(\mathbf{0}, 0)$ is, according to (72),

$$\frac{-y^1}{(x^1)^2+(y^1)^2} + \frac{-y^2}{(x^2)^2+(y^2)^2} + \frac{-y^3}{(x^3)^2+(y^3)^2} + 2\pi u_0 = 0,$$
$$\frac{x^1}{(x^1)^2+(y^1)^2} + \frac{x^2}{(x^2)^2+(y^2)^2} + \frac{x^3}{(x^3)^2+(y^3)^2} - 2\pi v_0 = 0.$$

To apply Theorem 17, I now define z^{11} and z^{12} by the left sides of the preceding equations, so that the constraint submanifold is described locally by $z^{11} = z^{12} = 0$. Now define the Dirac bracket according to (71) and (69). With the point-vortex Hamiltonian H given by (68), the unconstrained and constrained equations of motion are

$$\dot{x}^i = \{x^i, H\}, \qquad \dot{y}^i = \{y^i, H\}, \qquad \text{(unconstrained dynamics)}$$
$$\dot{x}^i = [x^i, H], \qquad \dot{y}^i = [y^i, H], \qquad \text{(constrained dynamics)}.$$

For the unconstrained N-vortex problem, the Hamiltonian exhibits translational and rotational symmetries, so by Noether's theorem there are corresponding conserved

quantities. In fact, four integrals of motion are known,

$$\begin{aligned} H &= \frac{-1}{4\pi} \sum_{j>i} \Gamma_i \Gamma_j \log ||\mathbf{x}_i - \mathbf{x}_j||^2, \\ Q &= \sum_i \Gamma_i x^i, \\ P &= \sum_i \Gamma_i y^i, \\ J &= \sum_i \Gamma_i ||\mathbf{x}_i||^2. \end{aligned} \tag{73}$$

The first of these is just the Hamiltonian (68), encoding the system's total energy. The quantities Q and P are the components of the system's *linear impulse*, and J is the *angular impulse*. The reader is referred to [46] and [34] for further details. In this and the following examples, I plot these four quantities for both the unconstrained and constrained dynamics; in the former case to verify accuracy of the numerical integration, and in the latter case to investigate the energy or momentum imparted to the fluid by the constraints.

I now consider, for a typical set of parameters, the unconstrained and constrained dynamics. The unconstrained vortex trajectories are shown in Figure 49. They are seen to orbit around the *center of vorticity* $\mathbf{x}_*$ defined by

$$\mathbf{x}_* \coloneqq \frac{1}{\sum_i \Gamma_i} \sum_i \mathbf{x}_i,$$

which for this problem is $\mathbf{x}_* = (1/3, 0)$. As time evolves, their trajectories seem to densly fill a certain subset of the plane. Next, Figure 50 shows the energy H, components Q, P of linear impulse, and angular impulse J for the unconstrained motion of the vortices. Note that, as expected, these quantities are all conserved.

The fluid velocity $\mathbf{u}(\mathbf{0}, t) = (u(0, t), v(0, t))$ is graphed in Figure 51. Note that as the vortices evolve in the fluid, the velocity at the origin is changing in a periodic fashion that corresponds to the periodic motion of the vortices.

Turning to the constrained dynamics, the vortex trajectories are shown in Figure 52. Qualitatively, these trajectories exhibit similar periodic behavior as for the unconstrained dynamics, and although they still appear to densly fill a subregion of the plane, the vortices no longer orbit the center of vorticity; instead, the center of their orbit has been shifted to the left half-plane. In Figure 53, the energy H, components Q, P of linear impulse, and angular impulse J are shown, but now we see that the constraint breaks the conservation of both linear and angular impulse, although it does conserve the energy H. Furthermore, the magnitude of the linear impulse $\sqrt{P^2 + Q^2}$ and that of the angular impulse $|J|$ of the fluid are fluctuating periodically. Finally, the fluid velocity $\mathbf{u}(\mathbf{0}, t) = (u(0, t), v(0, t))$ is graphed in Figure 54, and we see that the method introduced here succeeds in forcing the fluid velocity to maintain its initial value at the origin.

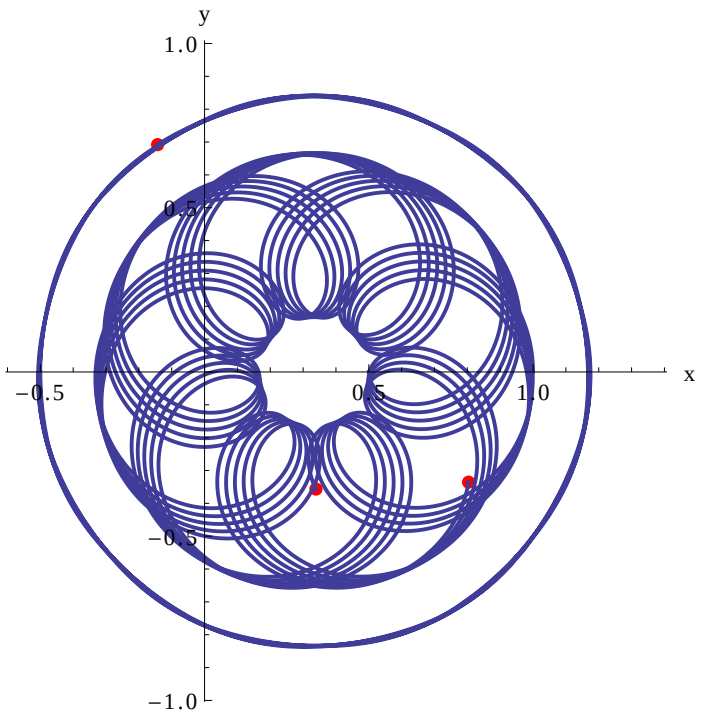

$0 \le t \le 100,\ \Gamma_1 = 1,\ \Gamma_2 = 1,\ \Gamma_3 = 1,\ x_1 = (-0.5, 0.),\ x_2 = (0.5, 0.),\ x_3 = (1., 0.)$

Figure 49: Unconstrained vortex dynamics.

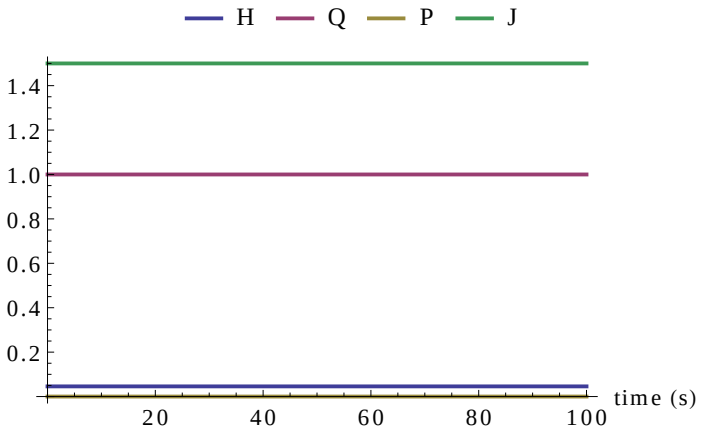

$0 \le t \le 100,\ \Gamma_1 = 1,\ \Gamma_2 = 1,\ \Gamma_3 = 1,\ x_1 = (-0.5, 0.),\ x_2 = (0.5, 0.),\ x_3 = (1., 0.)$

Figure 50: Energy H, components Q, P of linear impulse, and angular impulse J for the motion of the vortices in Figure 49.

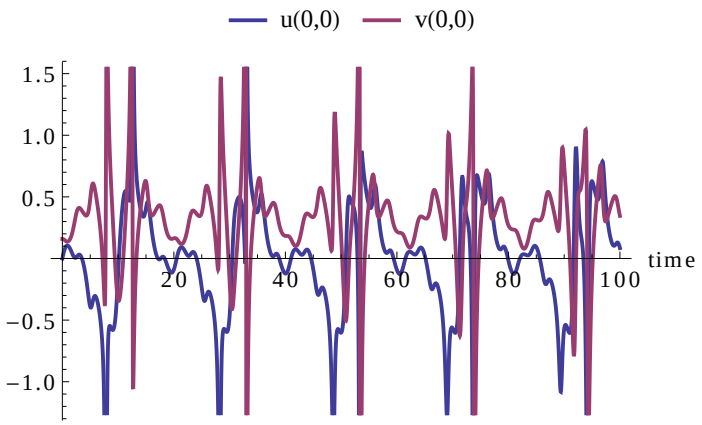

$0 \le t \le 100,\ \Gamma_1 = 1,\ \Gamma_2 = 1,\ \Gamma_3 = 1,\ x_1 = (-0.5, 0.),\ x_2 = (0.5, 0.),\ x_3 = (1., 0.)$

Figure 51: Fluid velocity at the origin for the motion of the vortices in Figure 49.

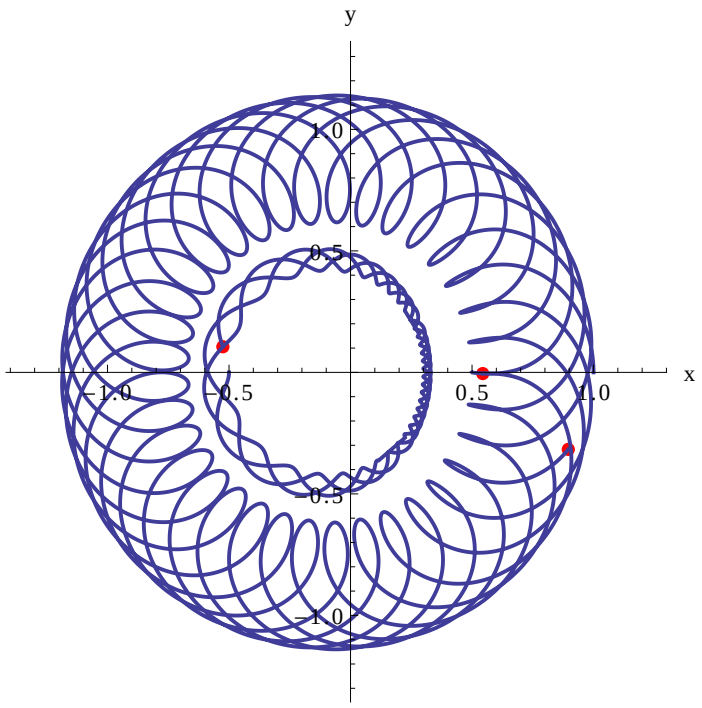

$0 \le t \le 100,\ \Gamma_1 = 1,\ \Gamma_2 = 1,\ \Gamma_3 = 1,\ x_1 = (-0.5, 0.),\ x_2 = (0.5, 0.),\ x_3 = (1., 0.)$

Figure 52: Trajectories of the vortices considered in Figure 49, but subject now to the constraint the fluid velocity at the origin maintains its initial value.

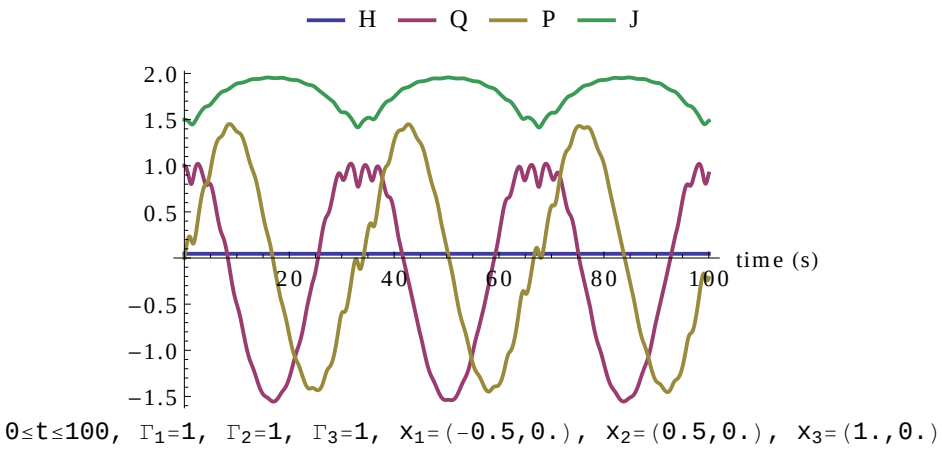

Figure 53: Energy H, components Q, P of linear impulse, and angular impulse J for the motion of the vortices in Figure 52

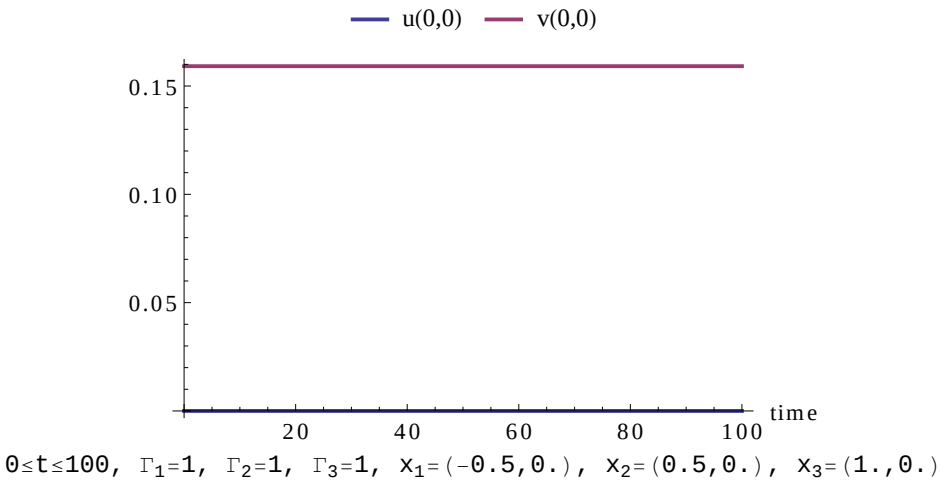

Figure 54: Fluid velocity at the origin for the motion of the vortices in Figure 52.

6.5 Direction Constraint

I now consider a different kind of hydrodynamic constraint, one that might arise from the presence of an infinitesimal fin immersed in the fluid, as shown in the middle panel of Figure 48. Such a fin would not constrain the speed of the fluid at the given point, but only its direction — which must be tangent to the fin. This is, therefore, the hydrodynamic analog of the nonholonomic no-slip constraint appearing in the

Chaplygin control systems of Chapter 4.

If a fin tangent to the vector $\mathbf{v}$ is placed at a point $\mathbf{p}$, the resulting constraint is that $\mathbf{u}(\mathbf{p}, t) \cdot \mathbf{v} = 0$ for all time t. Unlike the velocity constraint considered in the previous section, this is a scalar constraint. Since an even number of constraint equations is needed for Dirac's method, I place two fins in the fluid at points $\mathbf{p}_1, \mathbf{p}_2$ with corresponding orientations $\mathbf{v}_1, \mathbf{v}_2$. Furthermore, since the initial conditions must satisfy the constraints, I chose the initial vortex positions arbitrarily, determined the resulting velocity field according to (66), and then selected arbitrary locations $\mathbf{p}_1, \mathbf{p}_2$ for the fins and set $\mathbf{v}_1, \mathbf{v}_2$ equal to the initial fluid velocity at these points. In other words, I placed the fins so that the initial fluid velocity was guaranteed to satisfy the constraints. The two constraint equations are

$$\mathbf{u}(p_1, t) \cdot \mathbf{v}_1 = 0,$$

$$\mathbf{u}(p_2, t) \cdot \mathbf{v}_2 = 0.$$

The unconstrained vortex trajectories are shown in Figure 55. Next, Figure 56 shows the energy H, components Q, P of linear impulse, and angular impulse J for the unconstrained motion of the vortices. As before, these quantities are all conserved. The component u_n of the fluid velocity normal to the two fins appearing in Figure 58 is graphed in Figure 57. Note that the fluid velocity at the origin is always horizontal, even in the unconstrained system, by symmetry of the vortex locations. Since all the vortices are of equal strength and symetrically aligned along the vertical axis, the fluid velocity at the origin must be horizontal by symmetry. At the other fin location, however, the normal component of the fluid velocity is not conserved, and there is no

reason it should be.

Turning to the constrained dynamics, the vortex trajectories are shown in Figure 58. Here — unlike for the velocity constraint — the unconstrained and constrained vortex trajectories are dramatically different. The introduction of the constraints has pushed the dynamics from a symmetric periodic orbit to an asymmetric scattering orbit. In Figure 59, the energy H, components Q, P of linear impulse, and angular impulse J are shown. As before, energy is still conserved, but the constraint breaks the conservation of both linear and angular impulse. The magnitude $\sqrt{P^2+Q^2}$ of the linear impulse and that of the angular impulse $|J|$ are increasing with time as well, so the constraint is injecting linear and angular momentum into the fluid. Finally, Figure 60 graphs the normal velocity of the fluid at the location of the two fins. It is effectively zero at both locations, which means the velocity field is indeed tangent to the two fins, as required.

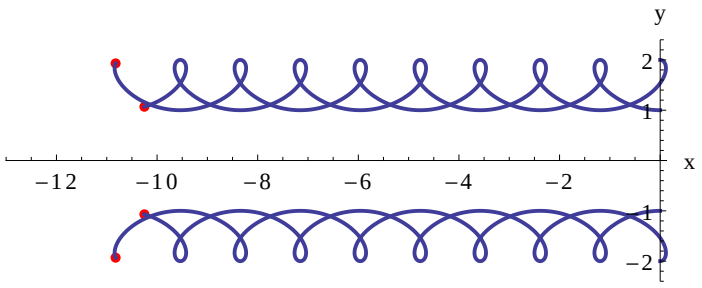

$0 \le t \le 100,\ \Gamma_1 = 1,\ \Gamma_2 = 1,\ \Gamma_3 = -1,\ x_1 = (0., -2.),\ x_2 = (0., -1.),\ x_3 = (0., 1.),\ x_4 = (0., 2.)$

Figure 55: Unconstrained vortex dynamics.

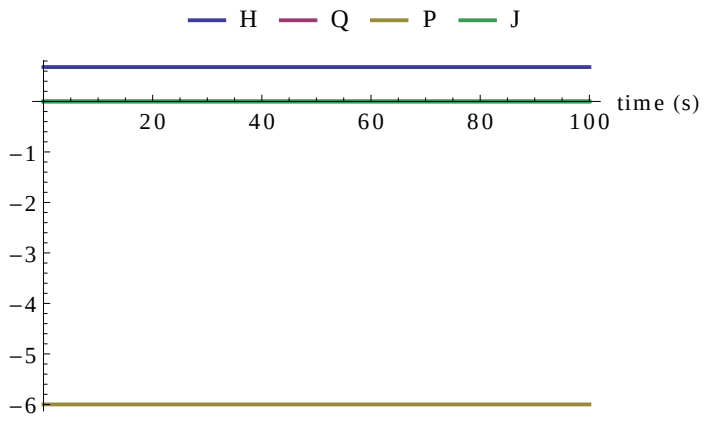

$0 \le t \le 100$, $\Gamma_1 = 1$, $\Gamma_2 = 1$, $\Gamma_3 = -1$, $x_1 = (0., -2.)$, $x_2 = (0., -1.)$, $x_3 = (0., 1.)$, $x_4 = (0., 2.)$

Figure 56: Energy H, components Q, P of linear impulse, and angular impulse J for the motion of the vortices in Figure 55.

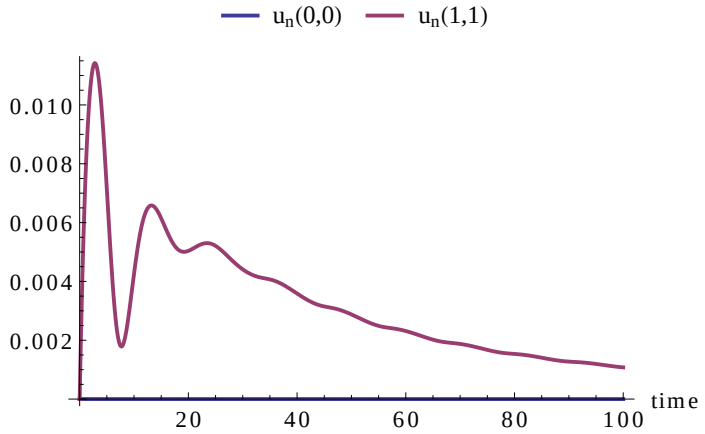

$0 \le t \le 100$, $\Gamma_1 = 1$, $\Gamma_2 = 1$, $\Gamma_3 = -1$, $x_1 = (0., -2.)$, $x_2 = (0., -1.)$, $x_3 = (0., 1.)$, $x_4 = (0., 2.)$

Figure 57: Component u_n of the fluid velocity normal to the infinitesimal fins at $(0, 0)$ and $(1, 1)$ for the unconstrained vortices of Figure 55.

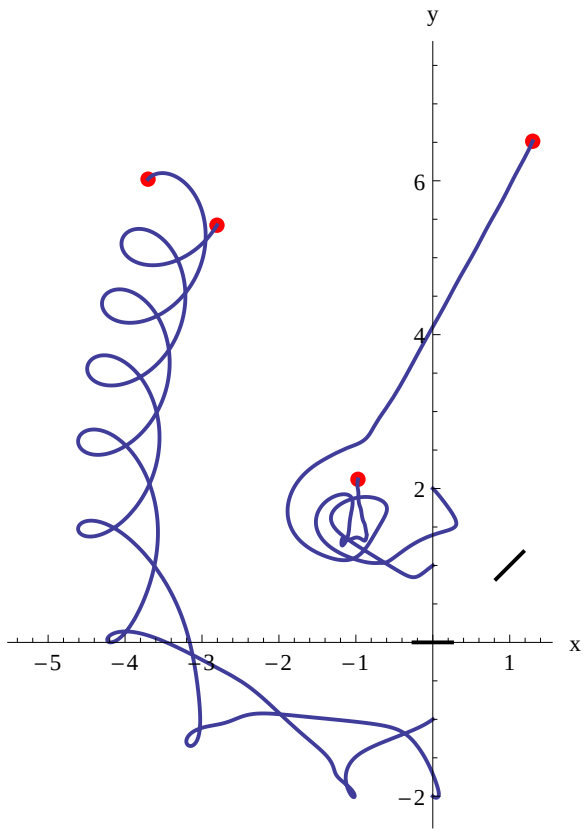

$0 \le t \le 100,\ \Gamma_1 = 1,\ \Gamma_2 = 1,\ \Gamma_3 = -1,\ x_1 = (0., -2.),\ x_2 = (0., -1.),\ x_3 = (0., 1.),\ x_4 = (0., 2.)$

Figure 58: Trajectories of the vortices considered in Figure 55, but subject now to the constraint that the fluid velocity is tangent to the two infinitesimal fins shown in the figure as thick black line segments.

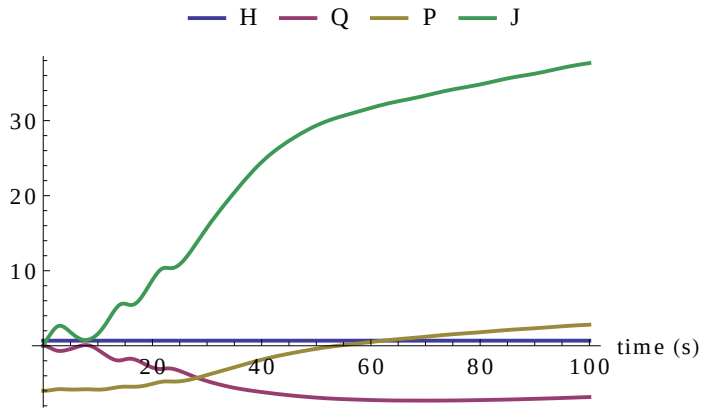

$0 \le t \le 100,\ \Gamma_1 = 1,\ \Gamma_2 = 1,\ \Gamma_3 = -1,\ x_1 = (0., -2.),\ x_2 = (0., -1.),\ x_3 = (0., 1.),\ x_4 = (0., 2.)$

Figure 59: Energy H, components Q, P of linear impulse, and angular impulse J for the motion of the vortices in Figure 58

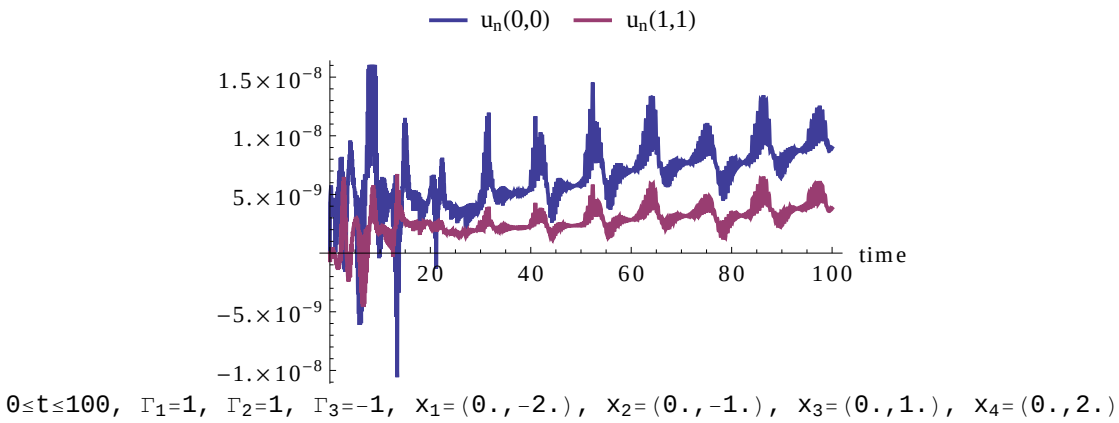

Figure 60: Component u_n of the fluid velocity normal to the infinitesimal fins at $(0,0)$ and $(1,1)$ for the constrained vortices of Figure 58.

6.6 Distance Constraint

Now I consider a third kind of hydrodynamic constraint, a distance constraint. I require the distance between a pair of vortices to maintain their initial values, as illustrated in the third panel of Figure 48. If the two vortices have positions $\mathbf{x}_1, \mathbf{x}_2$ and are initially separated by a distance d_0, the constraint is that $||\mathbf{x}_1 - \mathbf{x}_2|| = d_0$ for all time. That is, $\sqrt{(\mathbf{x}_1 - \mathbf{x}_2) \cdot (\mathbf{x}_1 - \mathbf{x}_2)} = d_0$. To avoid numerical complications with square roots, I use the equivalent formulation that

$$(\mathbf{x}_1 - \mathbf{x}_2) \cdot (\mathbf{x}_1 - \mathbf{x}_2) - d_0^2 = 0.$$

This is a single scalar equation. To get an even number of constraint equations for Dirac's method, I consider the three-vortex problem and impose the constraints that the distances between $\mathbf{x}_1$ and $\mathbf{x}_2$ and between $\mathbf{x}_2$ and $\mathbf{x}_3$ remain constant.

The unconstrained vortex trajectories for a typical set of parameters are shown in Figure 61. The vortices orbit around their center of vorticity, located at approxi-

mately $(0.60, -0.17)$. Next, Figure 62 shows the energy H, components Q, P of linear impulse, and angular impulse J for the unconstrained motion of the vortices. These quantities are all conserved. The distances between the first and second and between the second and third vortices, graphed in Figure 63, are seen to undergo periodic variations consistent with Figure 61.

Turning to the constrained dynamics, the vortex trajectories are shown in Figure 64. Here we see that the motion is simply rigid body rotation, which is also verified by the graphs of the distances between the two pairs of vortices shown in Figure 66. This may be explained heuristically as follows. It is known that two vortices of equal strength orbit one another in a circular fashion about their center of vorticity (see [46] or [53]), so one of these two distance constraints adds nothing. The third vortex is constrained to move at a fixed distance from the second, so this leaves two possibilities — an orbit resembling the Sun-Earth-Moon system (circles within circles), or a rigid body rotation. I don't have a good explanation for why the latter motion is chosen, and perhaps the former is possible in other cases. In Figure 65, the energy H, components Q, P of linear impulse, and angular impulse J are shown. We see that all of them are conserved by the system, consistent with the uniform rotation of a rigid body.

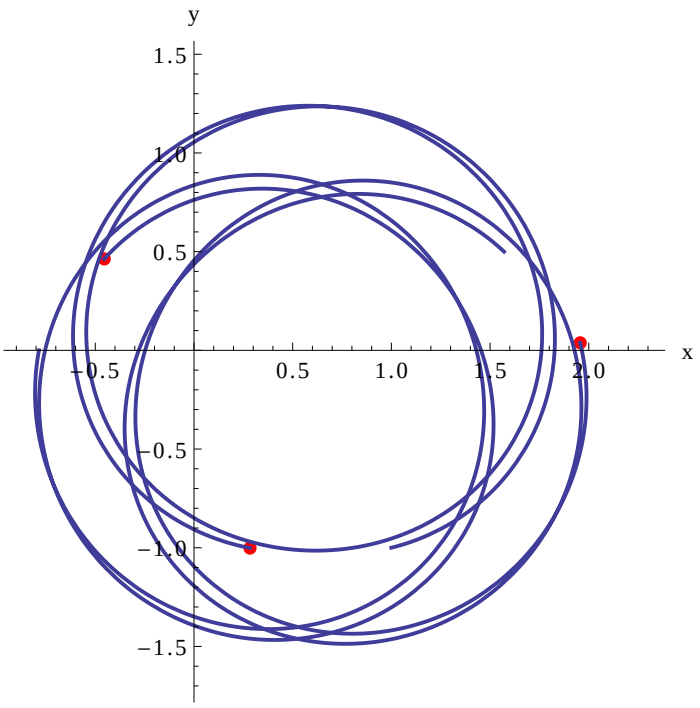

$0 \le t \le 100,\ \Gamma_1 = 1,\ \Gamma_2 = 1,\ \Gamma_3 = 1,\ x_1 = (-0.785398, 0.),\ x_2 = (1.5708, 0.5),\ x_3 = (1., -1.)$

Figure 61: Unconstrained vortex dynamics.

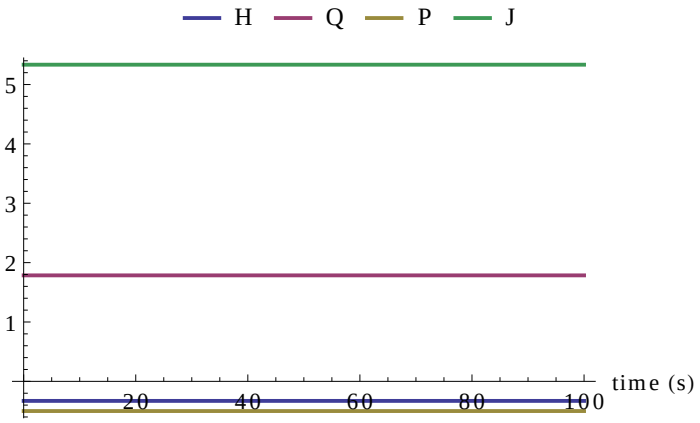

$0 \le t \le 100,\ \Gamma_1 = 1,\ \Gamma_2 = 1,\ \Gamma_3 = 1,\ x_1 = (-0.785398, 0.),\ x_2 = (1.5708, 0.5),\ x_3 = (1., -1.)$

Figure 62: Energy H, components Q, P of linear impulse, and angular impulse J for the motion of the vortices in Figure 61.

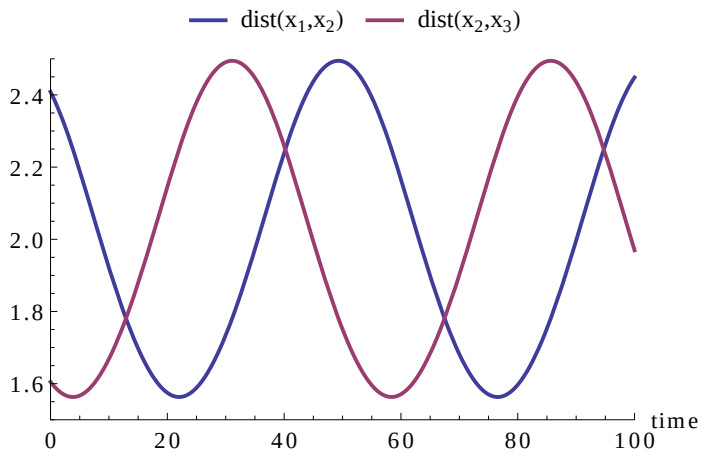

$0 \le t \le 100,\ \Gamma_1=1,\ \Gamma_2=1,\ \Gamma_3=1,\ \mathbf{x}_1=(-0.785398, 0.),\ \mathbf{x}_2=(1.5708, 0.5),\ \mathbf{x}_3=(1., -1.)$

Figure 63: Inter-vortex distances for the unconstrained motion of the vortices in Figure 61.

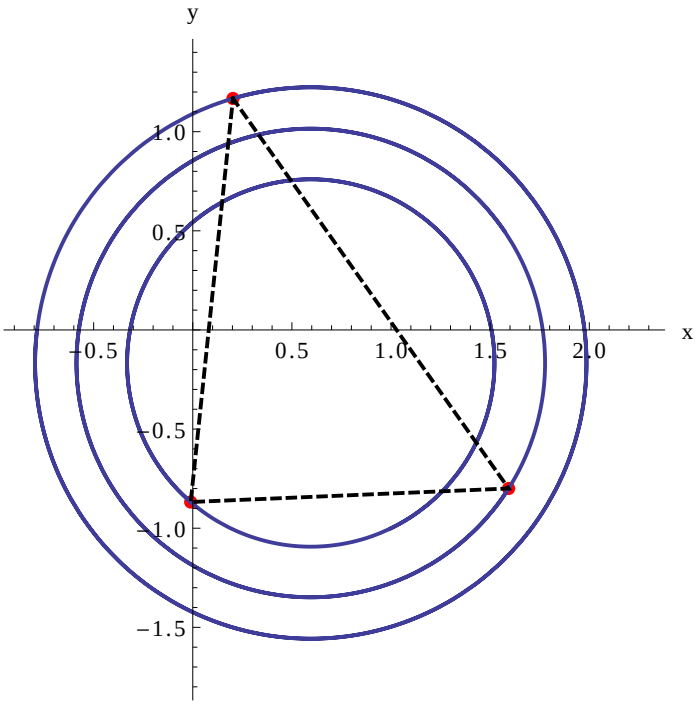

$0 \le t \le 100,\ \Gamma_1=1,\ \Gamma_2=1,\ \Gamma_3=1,\ \mathbf{x}_1=(-0.785398, 0.),\ \mathbf{x}_2=(1.5708, 0.5),\ \mathbf{x}_3=(1., -1.)$

Figure 64: Trajectories of the vortices considered in Figure 61, but subject now to the constraint the distances between $\mathbf{x}_1$ and $\mathbf{x}_2$, and between $\mathbf{x}_2$ and $\mathbf{x}_3$ are constant. The vortices evolve so that the triangle, signified with a dashed line, rotates as if it were a rigid body.

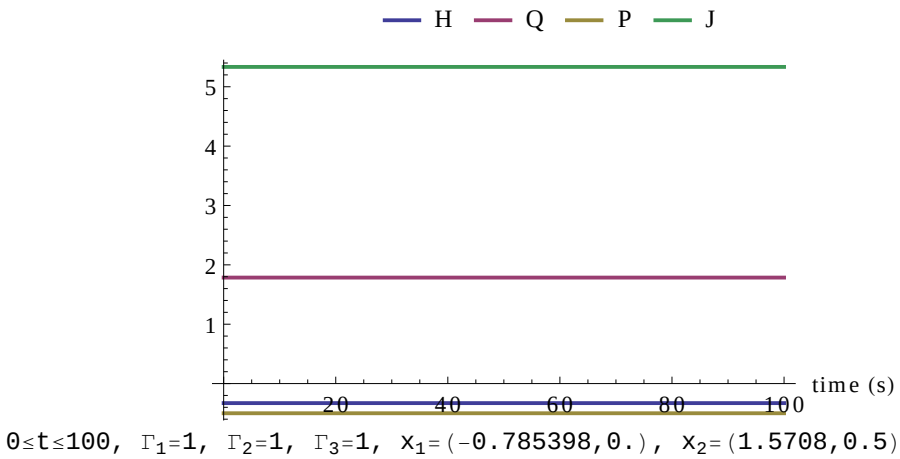

Figure 65: Energy H, components Q, P of linear impulse, and angular impulse J for the motion of the vortices in Figure 64

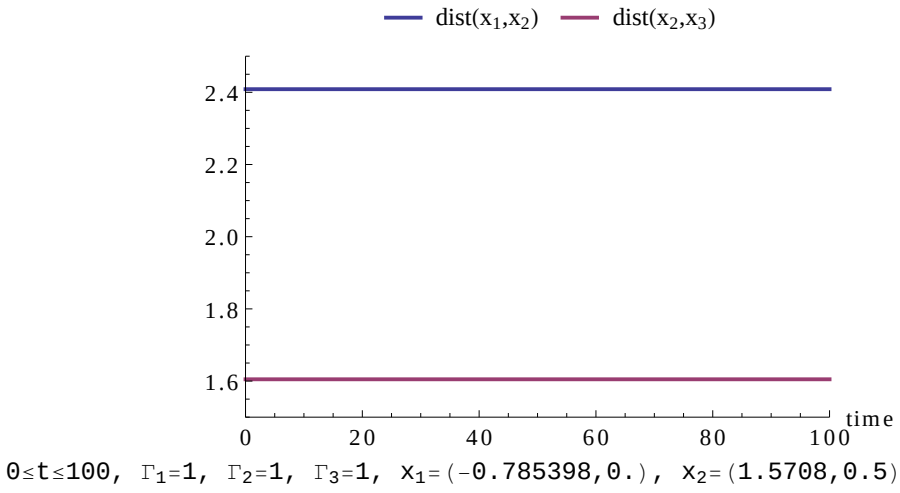

Figure 66: Inter-vortex distance for the constrained motion of the vortices in Figure 58.

6.7 Point Vortex and a Rigid Body

The final problem I consider is using constrained vortex dynamics as a reduced-order model for the interaction of rigid bodies with point vortices. The most basic problem of this form is the dynamic interaction of a rigid cylinder and a single external point vortex. As mentioned in the introduction to this chapter, the fully nonlinear equations of motion for this system — in terms of an exact reduced-order model —

were only recently discovered in [55] and [10]. The dynamics of a cylinder and a single external point vortex given by the equations in [55] are shown in Figure 67. This paper demonstrated that if the vortex strengths sum to zero and the cylinder has circular cross section, then the resulting equations are Hamiltonian relative to a Poisson bracket that is the sum of the rigid body Lie-Poisson bracket on the dual of the Lie algebra $\mathfrak{se}(2)$ and the standard Poisson bracket for point vortices in the unbounded plane, (69). The equations of motion were derived by a lengthy and ad hoc control volume analysis, and the Hamiltonian formulation was essentially discovered by accident. The equations in [10] were derived by a different method, but [61] showed that they are ultimately equivalent to those in [55]. The question I ask in this section is — rather than carrying out a difficult control-volume analysis, to what extent can the dynamic interaction of rigid bodies with an inviscid incompressible fluid with vorticity be modeled by judiciously introducing constraints into the classical N-vortex problem? If this is possible at all, it should be so for the simplest case of a rigid circular cylinder interacting with a single external point vortex.

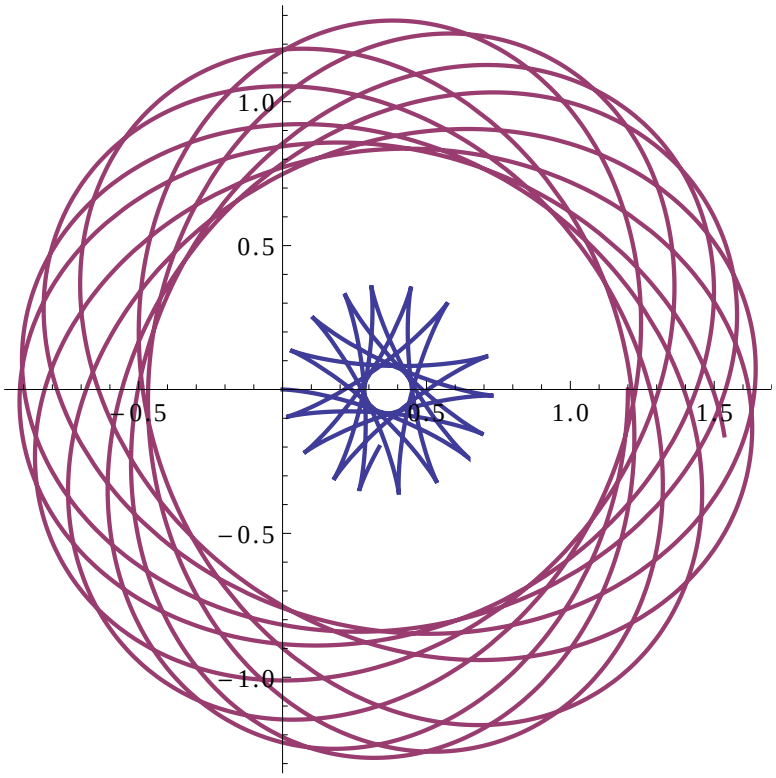

Figure 67: Trajectories over the interval $0 \leq t \leq 250$ for a rigid cylinder and a vortex of unit strength interacting dynamically according to the equations in [55]. The cylinder is taken to have unit radius and mass-plus-added-mass equal to 2π. The central trajectory gives the position of the center of the cylinder, and the outer trajectory depicts the position of the external vortex.

To obtain an approximate model using constrained vortex dynamics, I will use the method of images. Recall that the *complex potential* for an ideal fluid with flow velocity $\mathbf{u}$ in the complex plane is the function $f : \mathbb{C} \to \mathbb{C} : z \mapsto \phi(z) + i\psi(z)$, where ϕ is the *velocity potential* satisfying $\mathbf{u} = \nabla\phi$ and ψ is the *stream function* satisfying $(\mathbf{u} \cdot \nabla)\psi = 0$. The complex potential for a single point vortex of strength Γ at z_0 is shown in [2] to be the function $z \mapsto \frac{\Gamma}{2\pi i} \log(z - z_0)$. By superposition, the complex potential $f(z)$ for N point vortices of strengths $\Gamma_1, \ldots, \Gamma_N$ is

$$f(z) = \frac{1}{2\pi i} \sum_{i=1}^{N} \Gamma_i \log(z - z_i).$$

Recall now the Milne-Thomson circle theorem, also appearing in [2], which is a method of images for the Laplace problem in circular domains.

THEOREM 18 (Milne-Thomson Circle). *If $f : \mathbb{C} \to \mathbb{C}$ is the complex potential for a flow whose singularities are external to the circle $|z| = a$, then the complex potential $w : \mathbb{C} \to \mathbb{C}$ for a flow with this circle as a streamline and having the same singularities external to this circle is given by*

$$w(z) \coloneqq f(z) + \overline{f(a^2/\overline{z})}.$$

Note that if a point vortex singularity is located at a point z_0 outside the circle $|z| = a$, then $a^2/\overline{z}_0$ lies interior to this circle. In effect, the theorem makes the circle a streamline at the cost of introducing new singularities at certain image points inside the circle.

Returning to the cylinder and vortex problem, assume the vortex has strength Γ. At all times the boundary of the cylinder is a streamline of the fluid flow. Coupled with the Milne-Thomson theorem, this suggests that the dynamics may be modeled by a constrained 3-vortex problem such that one vortex of strength Γ lies exterior to the cylinder, another vortex of strength $-\Gamma$ is constrained to reside at the Milne-Thomson image location, and a third vortex of strength Γ is placed at the location where the cylinder's center would be in order to cancel — or more generally, set to any desired value — the circulation around the cylinder. For this constrained 3-vortex problem, the circulation around the cylinder matches that of the cylinder+vortex problem, and there is a streamline where the cylinder would be.

To make the foregoing considerations more definite, let a be the radius of the

cylinder. Let $z_1 = (x^1, y^1)$ denote the position of the vortex where the cylinder's center would be, let $z_2 = (x^2, y^2)$ be the position of the Milne-Thomson image vortex, and let $z_3 = (x^3, y^3)$ denote the position of the external vortex. The Milne-Thomson constraint becomes the pair of equations

$$x^2 - x^1 - \frac{a^2(x^3 - x^1)}{(x^3 - x^1)^2 + (y^3 - y^1)^2} = 0,$$
$$y^2 - y^1 - \frac{a^2(y^3 - y^1)}{(x^3 - x^1)^2 + (y^3 - y^1)^2} = 0.$$

If one applies Dirac's method with these constraint equations in the same manner as in the previous examples, the resulting vortex trajectories are shown in Figure 68. The innermost trajectory near the origin shows the cylinder's location, the middle trajectory is of the image vortex, and the outer trajectory is that of the external point vortex. On the scale shown in the figure, the motion of the central vortex is not so clear, so a blown-up version of it is shown in Figure 69. We see that the motion of the cylinder and external point vortex are qualitatively similar, but different in detail, to those given by Figure 67. In particular, the exterior vortex is seen to orbit around the cylinder in a Lissajous-like pattern, and the central vortex (cylinder location) undergoes quasiperiodic motion, both of which resemble the motion in Figure 67. These encouraging results demonstrate that it may be appropriate in certain situations to model complicated interactions of solids and fluids with conceptually simpler point vortex dynamics.

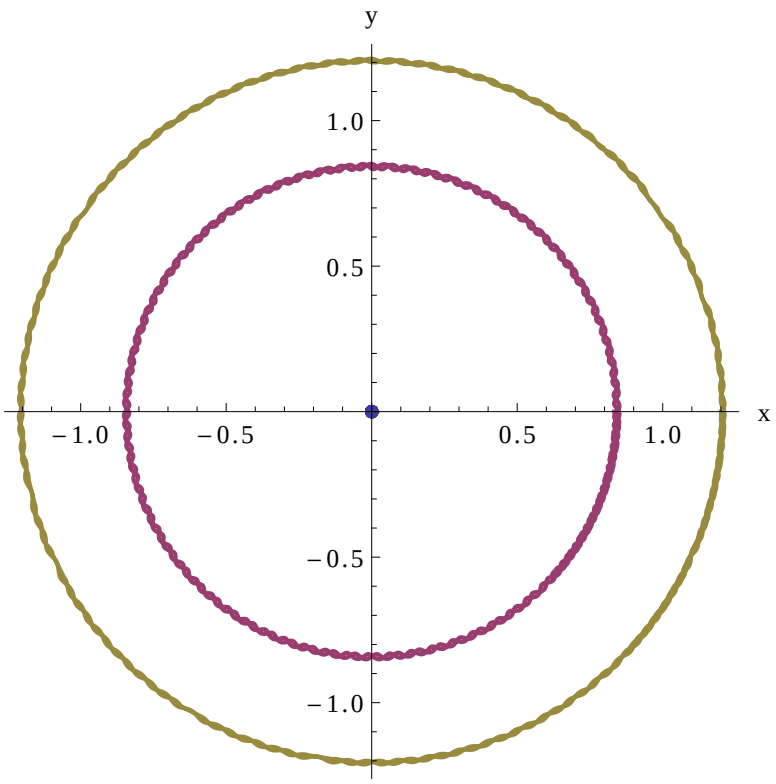

Figure 68: Motion of three vortices of strengths $\Gamma_1 = 1$, $\Gamma_2 = -1$, and $\Gamma_3 = 1$ modeling a circular cylinder interacting with a single external point vortex over the interval $0 \leq t \leq 100$.

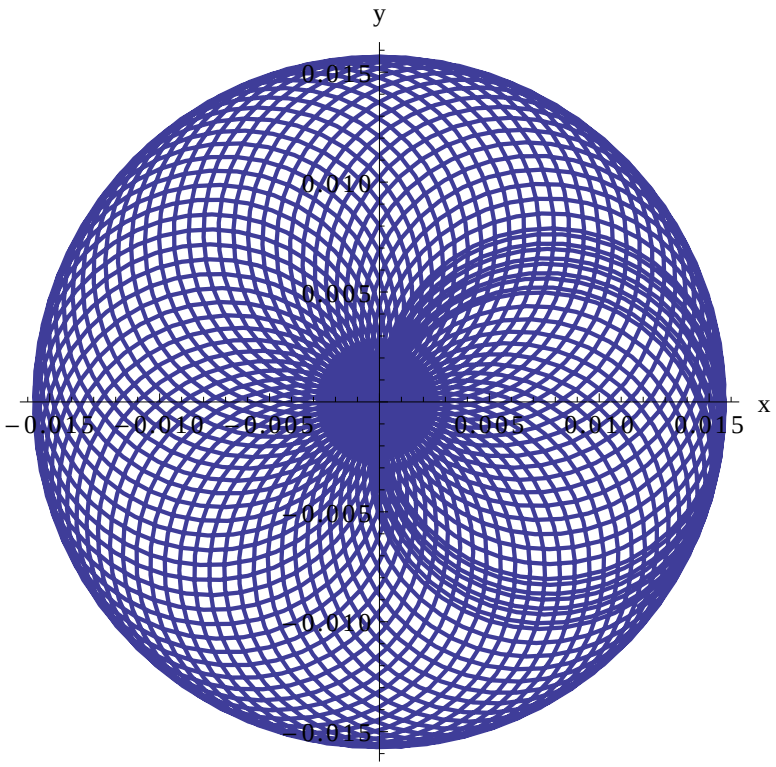

Figure 69: Motion for $0 \leq t \leq 50$ of the central vortex in Figure 68.

6.8 Summary

In this chapter I devised new reduced-order models for hydrodynamic constraints arising from fixed rigid bodies immersed in inviscid incompressible fluids with point vorticity by applying Dirac's method to judiciously chosen constraints in the Hamiltonian formulation of the classical N-vortex problem for four different classes of constraints — velocity, direction, distance, and position. I found that the constraints generally preserve energy while modifying the linear and angular impulse of the system, and that they may change the qualitative nature of the dynamics, for example changing a periodic orbit to a scattering orbit. Finally, I showed that constrained vortex dynamics may be used to develop approximate reduced-order models for the interaction of moving rigid bodies and vortical fluids.

CHAPTER 7: FUTURE WORK

There are several lines of research suggested by the results in this dissertation. For Chaplygin control systems, a natural extension is to design controllers for motion planning and optimal control. In the former one seeks to steer the system along a particular path through its environment, and in the latter one seeks to achieve a control objective while at the same time minimizing a cost function. It may also be possible to achieve control in finite time, rather than mere asymptotic control, by allowing for multiple control inputs for the unbalanced sleigh. Yet another avenue for research is the coordinated control of multiple Chaplygin control systems, in which multiple robots mutually interact to achieve a shared goal.

Turning to articulated swimmers, the same optimal control and motion planning suggestions discussed for Chaplygin control systems pertain here as well. Furthermore, an investigation into the numerically suggested geometric phase seems warranted; perhaps by factoring the system into its symmetric and asymmetric parts, it may be possible to find a connection on the symmetric factor that governs the motion. Also, the validity of the hydrodynamic decoupling assumption — although widely used in the literature — should still be revisited, perhaps by including first-order interactions between the spheres.

In the treatment of hydrodynamic constraints via Dirac's method, one obvious drawback is the requirement that there be an even number of scalar constraints due

to the Hamiltonian formulation of the problem. However, the point vortex equations are also known to have a Lagrangian form, and the usual treatment of constraints in Lagrangian mechanics is able to accommodate any number — even or odd — of constraints. It also seems advisable to compare the reduced-order models discussed in this work to high-fidelity Navier-Stokes simulations and to physical experiments. A full accounting should be made of the discrepancy between the constrained-vortex model of a cylinder interacting with an external vortex vs. the known dynamics. In particular, since both are governed by Poisson brackets, an understanding of the differences between their brackets might lead to insight. Finally, another idea is to allow the infinitesimal rigid bodies imposing the constraints to move, rather than be fixed; equivalently, to consider time-dependent constraints. Since the constraints affect the vortex dynamics, it is conceivable that time-dependent constraints may be used to *control* the vortex dynamics.

REFERENCES

[1] R. Abraham and J. E. Marsden. *Foundations of Mechanics*. Addison Wesley, 2nd edition, 1978.

[2] D. J. Acheson. *Elementary Fluid Dynamics*. Oxford, 1990.

[3] H. Aref. Point vortex dynamics: A classical mathematics playground. *Journal of Mathematical Physics*, 48, 2007.

[4] V. I. Arnold. Sur la géométrie différentielle des groupes de lie de dimension infinie et ses applications à l'hydrodynamique des fluides parfaits. *Annales de l'Institut Fourier*, 16(1):319–361, 1966.

[5] J. Baez and J. P. Muniain. *Gauge Fields, Knots and Gravity*. World Scientific, 1994.

[6] D. Bleecker. *Gauge Theory and Variational Principles*. Dover, 2005.

[7] A. M. Bloch. *Nonholonomic Mechanics and Control*. Springer, 2003.

[8] A. M. Bloch, P. Krishnaprasad, J. E. Marsden, and R. M. Murray. Nonholonomic mcehanical systems with symmetry. *Archive for Rational Mechanics and Analysis*, 136:21–99, 1996.

[9] W. M. Boothby. *An Introduction to Differentiable Manifolds and Riemannian Geometry*. Academic Press, 2nd edition, 1986.

[10] A. V. Borisov, I. S. Mamaev, and S. M. Ramodanov. Motion of a circular cylinder and N point vortices in a perfect fluid. *Regular and Chaotic Dynamics*, 8:449–462, 2003.

[11] H. Cendra, J. E. Marsden, and T. S. Ratiu. *Lagrangian Reduction by Stages*. American Mathematical Society, 2001.

[12] S. A. Chaplygin. On the theory of motion of nonholonomic systems. The theorem on the reducing multiplier. *Math. Sbornik*, XXVIII:303–314, 1911.

[13] C. Chicone. *Ordinary Differential Equations with Applications*. Springer, 2006.

[14] P. A. Dirac. Generalized Hamiltonian dynamics. *Canadian Journal of Mathematics*, 2:129–148, 1950.

[15] P. A. Dirac. *Lectures on Quantum Mechanics*. Dover, 2001.

[16] M. P. Do Carmo. *Riemannian Geometry*. Birkhäuser, 2nd edition, 1992.

[17] M. J. Fairchild, P. M. Hassing, S. D. Kelly, P. Pujari, and P. Tallapragada. Single-input planar navigation via proportional heading control exploiting nonholonomic mechanics or vortex shedding. *Proceedings of the ASME Dynamic Systems and Control Conference*, 2011.

[18] M. J. Fairchild and S. D. Kelly. Self-propulsion of jointed bodies near a wall in an ideal fluid. *Proceedings of the International Conference on Control, Dynamic Systems, and Robotics*, 2014.

[19] Y. N. Fedorov and L. C. García-Naranjo. The hydrodynamic Chaplygin sleigh. *J. Phys. A: Math. Theor.*, 43, 2010.

[20] Y. N. Fedorov, L. C. García-Naranjo, and J. Vankerschaver. The motion of the 2D hydrodynamic Chaplygin sleigh in the presence of circulation. *arXiv:1201.5054*, 2012.

[21] Y. N. Fedorov and D. V. Zenkov. Dynamics of the discrete Chaplygin sleigh. *Discrete and Continuous Dynamical Systems*, Supplement:258–267, 2005.

[22] T. Frankel. *The Geometry of Physics*. Cambridge University Press, 2nd edition, 2004.

[23] A. Guichardet. On rotation and vibration of molecules. *Annales de l'Institut Henri Poincaré, section A*, 40(3):329–342, 1984.

[24] H. v. Helmholtz. Uber Integrale der hydrodynamischen Gleichungen welche den Wirbelbewegungen entsprechen. *Crelle*, lv, 1858.

[25] D. D. Holm. *Geometric Mechanics and Symmetry: From Finite to Infinite Dimensions*. Oxford, 2006.

[26] E. Kanso, J. E. Marsden, C. W. Rowley, and J. B. Melli-Huber. Locomotion of articulated bodies in a perfect fluid. *Journal of Nonlinear Science*, 15:255–289, 2005.

[27] S. D. Kelly. *The Mechanics and Control of Robotic Locomotion with Applications to Aquatic Vehicles*. PhD thesis, California Institute of Technology, 1998.

[28] S. D. Kelly, M. J. Fairchild, P. M. Hassing, and P. Tallapragada. Proportional heading control for planar navigation: the Chaplygin beanie and fishlike robotic swimming. *Proceedings of the American Control Conference*, 2012.

[29] S. D. Kelly and R. M. Murray. Geometric phases and robotic locomotion. Technical Report 94-014, California Institute of Technology, 1994.

[30] S. D. Kelly, P. Pujari, and H. Xiong. Geometric mechanics, dynamics, and control of fishlike swimming in a planar ideal fluid. In S. Childress, A. Hosoi, W. W. Schultz, and Z. J. Wang, editors, *Natural Locomotion in Fluids and on Surfaces: Swimming, Flying, and Sliding*. Springer, 2012.

[31] G. R. Kirchhoff. *Vorlesungen uber Mathematische Physik, I.* Teubner, 1876.

[32] S. Kobayashi and K. Nomizu. *Foundations of Differential Geometry.* Wiley, 1963.

[33] J. Koiller, K. Ehlers, and R. Montgomery. Problems and progress in microswimming. *Journal of Nonlinear Science*, 6:507–541, 1996.

[34] S. H. Lamb. *Hydrodynamics.* Cambridge, 6th edition, 1932.

[35] J. M. Lee. *Introduction to Smooth Manifolds.* Springer, 2nd edition, 2012.

[36] J. E. Marsden. *Lectures on Mechanics.* Cambridge, 1992.

[37] J. E. Marsden, R. Montgomery, and T. S. Ratiu. *Reduction, Symmetry, and Phases in Mechanics.* American Mathematical Society, 1990.

[38] J. E. Marsden and T. Ratiu. *Introduction to Mechanics and Symmetry.* Springer, 2nd edition, 1999.

[39] J. E. Marsden and A. Weinstein. Coadjoint orbits, vortices, and Clebsch variables for incompressible fluids. *Physica D*, 7:305–323, 1983.

[40] J. M. Maruskin. *Introduction to Dynamical Systems and Geometric Mechanics.* Solar Crest, 2012.

[41] L. M. Milne-Thomson. *Theoretical Hydrodynamics.* Macmillan, 5th edition, 1968.

[42] R. Montgomery. *The Bundle Picture in Mechanics.* PhD thesis, University of California, Berkeley, 1986.

[43] S. Morita. *Geometry of Differential Forms.* American Mathematical Society, 2001.

[44] R. M. Murray, Z. Li, and S. S. Sastry. *A Mathematical Introduction to Robotic Manipulation.* CRC Press, 1994.

[45] J. Neimark and N. Fufaev. *Dynamics of Nonholonomic Systems.* American Mathematical Society, 1972.

[46] P. K. Newton. *The N-Vortex Problem.* Springer, 2001.

[47] S. Nguyen and L. A. Turski. Examples of the dirac approach to dynamics of systems with constraints. *Pusica A*, 290:431–444, 2001.

[48] J. M. Osborne and D. V. Zenkov. Steering the Chaplygin sleigh by a moving mass. *IEEE Conference on Decision and Control*, 44(2), 2005.

[49] J. P. Ostrowski. *The Mechanics and Control of Undulatory Robotic Locomotion.* PhD thesis, California Institute of Technology, 1996.

[50] E. M. Purcell. Life at low Reynolds number. *American Journal of Physics*, 45(1):3–11, 1977.

[51] J. Radford. *Symmetry, Reduction and Swimming in a Perfect Fluid*. PhD thesis, California Institute of Technology, 2003.

[52] S. D. Ross. Optimal flapping strokes for self-propulsion in a perfect fluid. *Proceedings of the 2006 American Control Conference*, June 2006.

[53] P. G. Saffman. *Vortex Dynamics*. Cambridge University Press, 1992.

[54] A. Shapere and F. Wilczek. Geometry of self-propulsion at low Reynolds number. *Journal of Fluid Mechanics*, 198:557–585, 1989.

[55] B. N. Shashikanth, J. E. Marsden, J. W. Burdick, and S. D. Kelly. The Hamiltonian structure of a two-dimensional rigid cylinder interacting dynamically with N point vortices. *Physics of Fluids*, 14(3):1214–1227, 2002.

[56] S. Smale. Topology and mechanics, I. *Inventiones math.*, 10:305–331, 1970.

[57] S. Smale. Topology and mechanics, II. *Inventiones math.*, 11:45–64, 1970.

[58] N. Steenrod. *The Topology of Fibre Bundles*. Princeton University Press, 1951.

[59] S. Sternberg. Lie algebras, 2004.

[60] W. Thomson. On vortex motion. *Edin. Trans.*, xxv, 1869.

[61] J. Vankerschaver, E. Kanso, and J. E. Marsden. The geometry and dynamics of interacting rigid bodies and point vortices. *Journal of Geometric Mechanics*, 1(2):223–266, 2009.

[62] F. W. Warner. *Foundations of Differentiable Manifolds and Lie Groups*. Springer, 1983.

APPENDIX A: MORE ABOUT CONNECTIONS

A.1 Factoring an Ehresmann Connection

Since local coordinates in a bundle factor as $q = (r, s)$, with r encoding position in the base and s encoding position along the fiber, it makes sense that the connection form of an Ehresmann connection might factor in a way that respects this coordinate factorization.

Indeed, let $\pi : Q \to M$ be an n-dimensional bundle with p-dimensional fiber, and let $A : TQ \to V$ be the connection form of an Ehresmann connection on this bundle. If we choose any local trivialization $\pi^{-1}(U) \to U \times F$ with bundle coordinates $q = (r, s)$, and if v_q is any tangent vector in $T(\pi^{-1}(U))$, then in these bundle coordinates we may write $v_q = \dot{r}^\alpha \frac{\partial}{\partial r^\alpha} + \dot{s}^a \frac{\partial}{\partial s^a}$, where $\alpha = 1, \ldots, n-p$ and $a = 1, \ldots, p$. Now v_q is vertical if and only if $T_q\pi \cdot v_q = 0$, if and only if $\dot{r}^\alpha = 0$ for all α.[6] Since $A : TQ \to V$ is vertical-valued and linear in each fiber, it follows that there are locally defined 1-forms ω^a on $\pi^{-1}(U)$ such that

$$A(v_q) = \omega^a(v_q) \left.\frac{\partial}{\partial s^a}\right|_q .$$

For each $a, b = 1, \ldots, p$ and $\alpha = 1, \ldots, n-p$, let $A^a_\alpha : \pi^{-1}(U) \to \mathbb{R}$ and $B^a_b : \pi^{-1}(U) \to \mathbb{R}$ be the functions such that $\omega^a = A^a_\alpha \mathbf{d}r^\alpha + B^a_b \mathbf{d}s^b$. Now recall that A is a projection

[6] *Warning*: it is *not* true that v_q is horizontal if and only if $\dot{s}^a = 0$ for all a, as will be seen in the example to follow.

on vertical vectors. Therefore, for $c = 1, \ldots, p$ it follows that

$$\frac{\partial}{\partial s^c} = A\left(\frac{\partial}{\partial s^c}\right) = \left[A^a_\alpha \mathbf{d}r^\alpha\left(\frac{\partial}{\partial s^c}\right) + B^a_b \mathbf{d}s^b\left(\frac{\partial}{\partial s^c}\right)\right]\frac{\partial}{\partial s^a} = B^a_c \frac{\partial}{\partial s^a},$$

which implies that $B^a_c = \delta^a_c$, and hence

$$\omega^a = A^a_\alpha \, \mathbf{d}r^\alpha + \mathbf{d}s^a.$$

Meanwhile, since the connection form returns the vertical part of a vector,

$$\mathrm{ver}(v_q) = A(v_q) = (A^a_\alpha(q)\dot{r}^\alpha + \dot{s}^a)\frac{\partial}{\partial s^a}.$$

Then the horizontal part is

$$\mathrm{hor}(v_q) = v_q - \mathrm{ver}(v_q) = \dot{r}^\alpha \frac{\partial}{\partial r^\alpha} - A^a_\alpha(q)\dot{r}^\alpha \frac{\partial}{\partial s^a}.$$

This discussion proves the following.

THEOREM 19 (Factorization of an Ehresmann connection). *Let A be the connection form of an Ehresmann connection on a fiber bundle (Q, π, M, F). Let $n = \dim Q$ and $p = \dim F$. Then in every local trivialization $\pi^{-1}(U) \to U \times F$ with bundle coordinates $q = (r, s)$ there exist locally defined 1-forms ω^a on $\pi^{-1}(U)$ and smooth functions $A^a_\alpha : \pi^{-1}(U) \to \mathbb{R}$ such that*

$$A = \omega^a \frac{\partial}{\partial s^a} = (\mathbf{d}s^a + A^a_\alpha \mathbf{d}r^\alpha)\frac{\partial}{\partial s^a}, \qquad (a = 1, \ldots, p \text{ and } \alpha = 1, \ldots, n-p). \tag{74}$$

Furthermore, if $v_q = \dot{r}^\alpha \frac{\partial}{\partial r^\alpha} + \dot{s}^a \frac{\partial}{\partial s^a}$ is any tangent vector in $T(\pi^{-1}(U))$ then

$$\begin{aligned} \mathrm{ver}(v_q) &= (\dot{s}^a + A^a_\alpha(q)\dot{r}^\alpha)\frac{\partial}{\partial s^a}, \\ \mathrm{hor}(v_q) &= \dot{r}^\alpha \frac{\partial}{\partial r^\alpha} - A^a_\alpha(q)\dot{r}^\alpha \frac{\partial}{\partial s^a}. \end{aligned} \tag{75}$$

I now give a simple, concrete example of an Ehresmann connection and the factorization of its connection form. Consider the bundle $\pi : \mathbb{R}^3 \to \mathbb{R}^2 : (x, y, z) \mapsto (x, y)$. The fiber over $p \coloneqq (x_0, y_0) \in \mathbb{R}^2$ is $\pi^{-1}(p) = \{(x_0, y_0, z) : z \in \mathbb{R}\} \cong \mathbb{R}$. Let $q = (x, y, z) \in \mathbb{R}^3$ and $v_q = \dot{x}\frac{\partial}{\partial x} + \dot{y}\frac{\partial}{\partial y} + \dot{z}\frac{\partial}{\partial z} \in T_qQ$. Then $T_q\pi \cdot v_q = \dot{x}\frac{\partial}{\partial x} + \dot{y}\frac{\partial}{\partial y}$, which is zero if and only if $\dot{x} = \dot{y} = 0$. Hence $V_q = \ker(T_q\pi) = \mathrm{Span}\{\frac{\partial}{\partial z}\}$. Let $q \mapsto H_q$ be the distribution spanned by the vector fields $(1 + y^2)\frac{\partial}{\partial x} - \frac{\partial}{\partial z}$ and $\frac{\partial}{\partial y} + xz\frac{\partial}{\partial z}$. Then

$$V_q = \mathrm{Span}\left\{\frac{\partial}{\partial z}\right\}, \quad H_q = \mathrm{Span}\left\{(1 + y^2)\frac{\partial}{\partial x} - \frac{\partial}{\partial z},\ \frac{\partial}{\partial y} + xz\frac{\partial}{\partial z}\right\}.$$

Since the distribution $q \mapsto H_q$ is smooth and $T_qQ = H_q \oplus V_q$ everywhere, it defines an Ehresmann connection. Let us determine the horizontal and vertical parts of v_q. Since $T_qQ = H_q \oplus V_q$, there are unique scalars a, b, c such that

$$\begin{aligned} v_q = \dot{x}\frac{\partial}{\partial x} + \dot{y}\frac{\partial}{\partial y} + \dot{z}\frac{\partial}{\partial z} &= a\left((1 + y^2)\frac{\partial}{\partial x} - \frac{\partial}{\partial z}\right) + b\left(\frac{\partial}{\partial y} + xz\frac{\partial}{\partial z}\right) + c\frac{\partial}{\partial z} \\ &= a(1 + y^2)\frac{\partial}{\partial x} + b\frac{\partial}{\partial y} + (bxz + c - a)\frac{\partial}{\partial z}. \end{aligned}$$

Comparing coefficients on each side of the equation gives the system of equations

$$a(1 + y^2) = \dot{x}, \quad b = \dot{y}, \quad bxz + c - a = \dot{z}$$

whose solution is

$$a = \frac{\dot{x}}{1 + y^2}, \quad b = \dot{y}, \quad c = \frac{\dot{x}}{1 + y^2} - xz\dot{y} + \dot{z}.$$

Therefore,

$$\operatorname{hor} v_q = a\left((1+y^2)\frac{\partial}{\partial x} - \frac{\partial}{\partial z}\right) + b\left(\frac{\partial}{\partial y} + xz\frac{\partial}{\partial z}\right) = \dot{x}\frac{\partial}{\partial x} + \dot{y}\frac{\partial}{\partial y} + \left(xz\dot{y} - \frac{\dot{x}}{1+y^2}\right)\frac{\partial}{\partial z},$$
$$\operatorname{ver} v_q = c\frac{\partial}{\partial z} = \left(\frac{\dot{x}}{1+y^2} - xz\dot{y} + \dot{z}\right)\frac{\partial}{\partial z}.$$

Referring to Theorem 19, the connection form is $A : TQ \to V : \dot{x}\frac{\partial}{\partial x} + \dot{y}\frac{\partial}{\partial y} + \dot{z}\frac{\partial}{\partial z} \mapsto (\frac{\dot{x}}{1+y^2} - xz\dot{y} + \dot{z})\frac{\partial}{\partial z}$, and since the fiber is 1-dimensional, A is represented locally by the single 1-form $\omega^z = \mathbf{d}z + \frac{1}{1+y^2}\mathbf{d}x - xz\mathbf{d}y$ in the sense that $A = \omega^z\frac{\partial}{\partial z}$. The corresponding connection coefficients are $A^z_x = \frac{1}{1+y^2}$ and $A^z_y = -xz$.

A.2 Principal Connections

A principal bundle has additional structure beyond that of a general fiber bundle, namely a Lie group action relative to which the local trivializations are equivariant. The natural way to specialize an Ehresmann connection to a principal bundle in a manner that respects this additional structure is to require that horizontal spaces at two different points along a fiber should be related by the group action: a *principal connection* on a principal G-bundle $Q \to Q/G$, whose action is denoted Φ, is an Ehresmann connection $q \mapsto H_q$ such that if $q \in Q$ and $g \in G$ then

$$H_{\Phi_g q} = T_q\Phi_g \cdot H_q.$$

Turning to the connection form, the isomorphism $\lambda : \mathfrak{g} \to V_q : \xi \mapsto \xi_Q(q)$ of vector spaces induces the map $\Gamma : TQ \to \mathfrak{g}$ such that $\Gamma(v_q)$ is the unique Lie algebra element $\xi \in \mathfrak{g}$ such that $\operatorname{ver} v_q = \xi_Q(q)$. In words, $\Gamma(v_q)$ returns the Lie algebra element whose infinitesimal generator at q equals the vertical part of v_q. Hence $\Gamma(v_q)_Q(q) = \operatorname{ver} v_q$.

Since infinitesimal generators are everywhere vertical,

$$\Gamma(\xi_Q(q)) = \xi \tag{76}$$

for every $\xi \in \mathfrak{g}$, which I call the *projection property* of Γ. Note that Γ is fiberwise linear, in the sense that each $\Gamma_q : T_qQ \to \mathfrak{g}$ is linear, precisely because $\xi \mapsto \xi_Q(q)$ is linear. Moreover, $T_qQ = H_q \oplus V_q$ implies $H_q = \{v_q \in T_qQ : \mathrm{ver}(v_q) = 0\} = \{v_q \in T_qQ : \Gamma(v_q)_Q(q) = 0\} = \{v_q \in T_qQ : \Gamma(v_q) = 0\} = \ker \Gamma_q$, where the penultimate equality holds because λ is an isomorphism. Hence $H_q = \ker \Gamma_q$, just as for the connection form of an Ehresmann connection. It remains to account for equivariance. Recall that $(\Phi_g)_* \xi_Q = (\mathrm{Ad}_g\, \xi)_Q$ for a left action, and $(\Phi_g)_* \xi_Q = (\mathrm{Ad}_{g^{-1}}\, \xi)_Q$ for a right action (see [1]). From this the *equivariance property* of Γ follows, namely that $\Phi_g^* \Gamma = \mathrm{Ad}_g \circ \Gamma$ for a left action, and that $\Phi_g^* \Gamma = \mathrm{Ad}_{g^{-1}} \circ \Gamma$ for a right action. It is sometimes more convenient to write these equations in the equivalent form

$$\begin{aligned} &\Gamma(T\Phi_g \cdot v_q) = \mathrm{Ad}_g\, \Gamma(v_q) \qquad \text{(left action)}, \\ &\Gamma(T\Phi_g \cdot v_q) = \mathrm{Ad}_{g^{-1}}\, \Gamma(v_q) \qquad \text{(right action)}. \end{aligned} \tag{77}$$

These considerations motivate the following definition. A *principal connection form* on a principal bundle $Q \to Q/G$ is a Lie algebra-valued 1-form $\Gamma : TQ \to \mathfrak{g}$ satisfying the projection and equivariance properties. Define a connection and a connection form to be *compatible* if they induce the same distribution. Then we have the following theorem.

THEOREM 20. *If $q \mapsto H_q$ is a principal connection on a principal bundle $Q \to Q/G$, there is a unique principal connection form with which it is compatible, namely Γ :*

$TQ \to \mathfrak{g}$ defined such that $\Gamma(v_q)_Q(q) = \operatorname{ver} v_q$. Conversely, to each principal connection form $\Gamma : TQ \to \mathfrak{g}$ there is a unique principal connection with which it is compatible, namely $q \mapsto H_q \coloneqq \ker \Gamma_q$.

I now show how to locally factor a principal connection form $\Gamma : TQ \to \mathfrak{g}$ on a principal bundle $Q \to Q/G$. Let $\pi^{-1}(U) \to U \times G$ be any local trivialization and write the induced bundle coordinates $q = (r, g)$. If $(q, \dot{q})$ is any tangent vector in $T(\pi^{-1}(U))$, then in tangent-lifted coordinates $(q, \dot{q}) = (r, g, \dot{r}, \dot{g})$, and it follows from linearity of $\Gamma(q, \cdot) : T_qQ \to \mathfrak{g}$ that

$$\Gamma(q, \dot{q}) = \Gamma(r, g, \dot{r}, \dot{g}) = \Gamma(r, g, \dot{r}, 0) + \Gamma(r, g, 0, \dot{g}). \tag{78}$$

Assume the action is to the left. Since $(r, g, \dot{r}, 0) = T\Phi_g \cdot (r, e, \dot{r}, 0)$, the equivariance property (77) implies $\Gamma(r, g, \dot{r}, 0) = \operatorname{Ad}_g(r, e, \dot{r}, 0)$. Define the *local connection form* $A : TU \to \mathfrak{g}$ by

$$A(r, \dot{r}) \coloneqq \Gamma(r, e, \dot{r}, 0). \tag{79}$$

Then I have just shown that $\Gamma(r, g, \dot{r}, 0) = \operatorname{Ad}_g A(r, \dot{r})$. Meanwhile, for every $\xi \in \mathfrak{g}$ the infinitesimal generator for the left action is given in bundle coordinates on $\pi^{-1}(U)$ by $\xi_Q(r, g) = (0, \xi g)$. In particular, taking $\xi \coloneqq \dot{g}g^{-1} \in \mathfrak{g}$ gives $\dot{g} = \xi g$, so the projection property (76) implies $\Gamma(r, g, 0, \dot{g}) = \Gamma(r, g, 0, \xi g) = \Gamma(\xi_Q(r, g)) = \xi = \dot{g}g^{-1} = \operatorname{Ad}_g(g^{-1}\dot{g})$. Therefore, (78) becomes $\Gamma(r, g, \dot{r}, \dot{g}) = \operatorname{Ad}_g(g^{-1}\dot{g} + A(r, \dot{r}))$, for a left action. Hence as a $\mathfrak{g}$-valued 1-form, $\Gamma = \operatorname{Ad}_g(g^{-1}\,\mathbf{d}g + A(r)\,\mathbf{d}r)$ on $\pi^{-1}(U) \subset Q$, for a left action. The proof for a right action is similar, except then the infinitesimal generator is $\xi_Q(r, g) = (0, g\xi)$ and one uses the equivariance condition for a right

action in (77). This discussion proves the following.

THEOREM 21 (Factorization of a principal connection). *If Γ is a principal connection form on the principal bundle $\pi : Q \to Q/G$, if $\pi^{-1}(U) \to U \times G$ is a local trivialization with induced bundle coordinates $q = (r, g)$ and tangent-lifted coordinates $(q, \dot{q}) = (r, g, \dot{r}, \dot{g})$, and if $A : TU \to \mathfrak{g}$ is the local connection form defined in* (79)*, then as a $\mathfrak{g}$-valued 1-form,*

$$\Gamma = \mathrm{Ad}_g(g^{-1}\,\mathbf{d}g + A(r)\,\mathbf{d}r) \qquad (\textit{left action}),$$

$$\Gamma = \mathrm{Ad}_{g^{-1}}((\mathbf{d}g)g^{-1} + A(r)\,\mathbf{d}r) \quad (\textit{right action}).$$

In particular, for any $(q, \dot{q}) = (r, g, \dot{r}, \dot{g}) \in T\pi^{-1}(U) \cong T_{(r,g)}(U \times G)$,

$$\Gamma(r, g, \dot{r}, \dot{g}) = \mathrm{Ad}_g(g^{-1}\dot{g} + A(r, \dot{r})) \qquad \textit{(left action)},$$

$$\Gamma(r, g, \dot{r}, \dot{g}) = \mathrm{Ad}_{g^{-1}}(\dot{g}g^{-1} + A(r, \dot{r})) \quad \textit{(right action)}.$$

I have shown that a principal connection on $Q \to Q/G$ may be defined equivalently as an Ehresmann connection whose horizontal spaces are invariant under the group action or as an equivariant connection form $\Gamma : TQ \to \mathfrak{g}$ that is a projection on vertical vectors. There is a third equivalent definition in terms of a family of 1-forms $\omega_U : U \to \mathfrak{g}$ (physicists call these *gauge potentials*), one for each local trivialization $\pi^{-1}(U) \to U \times G$, satisfying conditions analogous to that of the local connection form we derived above as well as compatability conditions on overlaps. This point of view is common in theoretical physics (see [6]), but I shall not pursue the matter here.

A.3 Parallel Transport in Principal Bundles

Let $\pi : Q \to Q/G$ be a left principal bundle endowed with a principal connection. Let $\Gamma : TQ \to \mathfrak{g}$ be the associated connection form. Let a base curve $r : [0, T] \to Q/G$ and a point $g_0 \in \pi^{-1}(r(0))$ be given. Suppose $\gamma : [0, T]$ is a horizontal lift of this curve. Then $\dot{\gamma}(t)$ is horizontal for all $t \in [0, T]$, and since horizontal vectors are sent to zero by the connection form, it follows that $\Gamma = 0$ along a horizontal lift. Working in local bundle coordinates $q = (r, g)$, Theorem 21 implies that

$$0 = \Gamma(r, g, \dot{r}, \dot{g}) = \mathrm{Ad}_g(g^{-1}\dot{g} + A(r, \dot{r})).$$

Applying Ad_g^{-1} to each side and rearranging gives $\dot{g} = -gA(r, \dot{r})$. Therefore, the evolution of the group variables are governed by the initial-value problem

$$\begin{aligned} \dot{g}(t) &= g(t)A(r(t), \dot{r}(t)), \\ g(0) &= g_0. \end{aligned} \tag{80}$$

Since $r(t)$ and hence $A(r(t), \dot{r}(t))$ are known, this initial-value problem may be integrated in order to *reconstruct* the evolution of the group variable $g(t)$, which encode the system's position and orientation in its environment, from the known initial conditions and the evolution of the shape variables.

For an *abelian* principal bundle, i.e. principal bundles whose fiber is an abelian Lie group, there is an explicit solution parallel transport problem given by

$$g(t) = g_0 \exp\left(-\int_0^t A(r(s), \dot{r}(s))\, ds\right), \tag{81}$$

where $\exp : \mathfrak{g} \to G$ is the Lie exponential map. As a special case, if the path in shape

space is a closed loop to which Stokes' theorem applies, then we recover the formula

$$g(T) = g_0 \exp\left(-\iint_S \mathbf{d}A\right),$$

where S is any oriented submanifold of M whose boundary coincides with the given path in shape space; this formula is called the *area rule for abelian bundles*, and — since it is manifestly independent of the time parameterization — it gives the geometric phase associated with the closed loop in shape space. The reconstruction formula (81) for abelian principal bundles is proved in [36] by making use of a powerful structure theorem that says every abelian Lie group is a product of tori and Euclidean spaces. Here I give a different proof that relies on a formula for the derivative of the exponential map. If $t \mapsto \eta(t)$ is a curve in the Lie algebra $\mathfrak{g}$, the derivative of $t \mapsto \exp \eta(t)$ is

$$\frac{d}{dt} \exp \eta(t) = (\exp \eta(t)) \sum_{n=0}^{\infty} \frac{(-1)^n}{(n+1)!} (\mathrm{ad}_{\eta(t)})^n \dot{\eta}(t),$$

where $(\mathrm{ad}_{\eta(t)})^n$ signifies the n-fold composition $\mathrm{ad}_{\eta(t)} \circ \cdots \circ \mathrm{ad}_{\eta(t)}$. This formula is derived, for example, in [59]. Since $\mathrm{ad}_{\eta(t)} \dot{\eta}(t) = [\eta(t), \dot{\eta}(t)]$, the preceding formula may be expressed as the following series involving iterated Lie algebra brackets,

$$\frac{d}{dt} \exp \eta(t) = \exp \eta(t) \Big(\dot{\eta}(t) - [\eta(t), \dot{\eta}(t)] + \frac{1}{2!} [\eta(t), [\eta(t), \dot{\eta}(t)]] - \frac{1}{3!} [\eta(t), [\eta(t), [\eta(t), \dot{\eta}(t)]]] + \cdots \Big).$$

All brackets in the preceding display are zero because G is abelian, and so $\frac{d}{dt} \exp \eta(t) = (\exp \eta(t)) \dot{\eta}(t)$. Let $\xi(t)$ denote $A(c(t), \dot{c}(t)) \in \mathfrak{g}$ and assume temporarily that $g_0 = e$ in the inital-value problem (80). Recall that the exponential map of a connected,

abelian Lie group is surjective. Therefore, if $t \mapsto g(t)$ is the solution to the initial-value problem, there is a curve $[0,T] \to \mathfrak{g} : t \mapsto \eta(t)$ such that $g(t) = \exp \eta(t)$. By the formula we just derived, this is equivalent to $\dot{g}(t) = \frac{d}{dt} \exp \eta(t) = (\exp \eta(t))\dot{\eta}(t) = g(t)\dot{\eta}(t)$. However, we also have $\dot{g}(t) = -g(t)\xi(t)$ from the initial-value problem. Setting these equal and cancelling $g(t)$ gives $\dot{\eta}(t) = -\xi(t)$, and integration gives $\eta(t) = -\int_0^t \xi(s)\, ds$. Hence the solution to the initial-value problem $\dot{g}(t) = -g(t)\xi(t)$ with $g(0) = e$ is $g(t) = \exp(-\int_0^t \xi(s)\, ds) = \exp(-\int_0^t A(c(s), \dot{c}(s))\, ds)$. To obtain the solution with $g(0) = g_0$, simply left translate by g_0 the solution just obtained for $g_0 = e$ to arrive (81).

A.4 The Mechanical Connection and the Master Formula

The mechanical connection was defined in [23], building on Smale's earlier work on the Kepler problem (see [56] and [57]). In much of the literature (e.g. [36]), the mechanical connection is *defined* by the formula for its connection form Γ,

$$\Gamma = \mathbb{I}^{-1} \circ \mathbf{J}, \tag{82}$$

which is shorthand for $\Gamma(v_q) = (\mathbb{I}(q))^{-1}(\mathbf{J}(v_q))$, where $\mathbf{J} : TQ \to \mathfrak{g}^*$ is the momentum map and $\mathbb{I}(q) : \mathfrak{g} \to \mathfrak{g}^*$ is defined such that for any two Lie algebra elements $\xi, \eta \in \mathfrak{g}$, $\langle \mathbb{I}(q)\xi, \eta \rangle = \langle \mathbb{F}L(\xi_Q(q)), \eta_Q(q) \rangle$. Here ξ_Q and η_Q are the infinitesimal generator vector fields on Q induced by the given Lie algebra elements and the group action, as defined in (11). The motivation for this formula is that $\mathbb{I}(q)$ represents the classical moment of inertia tensor for a mechanical linkage with all its internal joint angles "locked" into place, and that $\Gamma = \mathbb{I}^{-1} \circ \mathbf{J}$ gives the body angular velocity of this locked system

(see [36]). As pointed out in [37], the formula (82) is referred to as the "master formula" by Shapere and Wilczek, authors of the important paper [54] that addresses geometric phases in fluid locomotion.

In this appendix I *derive* the master formula as a consequence of a more geometric definition for the mechanical connection. For a simple mechanical system with configuration space a principal bundle $Q \to Q/G$ endowed with a Riemannian metric g and a Lagrangian $L : TQ \to \mathbb{R}$ of the form (4), the *mechanical connection* is the induced metric connection. That is, its horizontal spaces are defined to be metric orthogonal to vertical, as in (3). Because $Q \to Q/G$ is a principal bundle, the group action preserves vertical spaces, i.e. $T_q\Phi_h : V_q \to V_{\Phi_h q}$ is an isomorphism of vector spaces for every $q \in Q$ and every $h \in G$. If the metric is *invariant* in the sense that $\Phi_h^* g = g$ for every $h \in G$, then it follows that the horizontal spaces are also preserved, i.e. $T_q\Phi_h \cdot H_q = H_{\Phi_h q}$. This proves the following theorem.

THEOREM 22. *If the metric g on the total space of a principal bundle $Q \to Q/G$ is invariant, then the induced metric connection is a principal connection.*

Meanwhile, the metric and the group action interact to induce a natural family of inner products $(\cdot,\cdot)_q$ on the Lie algebra $\mathfrak{g}$, one for each $q \in Q$, defined by

$$(\xi,\eta)_q \coloneqq g(\xi_Q(q),\eta_Q(q)).$$

Each inner product induces an isomorphism $\mathbb{I}(q) : \mathfrak{g} \to \mathfrak{g}^*$ in a natural way, namely

$$\langle \mathbb{I}(q)\xi,\eta\rangle \coloneqq (\xi,\eta)_q = g(\xi_Q(q),\eta_Q(q)) = g_{ij}\xi_Q^i\eta_Q^j. \tag{83}$$

As already mentioned, we call $\mathbb{I}(q)$ the *locked inertia tensor* in this context. We

now have the following theorem.

THEOREM 23. *Let g be an invariant metric on the total space of a principal bundle $Q \to Q/G$ with momentum map $\mathbf{J} : TQ \to \mathfrak{g}^*$. If Γ is the connection form of the mechanical connection, then for every $v_q \in TQ$,*

$$\Gamma(v_q) = \mathbb{I}^{-1}(q)(\mathbf{J}(v_q)).$$

Proof. By decomposing each of $v_q, w_q \in T_qQ$ as the sum of vertical and horizontal vectors, bilinearity of the metric and $H_q = V_q^\perp$ imply that

$$g(v_q, w_q) = g(\operatorname{hor} v_q, \operatorname{hor} w_q) + g(\operatorname{ver} v_q, \operatorname{ver} w_q).$$

In particular, if w_q is either vertical or horizontal, then

$$g(v_q, w_q) = \begin{cases} g(\operatorname{ver} v_q, w_q), & \text{if } w_q \text{ is vertical,} \\ g(\operatorname{hor} v_q, w_q), & \text{if } w_q \text{ is horizontal.} \end{cases} \tag{84}$$

Since $\operatorname{ver} v_q = \Gamma(v_q)_Q(q)$ and $\xi_Q(q)$ are vertical, (10), (6), (84) and (83) imply

$$\langle \mathbf{J}(v_q), \xi \rangle = \langle \mathbb{F}L(v_q), \xi_Q(q) \rangle = g(v_q, \xi_Q(q)) = g(\Gamma(v_q)_Q(q), \xi_Q(q)) = \langle \mathbb{I}(q)\Gamma(v_q), \xi \rangle .$$

Since this holds for all $\xi \in \mathfrak{g}$, it follows that $\mathbf{J}(v_q) = \mathbb{I}(q)(\Gamma(v_q))$, or $\Gamma(v_q) = \mathbb{I}^{-1}(q)(\mathbf{J}(v_q))$. □

The foregoing constructions may summarized by saying that the following diagram commutes.

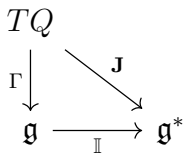

The horizontal spaces may also be characterized in terms of the momentum map. Indeed, note that $v_q \in T_qQ$ is horizontal if and only if $0 = \text{ver}(v_q) = \Gamma(v_q) = \mathbb{I}^{-1}(q)(\mathbf{J}(v_q))$, which is zero if and only if $\mathbf{J}(v_q) = 0$ because $\mathbb{I}(q)$ (and hence $\mathbb{I}^{-1}(q)$) is an isomorphism of vector spaces. Therefore,

$$H_q = \{v_q \in T_qQ : \mathbf{J}(v_q) = 0\}.$$

Hence *a trajectory in TQ evolves horizontally with respect to the mechanical connection if and only if the momentum* $\mathbf{J}$ *is identically zero along that trajectory.*

A.5 Elroy's Beanie

The simple mechanical system known as *Elroy's beanie* appears in [37]. It is a mechanical system comprising two planar rigid bodies pinned at their centers of mass but free to rotate relative to one another, as depicted in Figure 70. The configuration manifold for the system is the torus $Q = S^1 \times S^1$ with coordinates ϕ, θ that describe, respectively, the joint angle between the two bodies and the orientation of one body relative to a fixed inertial system.

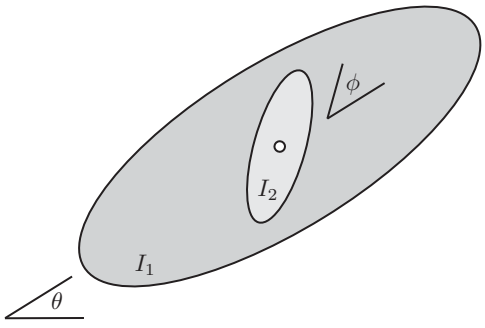

Figure 70: Elroy's beanie. The darkly shaded ellipse is Elroy, and the lightly shaded one is his beanie.

We assume there are no external forces or torques, but that an internal torque permits

variation of the joint angle. Let I_1, I_2 be the moments of inertia about the vertical axis through the pin. Conservation of angular momentum for this system implies $I_2\,\Delta\phi + (I_1 + I_2)\,\Delta\theta = 0$, and consequently

$$\Delta\theta = -\frac{I_2}{I_1 + I_2}\,\Delta\phi. \tag{85}$$

That is, if the beanie undergoes a rotation of $\Delta\phi$ relative to the first body, then Elroy undergoes a rotation of $-\frac{I_2}{I_1+I_2}\,\Delta\phi$ relative to the environment. As mentioned in [37], this result may be interpreted as geometric phase arising from the mechanical connection for this system, but no derivation is given. I give the derivation here in order to concretely illustrate the mechanical connection and the geometric phase formula (81).

The Lagrangian $L : TQ \to \mathbb{R}$ for the system is

$$L = \frac{1}{2}I_2(\dot\phi + \dot\theta)^2 + \frac{1}{2}I_1\dot\theta^2.$$

From this the fiber derivative $\mathbb{F}L : TQ \to T^*Q$, given in coordinates by $\mathbb{F}L(q, \dot q) = \frac{\partial L}{\partial \dot q^i}\,\mathbf{d}q^i$, is seen to be

$$\mathbb{F}L(\phi, \theta, \dot\phi, \dot\theta) = I_2(\dot\phi + \dot\theta)\,\mathbf{d}\phi + \Big(I_2(\dot\phi + \dot\theta) + I_1\dot\theta\Big)\,\mathbf{d}\theta.$$

There is a natural $G \coloneqq S^1$ action $\Phi : G \times Q \to Q$ given by

$$\Phi_\psi(\phi, \theta) = (\phi, \theta + \psi),$$

corresponding to rotation of the entire system through angle ψ. This action makes $Q \to Q/G$ into a trivial principal G-bundle over $Q/G \cong S^1$. The coordinate on

the base is, of course, ϕ. By inspection, the tangent lift of this action is given by $T\Phi_\psi : (\phi, \theta, \dot{\phi}, \dot{\theta}) \mapsto (\phi, \theta + \psi, \dot{\phi}, \dot{\theta})$, from which we also see that L is invariant under the tangent-lifted action. Since the Lie algebra $\mathfrak{g} \coloneqq T_1 S^1$ is one-dimensional, we identify it with $\mathbb{R}$. The exponential map $\exp : \mathfrak{g} \to S^1$ is computed to be $\exp(\xi) = \xi$. Using this, the fundamental vector field for the action corresponding to a Lie algebra element ξ is computed to be

$$\xi_Q = \xi \frac{\partial}{\partial \theta}.$$

Let $q = (\phi, \theta)$ denote a general point of Q, so in tangent-lifted coordinates, $(q, \dot{q}) = (\phi, \theta, \dot{\phi}, \dot{\theta})$. The momentum map $\mathbf{J} : TQ \to \mathfrak{g}^*$ is determined by

$$\begin{aligned}
\langle \mathbf{J}(q, \dot{q}), \xi \rangle &= \langle \mathbb{F}L(q, \dot{q}), \xi_Q(q) \rangle \\
&= \left\langle I_2(\dot{\phi} + \dot{\theta})\, \mathbf{d}\phi + \Big(I_2(\dot{\phi} + \dot{\theta}) + I_1 \dot{\theta} \Big)\, \mathbf{d}\theta, \xi \frac{\partial}{\partial \theta} \right\rangle \\
&= \Big(I_2(\dot{\phi} + \dot{\theta}) + I_1 \dot{\theta} \Big)\, \xi.
\end{aligned}$$

By identifying $\mathfrak{g}^* \cong \mathbb{R}^*$ with $\mathbb{R}$ via multiplication, it follows that

$$\mathbf{J}(q, \dot{q}) = I_2(\dot{\phi} + \dot{\theta}) + I_1 \dot{\theta},$$

which is nothing but the total angular momentum of the system about the axis through the pin. To compute the locked inertia tensor $\mathbb{I}(q) : \mathfrak{g} \to \mathfrak{g}^*$ at q, let $\xi, \eta \in \mathfrak{g}$.

Then

$$\begin{aligned}\langle \mathbb{I}(q)\xi, \eta\rangle &= \langle \mathbb{F}L(\xi_Q(q)), \eta_Q(q)\rangle \\ &= \left\langle \mathbb{F}L(\phi, \theta, 0, \xi), \eta\frac{\partial}{\partial\theta}\right\rangle \\ &= \left\langle I_2\xi\,\mathbf{d}\phi + (I_2 + I_1)\xi\,\mathbf{d}\theta, \eta\frac{\partial}{\partial\theta}\right\rangle \\ &= (I_2 + I_1)\xi\eta.\end{aligned}$$

In general, if $\dim\mathfrak{g} = n$ then the linear map $\mathbb{I}(q) : \mathfrak{g} \to \mathfrak{g}^*$, when identified with the bilinear map $\mathbb{I}(q) : \mathfrak{g}\times\mathfrak{g} \to \mathbb{R} : (\xi, \eta) \mapsto \langle \mathbb{I}(q)\xi, \eta\rangle$, is represented in coordinates by the $n \times n$ matrix $(\mathbb{I}(q)_{ij})$ such that if $\xi = \xi^i e_i$ and $\eta = \eta^j e_j$ relative to a basis $e_1, \ldots, e_n$ for $\mathfrak{g}$ then $\langle \mathbb{I}(q)\xi, \eta\rangle = \mathbb{I}(q)_{ij}\xi^i\eta^j$. In this case, $\dim\mathfrak{g} = 1$, so $\mathbb{I}(q)$ is simply a scalar, and the preceding computation implies

$$\mathbb{I}(q) = I_1 + I_2, \quad \mathbb{I}^{-1}(q) = \frac{1}{I_1 + I_2}.$$

Note that $\mathbb{I}(q) = I_1 + I_2$ is just the inertia of the "locked" system (i.e. with the joint angle ϕ fixed). The mechanical connection $\Gamma : TQ \to \mathfrak{g}$ is determined by

$$\Gamma(q, \dot{q}) = \mathbb{I}^{-1}(q) \circ \mathbf{J}(q, \dot{q}) = \frac{I_2(\dot{\phi} + \dot{\theta}) + I_1\dot{\theta}}{I_1 + I_2} = \frac{I_2}{I_1 + I_2}\dot{\phi} + \dot{\theta}.$$

It could be concluded here that since $\Gamma = 0$ along a horizontal trajectory, $\dot{\theta} = -\frac{I_2}{I_1+I_2}\dot{\phi}$, integration of which gives recovers (85). However, in order to illustrate the concepts of local connection and geometric phase, I continue. It follows from the previous display that as a $\mathfrak{g}$-valued 1-form on Q,

$$\Gamma = \frac{I_2}{I_1 + I_2}\,\mathbf{d}\phi + \mathbf{d}\theta.$$

The local connection form $A : T(Q/G) \to \mathfrak{g}$ is

$$A(\phi, \dot{\phi}) = \Gamma(\phi, e, \dot{\phi}, 0) = \frac{I_2}{I_1 + I_2}\dot{\phi},$$

where e denotes the identity element of S^1. Hence as a $\mathfrak{g}$-valued 1-form on $Q/G \cong S^1$,

$$A = \frac{I_2}{I_1 + I_2}\,\mathbf{d}\phi.$$

Now assume a curve $t \mapsto \phi(t)$ is given in the base S^1, and that initially $\theta(0) = \theta_0$. Since $G = S^1$ is abelian, according to (81) the horizontal lift of the base curve ϕ to Q is the curve $t \mapsto (\phi(t), \theta(t))$ where $\theta(t)$ is given by

$$\theta(t) = \theta_0 \exp\left(-\int_0^t A(\phi(s), \dot{\phi}(s))\,ds\right).$$

Since the group is additive, and since the exponential map on S^1 is $\exp(\xi) = \xi$, by putting $\Delta\theta = \theta(t) - \theta_0$ and $\Delta\phi = \phi(t) - \phi(0)$ this formula recovers (85),

$$\Delta\theta = -\int_0^t \frac{I_2}{I_1 + I_2}\dot{\phi}(s)\,ds = -\frac{I_2}{I_1 + I_2}\Delta\phi.$$

APPENDIX B: AN EXAMPLE OF DIRAC'S METHOD

I present here an expanded version of an example of Dirac's method appearing in [47]. Consider a particle of mass m moving in $Q = \mathbb{R}^2$ with Euclidean coordinates $q = (x, y)$. The phase space is the cotangent bundle $P \coloneqq T^*Q = T^*\mathbb{R}^2$ with coordinates (x, y, p_x, p_y) and endowed with the canonical symplectic form

$$\Omega \coloneqq \mathbf{d}x \wedge \mathbf{d}p_x + \mathbf{d}y \wedge \mathbf{d}p_y.$$

This induces the canonical Poisson bracket $\{f, g\} \coloneqq \Omega(X_f, X_g) = \sum_i \frac{\partial f}{\partial q^i}\frac{\partial g}{\partial p_i} - \frac{\partial f}{\partial p_i}\frac{\partial g}{\partial q^i}$. Explicitly, if $f, g : P \to \mathbb{R}$ are smooth functions, then

$$\{f, g\} = \left(\frac{\partial f}{\partial x}\frac{\partial g}{\partial p_x} + \frac{\partial f}{\partial y}\frac{\partial g}{\partial p_y}\right) - \left(\frac{\partial f}{\partial p_x}\frac{\partial g}{\partial x} + \frac{\partial f}{\partial p_y}\frac{\partial g}{\partial y}\right).$$

Assume the particle is constrained to move along the graph of

$$f(x, y) = 0 \tag{86}$$

for some smooth function f such that $\mathbf{d}f$ is never zero. This last condition implies that zero is regular value of f, and so $f^{-1}(0)$ is an embedded submanifold of P by the level set theorem. In applying the Dirac method, the constraint submanifold $S \subset P$ must be a symplectic submanifold, and so in particular S must be even dimensional. Therefore, an even number of independent constraints are required. To find another constraint, note that f is identically zero along the particle's trajectory. Since the

vector field $X = p_x \frac{\partial}{\partial x} + p_y \frac{\partial}{\partial y}$ is tangent to the particle's trajectory, it follows that $Xf = 0$; that is,

$$p_x \frac{\partial f}{\partial x} + p_y \frac{\partial f}{\partial y} = 0. \tag{87}$$

More prosaically, (87) says the particle's momentum is tangent to the graph of f. Now there are four coordinates and two constraint equations, (86) and (87). To apply Dirac's method, change coordinates from (x, y, p_x, p_y) to coordinates (x, y, z^3, z^4), where z^3 and z^4 are defined by

$$\begin{aligned} z^3 &\coloneqq f(x, y), \\ z^4 &\coloneqq p_x \frac{\partial f}{\partial x} + p_y \frac{\partial f}{\partial y}, \end{aligned}$$

so that in these coordinates the constraint submanifold S consists of the level set $\{z^3 = z^4 = 0\}$. The constraint matrix is

$$(C^{ij}) \coloneqq \begin{pmatrix} \{z^3, z^3\} & \{z^3, z^4\} \\ \{z^4, z^3\} & \{z^4, z^4\} \end{pmatrix} = \begin{pmatrix} 0 & \{z^3, z^4\} \\ -\{z^3, z^4\} & 0 \end{pmatrix},$$

the last equality following by antisymmetry of the Poisson bracket. Explicitly,

$$\begin{aligned} \{z^3, z^4\} &= \left(\frac{\partial z^3}{\partial x} \frac{\partial z^4}{\partial p_x} + \frac{\partial z^3}{\partial y} \frac{\partial z^4}{\partial p_y} \right) - \left(\frac{\partial z^3}{\partial p_x} \frac{\partial z^4}{\partial x} + \frac{\partial z^3}{\partial p_y} \frac{\partial z^4}{\partial y} \right) \\ &= \left(\frac{\partial f}{\partial x} \frac{\partial f}{\partial x} + \frac{\partial f}{\partial y} \frac{\partial f}{\partial y} \right) - \left(0 \frac{\partial z^4}{\partial x} + 0 \frac{\partial z^4}{\partial y} \right) = \left(\frac{\partial f}{\partial x} \right)^2 + \left(\frac{\partial f}{\partial y} \right)^2. \end{aligned}$$

Hence

$$(C^{ij}) = \left[\left(\frac{\partial f}{\partial x}\right)^2 + \left(\frac{\partial f}{\partial y}\right)^2\right] \begin{pmatrix} 0 & 1 \\ -1 & 0 \end{pmatrix},$$

$$(C_{ij}) = (C^{ij})^{-1} = \frac{1}{\left(\frac{\partial f}{\partial x}\right)^2 + \left(\frac{\partial f}{\partial y}\right)^2} \begin{pmatrix} 0 & -1 \\ 1 & 0 \end{pmatrix}.$$

To be definite, assume the particle is in a uniform gravitational field and has Hamiltonian $H \coloneqq \frac{p_x^2}{2m} + \frac{p_y^2}{2m} + mgy$. Assume further that $f(x, y) = y - x^2$, so that the particle is constrained to move along the graph of $y = x^2$. Then $\mathbf{d}f = -2x\,\mathbf{d}x + \mathbf{d}y \neq 0$, and $(\frac{\partial f}{\partial x})^2 + (\frac{\partial f}{\partial y})^2 = 1 + 4x^2$. A tedious computation leads to the following system of first-order equations

$$\begin{aligned}
\dot{x} &= [x, H] = \frac{p_x + 2xp_y}{m(1 + 4x^2)}, \\
\dot{y} &= [y, H] = \frac{2x(p_x + 2xp_y)}{m(1 + 4x^2)}, \\
\dot{p}_x &= [p_x, H] = -\frac{2(p_x p_y + m^2 gx)}{m(1 + 4x^2)}, \\
\dot{p}_y &= [p_y, H] = \frac{2(p_x^2 - 2m^2 gx^2)}{m(1 + 4x^2)}.
\end{aligned}$$

Note that $\dot{y} = 2x\dot{x}$, so that $\frac{dy}{dx} = 2x$ and $y = x^2 + \text{constant}$, as required.